FORMATION OF HETEROMERIC CHANNELS BY Cx26S17F SYNDROMIC DEAFNESS MUTANT AND Cx30 AND ITS CONSEQUENCES ON COCHLEAR PATHOLOGY

Tesis entregada a
LA UNIVERSIDAD DE VALPARAÍSO
en Cumplimiento Parcial de los requisitos para optar al grado de
Doctor en Ciencias con Mención en Neurociencia
Facultad De Ciencias

Por
ANA CAROLINA ABBOTT ROJAS
Agosto, 2020
Dirigida por: Dr. Agustín Martínez Carrasco
Co-Dirigida por: Dr. Helmuth Sánchez Riquelme

FACULTAD DE CIENCIAS

UNIVERSIDAD DE VALPARAÍSO

INFORME DE APROBACION

TESIS DE DOCTORADO

Se informa a la Facultad de Ciencias que la Tesis de Doctorado presentada por:

ANA CAROLINA ABBOTT ROJAS

Ha sido aprobada por la comisión de Evaluación de la tesis como requisito para optar al grado de Doctor en Ciencias con mención en Neurociencia, en el examen de Defensa de Tesis rendido el día del mes de de 2020

Director/a de Tesis:
Dr. Agustín Martínez Carrasco **..…… .....**
Co-Director de Tesis:
Dr. Helmuth Sánchez Riquelme **…….....**

Comisión de Evaluación de la Tesis
Dra. Ana María Cárdenas **…….....**

Dr. Juan Carlos Sáez **….....**

Dr. Juan Cristóbal Maass **.....**

Para Gabriel, mi mayor inspiración

AGRADECIMIENTOS

Mis primeros y más profundos agradecimientos son a mi familia, Gabriel, Osvaldo, mi mamá Sara y mi papá Joaquín, y a mis abuelos María y José, y a mi hermano Joaquín. Sin ellos, nada de esto habría sido posible. Gracias por acompañarme en este camino, por soportar mis cambios de humor y por sobre todo por alentarme a nunca rendirme, especialmente tú, Osvaldo. A ti, mi querido hijo, que sin decirlo, me motivabas cada día a continuar y nunca rendirme. Porque quiero que sepas que las mujeres podemos ser mamás y científicas, aun cuando a veces el mundo te diga lo contrario. Y a mis papás, que siempre me han apoyado y acompañado en todo lo que me he propuesto. Gracias infinitas.

A mis queridos tutores, Dr. Agustín Martínez y Dr. Helmuth Sánchez, a quienes no sólo les agradezco cada uno de sus comentarios, apoyo, enseñanza y dedicación; sino también su calidad humana. Sepan Uds. que son grandes personas y los admiro mucho.

Agradezco también a mi Comisión de Tesis, Dra. Ana María Cárdenas, Dr. Juan Carlos Sáez y Dr. Juan Cristóbal Maass, por todos sus aportes y comentarios durante todo el proceso de esta tesis. Sin duda fueron muy valiosos, y nos ayudaron a concluir este trabajo satisfactoriamente. También agradezco a todo el Claustro del Doctorado en Neurociencias de la UV, por sus fantásticas clases cuando tuvimos el año de Troncal, y también por cada una de sus contribuciones a la ciencia, desde sus distintas áreas de investigación.

A mi querido Laboratorio de Comunicación Intercelular, o Laboratorio de Conexinas para los amigos. Sin la ayuda técnica y las largas conversas, este trabajo no habría sido lo mismo. A Jaime por su ayuda con las células y todo lo que me enseñó, a Mauricio por su ayuda y conversaciones de Biología Molecular, a Coni por ser una científica inspiradora y por todas las conversas en el patio. A Paloma, Carolina, Joel, Ricardo, Yessenia y Jorge, porque todos me enseñaron mucho. Al Dr. García, por sus consejos para trabajar con la conexina mutante. Incluyo también a Enzo Seguel y Claudia Delgado, por haber cuidado mis ratones durante todo este proceso, y al laboratorio del Dr. Sáez por facilitarme el equipo de Fura-2. Muchas gracias.

Finalmente agradezco a mis amigos de la UV y de la vida, que siempre me han apoyado en todo. A Barbara Cádiz, Victoria Devia, Sarita Granados e Isa Benjumeda, por todos los tecitos en el confocal, por todas las conversas y grandes momentos. A mis amigos eternos Paula, Pamela, Carolina, Pato, y todos los que se me quedan en el tintero. Sepan que los quiero mucho y que agradezco todo el apoyo durante todo este largo proceso.

Muchas gracias.

*This thesis has been supported by the FONDECYT (ANID, Chile) grant 1171240 (**to ADM**) and ICN09-022-F from ICM-ANID, CINV. Centro Interdisciplinario de Neurociencia de Valparaíso (CINV) is a Millennium Institute supported by the Millennium Scientific Initiative of the Ministerio de Ciencia, Tecnología, Conocimiento e Innovación de Chile. **Ana Abbott** was funded by a PhD fellowship from UV (FIB-UV), ANID (Agencia Nacional de Investigación y Desarrollo. Ministerio de Ciencia Tecnología, Conocimiento e Innovación de Chile, grant 21150585) and a Bridge Scholarship from CINV.*

INDEX

AGRADECIMIENTOS iv

INDEX v

LIST OF ABBREVIATIONS xi

ABSTRACT xiv

INTRODUCTION 1

Connexins form hemichannels and gap junction channels 1

KID syndrome (keratitis, ichthyosis, deafness) 4

The KID mutation affects residues that are part of the pore of the Cx26, causing HC gain of function in the skin. 5

Connexins and purinergic receptors in the cochlea, and their role in auditory function. 8

Hearing and organ of Corti 8

Purinergic signaling in the cochlea and its relationship with intracellular calcium 11

Problem Statement and hypothesis 13

MATERIALS AND METHODS 17

I.- HeLa cell culture 17

1. Maintenance 17

2. Transfections 18

3. Protein distribution and quantification 20

4. Functional analyses of connexins channels 22

5. Ca^{2+} imaging in HeLa cells 24

6. Cell death quantification 25

II.- Cochlear explant cultures..... 26

1. Maintenance 26

2. Ca^{2+} imaging in cochlear explants 28

III.- Study design and statistical analysis..... 29

RESULTS..... 30

I.- Syndromic deafness mutation S17F does not affect the compatibility of Cx26 to interact with Cx30. 30

II.- Mutant Cx26S17F is functional *trans* dominant-negative of Cx30 gap junction channels.. 40

III.-. Heteromeric HC formed by Cx26S17F and Cx30 are hyperactive and less sensitive to extracellular Ca^{2+} and La^{3+}. 43

IV.- Co-expression of Cx26S17F and Cx30 HCs increases cellular damage and death 50

V.- Expression of Cx26S17F in mouse cochlear explants changes the sub-cellular distribution of connexins in supporting cells of the organ of Corti. 53

VI.- Expression of Cx26S17F produce HCs hyperactivity in supporting cells of the organ of Corti and damage of Hair cells 59

VII.- Expression of Cx26S17F in HeLa cells and cochlear supporting cells differentially affect purinergic signaling..... 64

DISCUSSION AND CONCLUSIONS 68

I.- Syndromic deafness mutation S17F does not affect the compatibility of Cx26 to interact with Cx30. 68

II.- Mutant Cx26S17F is functional *trans* dominant-negative of Cx30 gap junction channels.. 71

III.- Heteromeric HC formed by Cx26S17F and Cx30 are hyperactive and less sensitive to extracellular Ca^{2+} and La^{3+} 73

IV.- Co-expression of Cx26S17F/Cx30 HCs increases cellular damage and death 76

V.- Expression of Cx26S17F in mouse cochlear explants changes the sub-cellular distribution of connexins in supporting cells of the organ of Corti. 77

VI.- Expression of Cx26S17F produce HCs hyperactivity in supporting cells of the organ of Corti and damage of hair cells 78

VII.- Expression of Cx26S17F in HeLa cells and cochlea supporting cells differentially affect purinergic signaling 80

REFERENCES 84

LIST OF TABLES

Table 1. Correlation index Pearson values, SEM and p value of Cx26WT/Cx30 and Cx26S17F/Cx30 per subcellular area 33

Table 2. Correlation index Manders 1 (Cx26WT or Cx26S17F, green; over Cx30, red), SEM and p value of Cx26WT/Cx30 and Cx26S17F/Cx30 per subcellular area 33

Table 3. Correlation index Manders 2 (Cx30, red, over Cx26WT or Cx26S17F, green), SEM and p value of Cx26WT/Cx30 and Cx26S17F/Cx30 per subcellular area 34

Table 4. Intensities of homomeric Cx26WT, Cx30 or Cx26S17F expression in HeLa cells per subcellular area (Mean ±SEM, N, p value) 37

Table 5. Intensities Cx26WT and Cx30 in heteromeric configuration in HeLa cells per subcellular area (Mean ±SEM, N, p value) 37

Table 6. Intensities Cx26S17F and Cx30 in heteromeric configuration in HeLa cells per subcellular area (Mean ±SEM, N, p value) 38

Table 7. Relative intensity of Cx30 when interacting with Cx26WT or Cx26S17F in HeLa cells per subcellular area (Mean ±SEM, N, p value) 38

Table 8. Percentaje of GJ coverage of the apposition zone in HeLa cells expressing homomeric Cx26WT, Cx30 and heteromeric Cx26WT/Cx30 and Cx26S17F/Cx30 (Mean ±SEM, N, p value) 38

Table 9. FRAP recovery rates comparison of homomeric Cx26WT v/s Cx30, and heteromeric Cx26WT/Cx30 v/s Cx26S17F/Cx30 (Mean, SEM and p value) 42

LIST OF FIGURES

Figure 1. Summary of the life of Cx43. 2

Figure 2. Connexins form hemichannels and gap junction channels. 3

Figure 3. 3D model of the homomeric HC formed by Cx26 obtained from crystallographic structure. 4

Figure 4. Distribution of GJCs in the cochlea. 9

Figure 5. Cell types in the organ of Corti. 11

Figure 6. Working hypothesis model. The syndromic mutant Cx26S17F forms oligomers with Cx30 generating non-functional GJ and hyperactive HCs with reduced regulation by Ca^{2+}_e. 14

Figure 7. Mutant Cx26S17F colocalizes with Cx30 and change the distribution of heteromeric hemichannels in HeLa cells 32

Figure 8. Expression of mutant Cx26S17F significantly reduce localization of Cx30 in the appositional zone 34

Figure 9. Cx26S17F interacts with Cx30, forming mutant heteromeric HC 39

Figure 10. Co-expression of Cx26S17F with Cx30 strongly reduces intercellular gap junctional communication 40

Figure 11. Heteromeric HC formed by Cx26S17F/Cx30 have hyperactive function and do not respond to connexin blocker La^{3+}. 43

Figure 12. HeLa cells co-expressing mutated heteromeric Cx26S17F/Cx30 channels showed less sensibility to $[Ca^{2+}]_e$ compared to cells coexpressing WT heteromeric Cx26WT/Cx30 channels. 46

Figure 13. Expression of mutant heteromeric Cx26S17F/Cx30 HCs increase cell death in HeLa cells 50

Figure 14. Cochlear explants as a model to study inner ear connexins 53

Figure 15. Expression of Cx26S17F in cochlear explants change the distribution of the protein in supporting cells of the organ of Corti. 567
Figure 16. cKI Cx26S17F expression in cochlear explants increases activity of supporting cells HC 61
Figure 17. Mutation Cx26S17F affects morphology of hair cell's stereocilia in cochlear explants 62
Figure 18. ATP-induced intracellular Ca^{2+} response is reduced in cells expressing mutant Cx26S17F/Cx30 64
Figure 19. cKI Cx26S17F expression in cochlear explants show altered ATP-induced Ca^{2+} response in absence or presence of $[Ca^{2+}]_e$ 67
Figure 20. Graphic conclusions. 83

LIST OF ABBREVIATIONS

ATP	Adenosine triphosphate
Ca^{2+}	Calcium
Ca^{2+}_e	Extracellular calcium
Ca^{2+}_i	Intracellular calcium
CaM	Calmodulin
cAMP	Cyclic adenosine monophosphate
CBX	Carbenoxolone
cDNA	Complementary DNA
cGMP	Cyclic guanosine monophosphate
cKI	Conditional *knock-in*
CT	Carboxy terminal domain
Cx	Connexin
Cx26 WT	Connexin 26 wild type
Cx26S17F	Connexin 26 with S17F mutation
Cx26S17F/Cx30	Heteromeric HC formed by Cx26S17F with Cx30
Cx26WT/Cx30	Heteromeric HC formed by Cx26 WT with Cx30
Cx30	Connexin 30
$[Ca^{2+}]_e$	Extracellular calcium concentration
$[Ca^{2+}]_i$	Intracellular calcium concentration
dB	Decibel
DIV	Days *in vitro*
DMSO	Dimethyl sulfoxide
EL	Extracellular loop

Etd	Ethidium bromide
F	Fibrocytes
FBS	Fetal bovine serum
FRAP	Fluorescence recovery after photobleaching
GFP	Green fluorescent protein
GJB2	Gap Junction β 2 gene
GJC	Gap Junction Channels
HC	Hemichannel
HP	HeLa parental (non-transfected)
IHC	Inner hair cells
IL	Intracellular loop
IP_3	Inositol trisphosphate
ISC	Inner supporting cells
K^+	Potassium
KID	Keratitis-Ichthyosis-Deafness
La^{3+}	Lanthanum
LY	Lucifer yellow
MEM	Minimum Essential Medium
NAD^+	Nicotinamide adenine dinucleotide
NT	Amino terminal domain
OHC	Outer hair cells
OSC	Outer supporting cells
P2X	Purinergic ionotropic receptors
P2Y	Purinergic metabotropic receptors
P7	7 days post-natal
PC	Pillar cells
PI	Propidium iodide

PLA	Proximity ligation assay
S17F	Substitution of a serine by a phenylalanine at 17th residue
siRNA	Small interfering RNA
TM	Transmembrane domain
Vj gating	Transjunctional voltage gating
WT	Wild type

ABSTRACT

Deafness is the most common condition associated with mutations in connexin (Cxs) genes, being mutations in Cx26 gene (GJB2) the most prevalent. Specific mutations in Cx26 also produce syndromic deafness, like Keratitis-Ichthyosis-Deafness (KID) syndrome, in which patients with deafness show severe alterations in the skin. KID syndrome symptoms include deep deafness, hard skin in hands and feet (palmoplantar keratoderma), red spots of thick (erythrokeratoderma), and scaly skin (ichthyosis), alopecia, bad nail formation, autoamputation of the last phalanges and thickness in the cornea (keratitis) that in severe cases leads to blindness.

In the main organs affected by KID mutations, Cx26 is co-expressed with Cx30. In the skin they are co-expressed in keratinocytes, while in the inner ear, they are co-expressed in the supporting cells of the organ of Corti. One mutation observed in KID patients is mutation Cx26S17F, which affect the N-terminal of Cx26, a Cx segment that is involved in the closure and opening of hemichannels (HC).

In this doctoral thesis, we studied the functional properties of heteromeric channels formed by Cx26S17F and Cx30. Here, we describe that Cx26S17F interact with Cx30 in an exogenous expression system like transfected HeLa cells, forming mutant heteromeric hemichannels (HC). These mutant heteromeric HCs are localized mainly in intracellular compartment, but some of them reach the plasma membrane forming few and small gap junction (GJ) plaques in appositional cell membranes. On contrary, mutant HCs in non-appositional cell membranes are hyperactive and do not respond to HC blocker La^{3+}. In addition, these mutant HCs present altered response to extracellular calcium (Ca^{2+}_e) remaining open at extracellular 1 and 1.5 mM that normally close wild type HCs, which is consistent with altered intracellular Ca^{2+} homeostasis in cells expressing these HCs. Finally, expression of these mutant HCs increased cell damage and death in the cultures.

Ex vivo expression of Cx26S17F in cochlear explants from conditional *knock-in* transgenic mouse (cKI), changes the distribution of Cx26 and Cx30 in supporting cells of the

organ of Corti, with more intracellular localization and reduced gap junction plaques, which contrast with the honeycomb-like GJ network observed in control explants. Also, supporting cells of cKI Cx26S17F cochlear explants show increased uptake of an extracellular tracer, suggesting that expression of mutant in supporting cells form hyperactive HC, that do not respond to extracellular Ca^{2+} and nor to the HC blocker carbenoxolone. To our knowledge, is the first study in cochlear Cxs using a model of syndromic deafness.

Because ATP is a very relevant paracrine molecule in the cochlea, we briefly explored the ATP-induced Ca^{2+} response in HeLa cells expressing mutant or WT heteromeric HC, as well as in cKI Cx26S17F cochlear explants. In absence and presence of Ca^{2+}_e, HeLa cells expressing Cx26S17F/Cx30 HC showed decreased intracellular Ca^{2+} signal to the stimulation with ATP, suggesting purinergic receptor desensitization and/or loss of Ca^{+2} homeostasis in cells. Preliminary observations in cKI cochlear explants expressing Cx26S17F also indicates that expression of hyperactive heteromeric HCs produces dysregulation of intracellular Ca^{2+} and altered purinergic signaling in cochlear cells, which are linked to hair cell damage.

INTRODUCTION

Connexins form hemichannels and gap junction channels

Connexins (Cxs) are protein subunits that form two types of channels, the gap junction channels (GJCs) and hemichannels (HCs) or connexons. The GJCs connect directly the cytoplasms of two adjacent cells through the formation of an aqueous pore, which crosses both plasma membranes. A GJC consists of two HCs, each belonging to each of the joined cells (Harris, 2001). On the other hand, HCs are formed by the oligomerization of six Cxs, which organize as a tube to form a central pore; thus, communicating the interior of the cell with the extracellular environment (Harris, 2007, 2001; Sáez et al., 2003). GJCs and HCs are permeable to ions and small molecules such as ATP, glucose, NAD^+, second messengers (i.e. cAMP, IP_3, cGMP), nucleotides, small peptides and siRNAs. HCs have been implicated in the regulation of cell homeostasis, and autocrine and paracrine intracellular signaling through the release of signaling molecules, such as ATP (Kang et al., 2008; Zong et al., 2016)

The oligomerization process of the six Cxs to form a HC occurs in the Golgi apparatus or in the endoplasmic reticulum, depending on the Cx type, where once assembled it travels to the plasma membrane through the secretory pathway using vesicles that are guided by microtubules (Lauf et al., 2002) (reviewed by Sáez et al., 2003). The half-life of Cxs is approximately 5 hours, being subsequently degraded. The entire plaque is internalized in the form of an endosome forming a structure called "annular junction", which is degraded into lysosomal compartments, multivesicular bodies or autophagosomes. In addition, depending on the cell type and Cx subunit can be degraded through the ubiquitin proteasome pathway (Laird, 2006; Falk et al., 2014; Sáez et al., 2003)

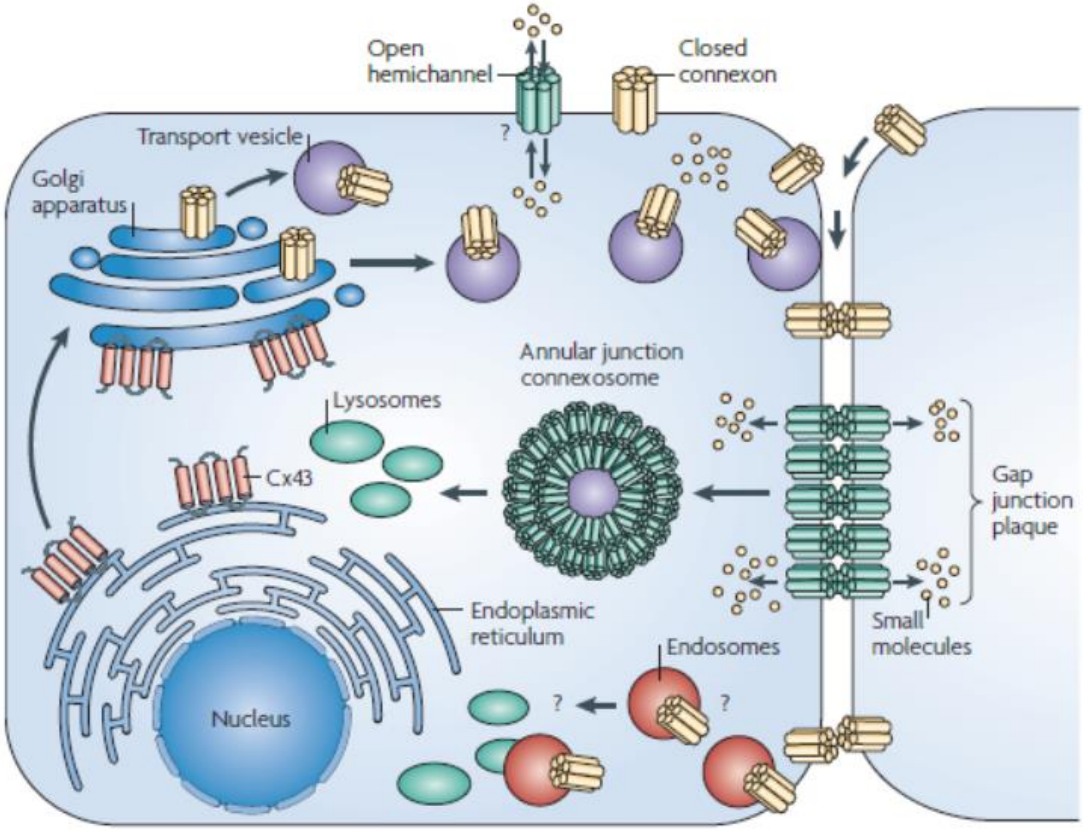

Figure 1. Summary of the life of Cx43. For explanation, see text. Modified from Naus and Dale, 2010.

The family of Cx genes has twenty one members in the human genome (Willecke et al., 2002; Söhl and Willecke, 2003). Cxs are differentially expressed in development and show a tissue-specific distribution in adulthood (Söhl et al., 2005). They have four transmembrane domains (TM1-4), two extracellular handles (EL1-2), an intracellular loop connecting TM2 with TM3 (IL), a short intracellular amino-terminal domain (NT) and an intracellular carboxy terminal domain (CT). The latter can be very short, as in Cx26; or long, as in Cx43 (Figure 2, panel A). TMs and ELs are highly conserved among the members of the Cx family, while the IL and CT domains are the most variable, containing sites that can be modified through phosphorylation, nitrosilation, ubiquitination and others; and participate in signaling pathways through protein-

protein interactions, including scaffolding, cytoskeleton binding proteins, and Ca^{2+}/Calmodulin (Sáez et al., 2003; Zou et al., 2014). In the membrane, Cxs can form different configurations of HCs and GJCs: when HCs are composed of the same isoform of Cx, they are called homomeric. When they are formed by different types of Cx, they are called heteromeric. As well, if a GJC is formed by two homomeric HCs, it is said to be homotypic, while if it is composed of homomeric HCs configured by different Cxs each, it is called heterotypic GJC (Figure 2, panel B) (Harris, 2001; Sáez et al., 2003). The configuration adopted by the HC and the GJC is extremely important because each Cx will give it specific permeability and voltage dependence properties to the channel (Martínez et al., 2002; Oh and Bargiello, 2015)

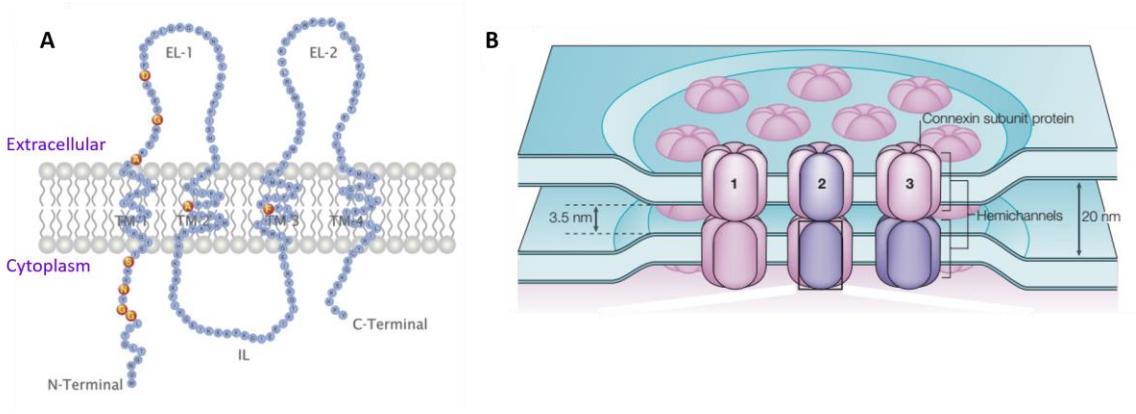

Figure 2. Connexins form hemichannels and gap junction channels. A) Structure of Cx26, where the amino terminal (N-Terminal), intracellular loop (IL) and carboxyl terminal (C-Terminal) domains are located towards the cytoplasm, while extracellular loops 1 and 2 (EL- 1 and EL-2) are located towards the outer side of the cell. Amino acids that suffer mutations and are associated with KID syndrome are highlighted in red (see text). B) Different configurations that can be adopted by each connexon or hemichannel, and by gap junction channels: 1) homomeric and homotypic 2) heteromeric and 3) heterotypic. Modified from (García et al., 2016a; Söhl et al., 2005).

The crystallographic structure of the channel formed by Cx26 indicates that the residues that form the pore belong mainly to the domains TM1, EL1 and NT. It is also possible to observe that the NT domain is part of the channel vestibule on the cytoplasmic face, and residues 1 through 10 are found inside the pore, forming a funnel-like structure towards the cytoplasmic side (Figure 3) (Maeda et al., 2009; Maeda and Tsukihara, 2011).

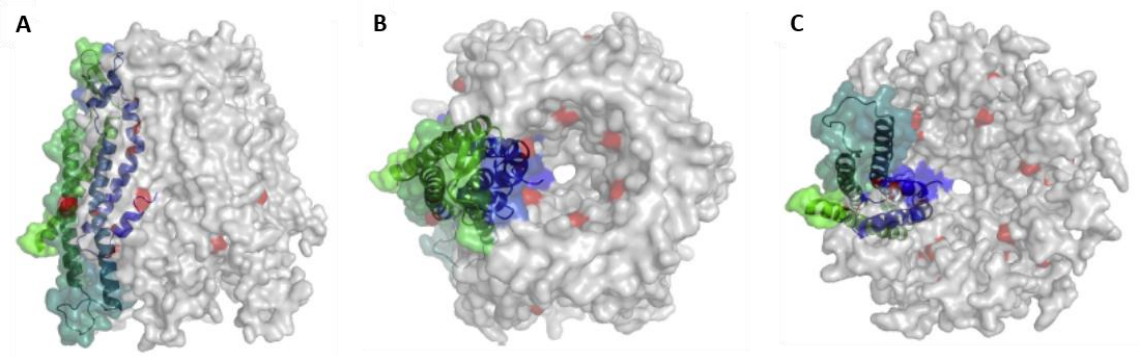

Figure 3. 3D model of the homomeric HC formed by Cx26 obtained from crystallographic structure. The funnel-shaped pore is observed, from A) side view, B) extracellular and C) cytoplasmic side. An isolated connexin is observed, marked with a blue-green gradient, where blue represents the amino terminal and green, the terminal carboxyl. Red marks sites of mutations associated with KID syndrome (see text). Modified by (García et al., 2016b), from (Maeda et al., 2009).

KID syndrome (keratitis, ichthyosis, deafness)

According to World Health Organization, deafness or hearing disability can be mild, moderate, severe or profound. It may occur in one or both ears, causing communicational problems and social impact to the affected person. Hearing loss implies an acoustic threshold of 25 dB above the normal hearing, while mild to profound deafness has an acoustic threshold above 45 dB normal hearing and can have different causes, some of them environmental and others congenital. Among environmental causes of deafness are infectious diseases in the ear, use of aminoglycoside-type antibiotics, acoustic trauma and others.

Congenital hearing loss and deafness can be caused by infectious disease during pregnancy, use of aminoglycoside-type antibiotics or cytotoxic drugs during pregnancy, and genetic mutations. Mutations in the Cx genes are related to several genetic diseases, being deafness the most frequent. Genetic deafness can be caused by mutations in several Cx genes, being Cx26 gene (*GJB2*) mutations responsible of 50% of genetic deafness causing sensorineural hearing loss due to cochlear malfunction in the inner ear (García et al., 2016a; b; Martínez et al., 2009; Mittal et al., 2018).

Most of the nonsense mutations in Cx26 are recessive, but some of them show a dominant pattern of inheritance and can produce syndromic deafness, including Keratitis-Ichthyosis-Deafness (KID) syndrome, in which deep deafness is associated with severe skin problems (Alvarez et al., 2003; García et al., 2016a; Skinner et al., 1981; Van Geel et al., 2002; Xu and Nicholson, 2013; Terrinoni et al., 2010; Avshalumova et al., 2014; Jonard et al., 2008; Godillot et al., 2019; Richard et al., 2002). The most common abnormalities of KID syndrome are deep deafness, and several skin conditions, such as palmoplantar keratoderma, thickening of the palms of the hands and palms of the feet; and erythrokeratoderma, characterized by ichthyosis, dry or flaky skin, and patches of red skin, which can be distributed throughout the body, but tend to concentrate on the neck and armpits (Jonard et al., 2008; García et al., 2016a; Lilly et al., 2019a; Skinner et al., 1981; Scott et al., 2012). In addition, patients have eye problems characterized by serious inflammatory conditions in the cornea (keratitis) that may lead to blindness (García et al., 2016a).

The KID mutation affects residues that are part of the pore of the Cx26, causing HC gain of function in the skin.

Most of the mutated Cxs associated with diseases do not form functional GJCs or have a drastic reduction in the functional status of the GJCs (García et al., 2016b), as in the case of

Cx26 mutations associated with non-syndromic deafness (Sanchez and Verselis, 2014). People who express these mutations have no other symptoms besides hearing loss. From an ultrastructural point of view, the mutations that produce non-syndromic deafness are not grouped in a specific domain within the Cx (Lee & White, 2009; Martínez et al., 2009).

On the other hand, in syndromic deafness, such as KID syndrome, it has been observed that HCs formed by mutated Cx26 show a gain of function with respect to Cx26 wild type (WT) (García et al., 2015, 2016a; Lee et al., 2009; Mhaske et al., 2013; Shuja et al., 2016). In some cases different mutations in the same residue may produce syndromic and non-syndromic deafness: for example, G12V and A40G mutations produce non-functional HCs and GJC, and deafness without problems to the skin (García et al., 2015; Jara et al., 2012; Martínez et al., 2009); while mutations in the same amino acid residues (G12R and A40V), have HCs with gain of function and produce syndromic deafness of the KID type (Sanchez and Verselis, 2014; García et al., 2016a; Marziano et al., 2003). To date, 9 mutations in Cx26 and 2 in Cx30 have been reported in patients with KID syndrome (Berger et al., 2014; Alvarez et al., 2003; Richard et al., 2002; Van Geel et al., 2002; Van Steensel et al., 2002; Yotsumoto et al., 2003; Gerido et al., 2007; Lilly et al., 2019b). Recently, the phenotype of syndromic mutation has been reported to begin at 32 weeks of gestation, *in utero*, where the human baby patient showed choroamniotic separation, facial deformation and protrusion in cerebellar vermis, caused by Cx26A88V. After birth, the baby only lived for 40 days, due to several skin infections (Okmen et al., 2019).

Most KID mutations are found in the NT and in the para-helix region of the transition zone between TM1 and EL1, in residues facing the pore of the canal. Both TM1 and EL1 are highly conserved regions in the Cxs family, critical for the opening and regulation of the channel (Harris, 2001; Maeda et al., 2009; Oh and Bargiello, 2015; Sanchez and Verselis, 2014). Our laboratory described that some KID mutations in the NT of the Cx26 produce highly hyperactive HCs when the mutant Cx26 is co-expressed with Cx43, suggesting that the disease is a consequence of an aberrant interaction between the two connexins, producing hyperactive HCs

and non-functional GJCs (García et al., 2015). The latter is consistent with the fact that in skin Cx26 is co-expressed with Cx43 (Suzuki et al., 2003; Wiszniewski et al., 2000). The molecular mechanism of hyperactivity of homo or heteromeric HC associated with KID syndrome is unknown; however, recent studies indicate that such mutations would affect the mechanism of channel gating (García, Bosen, et al., 2016; García et al., 2015).

Various properties of HCs and GJCs could be affected in syndromic deafness: A) mutations could affect the subtype of Cxs that make up each HC and GJC, giving the channels new functional properties, selectivity, regulation and unitary conductance. Consistent with the above, syndromic mutations appear to affect the oligomerization compatibility of Cx26 with Cxs that are incompatible in WT condition, such as Cx43, forming functionally aberrant heteromeric channels (García et al., 2015). B) Mutations could also affect the total number of channels in the plasma membrane, either by increasing the transport of the channels to the plasma membrane or by decreasing degradation (García et al., 2015, 2016b; Martínez et al., 2009; Sáez et al., 2003). C) Finally, the mutations could change the gate mechanisms of the channels. Preliminary results from our laboratory indicate that KID mutations in the NT of Cx26 eliminate the mechanism of fast gate or Vj gating, which normally closes the channel at depolarizing potential, leading the channels to remain open for longer periods (García et al., 2018; Sanchez et al., 2016). For example, the G12R syndromic mutation, located in the NT of Cx26, causes loss of the voltage-dependent fast gate by increasing the opening probability of the channel (García et al., 2018; Locke et al., 2011; Oh and Bargiello, 2015), which could explain the hyperactivity of this mutant. On the other hand, the syndromic mutant Cx26S17F interacts with the Cx43 forming heteromeric HCs that are hyperactive and non-functional GJCs. These aberrant channels favor the output of ATP and the intracellular increase of Ca^{2+} (García et al., 2015). The heteromeric channels formed by Cx26S17F and Cx43 also affect the HC fast gate, remaining open for a longer time than normal, which may explain the hyperactivity of the HC in KID (García et al., 2018; Sanchez et al., 2016).

Interestingly, it was observed that the expression of hyperactive heteromeric HCs formed by Cx43 and the syndromic mutants of Cx26, in particular Cx26S17F, increases the concentration of intracellular Ca^{2+} ($[Ca^{2+}]_i$) to 400-600 nM (García et al., 2015), values that are in the range necessary to increase the activity of Cx43 HC, through a mechanism dependent on Ca^{2+}/CaM (Zou et al., 2014; Peracchia, 2020). Cx43 have a CaM binding site in the IL, and CaM binding to the IL is required for the Cx43 HCs to open (Zou et al., 2014; Peracchia, 2020). Therefore, syndromic heteromeric channels containing Cx43 could also be regulated through the CaM pathway. However, the mechanism of intracellular Ca^{2+} increase is unknown. One possibility is that the ATP released through hyperactive HCs can act in an autocrine or paracrine manner on purinergic receptors of the P2Y or P2X type, which always favors increments in $[Ca^{2+}]_i$. (Retamal et al., 2015; García et al., 2016a) Therefore, the gain of function of the HCs in KID could generate a positive feedback with the release of ATP, the activation of purinergic receptors and the consequent increase in the concentration of $[Ca^{2+}]_i$, would contribute to the activation of Ca^{2+}/CaM and the opening of the HCs (Zou et al., 2014; Peracchia, 2020).

Connexins and purinergic receptors in the cochlea, and their role in auditory function.

Hearing and the organ of Corti

The conversion of sound waves into electrical impulses, allowing hearing, occurs in the inner ear, specifically in hair cells in the organ of Corti, within the cochlea. The cochlea is a snail-shaped structure, housed in a bone matrix that allow sounds with different frequencies to be perceived in specific areas within it (i.e. high frequencies in the basal part, and low frequencies at the apex of the snail). The spatial arrangement in the perception of different acoustic frequencies is called tonotopy. The cochlea contains three fundamental chambers, the *scala vestibularis* (vestibular duct), *the scala media* (cochlear duct) and the *scala tympani* (tympanic

duct). The vestibular and tympanic ducts are filled with a fluid called perilymph, of similar constitution to the cerebrospinal fluid (low K^+, high Na^+), while the cochlear duct is full of endolymph, high in K^+ and low in Na^+ and Ca^{2+}. The organ of Corti is located in the cochlear duct, where the inner and outer hair cells perceive the vibrations driven by the tympanic duct. When the acoustic waves travel along the tympanic duct, they cause the movement of the basal membrane, which is where the support cells are located (bathed by perilymph). Hair cells are located on top of supporting cells, bathed by perilymph in the basal area and by endolymph in the apical area. When hair cells move, the cilia in contact with the tectorial membrane also moves causing a deflection of the cilia, thereby allowing the passage of K^+, depolarizing the cell, and thereby, increasing Ca^{2+} into the hair cell. The K^+ will leave the hair cells by the basal part, thereby returning the hair cell to the resting state. The accumulation of Ca^{2+} allow the release of vesicles with glutamate to the auditory nerve, sending the auditory information to the brain (Pickles, 2015; Corey, 2009; Bulankina and Moser, 2012; Tritsch and Bergles, 2010; Hudspeth, 2008; Fisher et al., 2012).

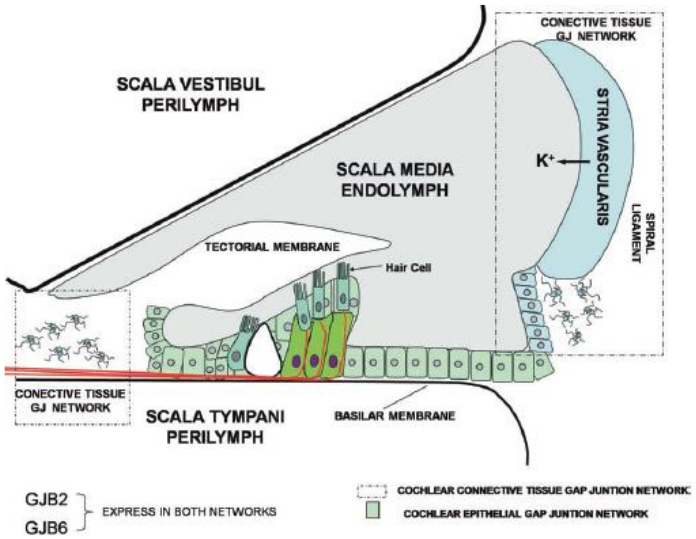

Figure 4. Distribution of GJCs in the cochlea. There are two main GJ networks in the cochlea: the network present in the connective tissue highlighted with doted lines, and the

GJ network in the epithelial tissue, which is the main focus of this research. (Martínez et al, 2009)

It has been proposed that supporting cells favor the exit of K^+ from the hair cells, recycling the K^+ and bringing it back to the endolymph, regulating the sensitivity of the ear and protecting it from hearing damage (Li–dong et al., 2008; Wan et al., 2013). There are several types of supporting cells: a) pillar cells, which form the Corti tunnel where the inner and outer hair cells rest; b) Deiters cells, which keep external hair cells supported and send a phalangeal process that extends obliquely between two or three of them; c) internal phalangeal cells, which support inner hair cells; d) Hensen cells, at the outer limit of the organ of Corti. They are also one of the places where the Cxs are located within the cochlea. Next to them, are the Böettcher and Claudius epithelial cells, which finish forming the network that regulates the ionic composition of extracellular fluids in the cochlea (Wan et al., 2013; Li–dong et al., 2008; Ramírez-Camacho et al., 2006). The supporting cells are those that have Cxs (Cx26, Cx30 and Cx31) (Jagger and Forge, 2015; Forge et al., 2003b), and have an important role in the regulation and recycling of K^+ and in homeostatic pH mechanisms, maintaining the sensitivity of hair cell (Li–dong et al., 2008; Wan et al., 2013; Ramírez-Camacho et al., 2006).

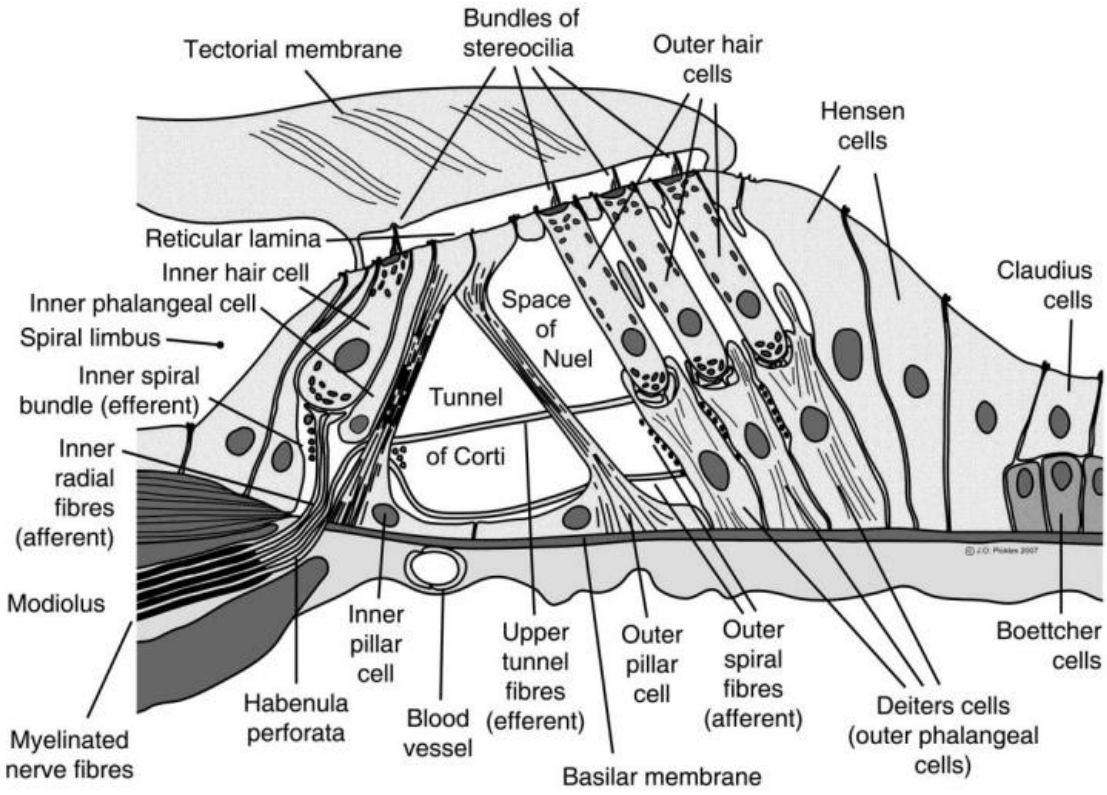

Figure 5. Cell types in the organ of Corti. Taken from (Pickles, 2015)

Purinergic signaling in the cochlea and its relationship with intracellular calcium

One of the molecules that can pass through HCs and GJ channels is adenosine triphosphate (ATP) (Baroja-Mazo et al., 2013; Kang et al., 2008; Verselis, 2017; Zhao et al., 2005), whose function is important for inner ear development (Leybaert et al., 2003; Taruno, 2018; Cotrina et al., 1998; Verselis, 2017). Adenosine triphosphate (ATP) is the main paracrine mediator in producing Ca^{2+} waves in the supporting and epithelial cells in the organ of Corti (Anselmi et al., 2008; Piazza et al., 2007). Extracellular signaling mediated by purinergic nucleotides has long been associated with sensory systems, where ATP functions as a co-transmitter or as a neuromodulator (Burnstock, 2006; Lee and Marcus, 2008; Thorne and Housley, 1996). ATP is one of the molecules that passes through HCs and GJCs (Baroja-Mazo

et al., 2013; Kang et al., 2008; Verselis, 2017; Zhao et al., 2005), so comprehend the effect of the Cx26 mutation on purinergic signaling is especially relevant for the understanding of syndromic deafness mechanism in the cochlea.

It has been described that all supporting cell types can respond to focal ATP applications by increasing intracellular Ca^{2+} transiently (Mammano, 2013). ATP activates purinergic receptors of the P2 type, which are subdivided into P2X and P2Y. P2X receptors correspond to ionotropic receptors, which when activated, allow the passage of ions directly, such as Ca^{2+}. P2Y receptors, on the other hand, correspond to G-protein coupled receptors, which when activated by ATP, generate a cascade of signals that can increase IP3 leading to an increase on $[Ca^{2+}]_i$. Therefore, the activation of purinergic receptors (either P2X or P2Y) generally increases $[Ca^{2+}]_i$, but with different kinetics and signaling pathways (Burnstock, 2006; Burnstock and Dale, 2015; Gossman and Zhao, 2008; Lee and Marcus, 2008; Piazza et al., 2007). In the cochlea of P15-P19 mice, still in developing stages and not fully active (Tritsch and Bergles, 2010; Bulankina and Moser, 2012), several types of P2X and P2Y have been observed through RT-PCR: P2X2, P2X3, P2X4, P2X6, P2Y1, P2Y2, P2Y6, P2Y12 and P2Y14 (Horváth et al., 2016).

ATP increases $[Ca^{2+}]_i$ in different cells of the organ of Corti, including hair cells and supporting cells (Ashmore and Ohmori, 1990; Sirko et al., 2019; Ceriani et al., 2019; Mammano, 2013). Extracellular ATP has the properties to be a fast-acting intercellular messenger: a) it is released in discrete quantities, b) it is bound to specific receptors in the membrane, generating specific signaling pathways and c) after it is released, there are ectoATPases that degrade it rapidly, to finish its action as a signaling molecule (Burnstock and Dale, 2015; Burnstock, 2006). Since ATP is one of the molecules that can pass through HCs and GJCs, and a gain-of-function in HCs has been observed in the syndromic deafness model, including an increase in ATP release and $[Ca^{2+}]_i$ concentration (García et al., 2015, 2016a), it is especially relevant to understand whether the increase in $[Ca^{2+}]_i$ produced by expression of syndromic deafness

mutations is ATP dependent. Ca^{2+} is strongly buffered in the extracellular environment, so the increase observed in syndromic deafness mutants could be due to an increase in IP3, and subsequent release of Ca^{2+} from intracellular reservoirs in supporting cells (Piazza et al., 2007).

It is important to mention that there are also mechanisms of ATP release that are Ca^{2+} dependent, such as exocytosis of ATP vesicles, and other independent ones, such as ATP release caused by change in cell volume, ABC transporters (which move different molecules through the plasma membrane using the energy of the hydrolysis of ATP), ATP synthase in the mitochondria and the aforementioned output of ATP through HC (Mammano, 2018; Lohman and Isakson, 2014; Verselis, 2017; Taruno, 2018). Also, if extracellular Ca^{2+} is decreased in supporting cells of the organ of Corti, the release of ATP increases (Zhao et al., 2005).

ATP can induce K^+ currents in Hensen cells, raise $[Ca^{2+}]_i$ in hair cells and stimulate their release from internal reservoirs in Deiters cells (but not Hensen cells) during development (Lee and Marcus, 2008). Subsequently, in rats between P14 and P21, ATP can stimulate the outflow of intracellular Ca^{2+} in Deiters, Hensen and pillar cells. In Deiters and Hensen cells, the mechanism occurs in a "Ca^{2+} induced, Ca^{2+} released" fashion, where Ca^{2+} is capable of generating more Ca^{2+} release from internal reservoirs; further suggesting that it works through several purinergic, ionotropic and metabotropic receptors (Horváth et al., 2016)

Problem Statement and hypothesis

However, and according to what was previously observed by our laboratory and others, KID Cx26S17F mutation would cause deregulation in the entire auditory circuitry. Until now, it is known that HCs conformed by Cx26S17F/Cx43 are hyperactive, while GJCs are not functional (García et al., 2015), but in the cochlea Cx26 is co-expressed with Cx30 instead of Cx43. The hyperactivity of the HC causes an increase in the output of ATP from the cells to the extracellular space, which could affect autocrine or paracrine signaling. Likewise, it is proposed that said ATP

could increase $[Ca^{2+}]_i$ in the cells, altering their survival or causing cell death in the organ of Corti. It is unknown how ATP could be causing physiological changes in the organ of Corti in KID model. Finally, until now we do not know if Cx26S17F is able to oligomerize with Cx30 and form HCs and GJCs with this Cx. The latter is fundamental since the previous background indicates that under WT condition Cx26 and Cx30 can form heteromeric channels (Forge et al., 2003a; Marziano et al., 2003; Ahmad et al., 2003; Sun et al., 2004), but it has not been studied whether Cx26 syndromic mutations affect this interaction, nor what is its effect on the function of HCs and GJCs formed by both Cxs.

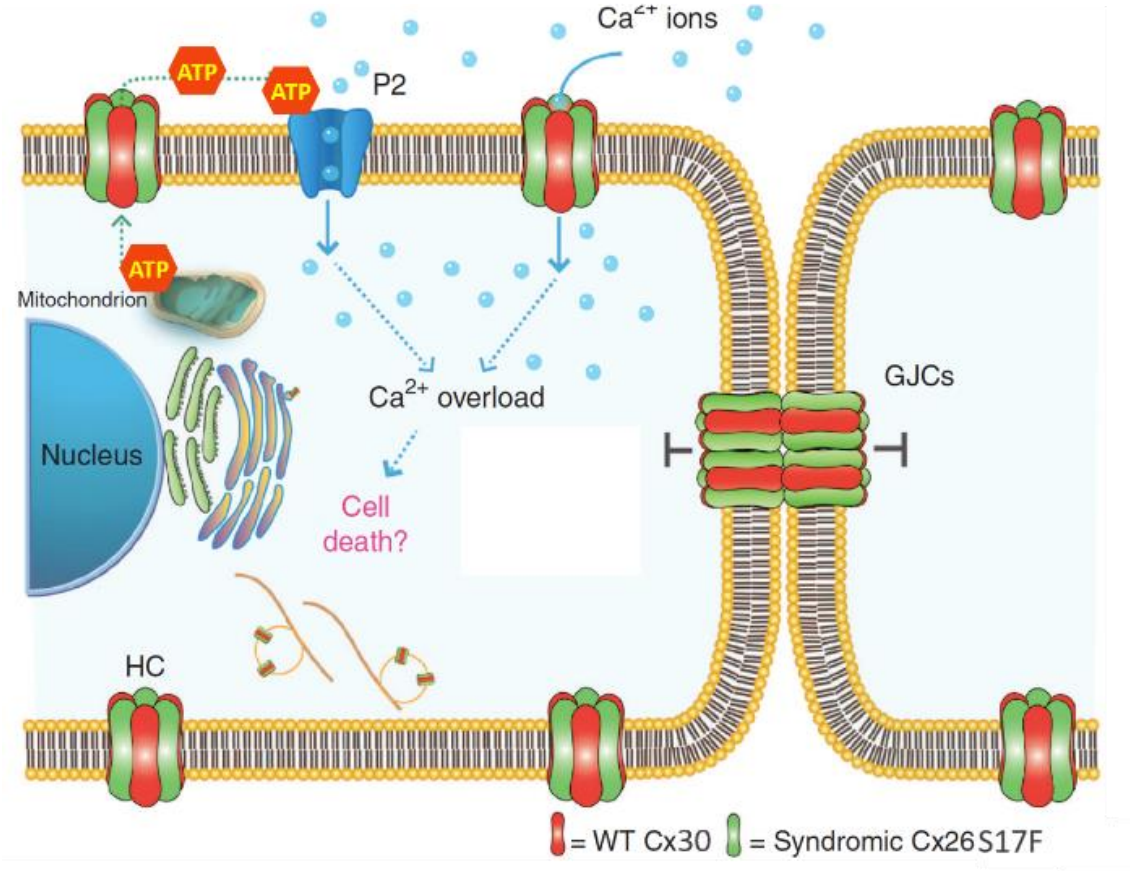

Figure 6. Working hypothesis model. The syndromic mutant Cx26S17F forms oligomers with Cx30 generating non-functional GJ and hyperactive HCs with reduced regulation by Ca^{2+}_e. ATP is released through hyperactive HC formed by Cx26S17F/ Cx30 leading to activation of P2

purinergic receptors (P2X or P2Y). The aberrant signal caused by hyperactive HC and non-functional GJC affects the viability of supporting and hair cells in the cochlea (Cartoon modified from García et al, 2015)

Considering the above, we have raised the following hypothesis:

The syndromic mutant Cx26S17F associates with Cx30 generating non-functional GJs and hyperactive HCs with reduced regulation of Ca^{2+}_e. Expression of these heteromeric HCs in cochlear tissue produce an increment in membrane permeability in the supporting cells and damage of hair cells in the organ of Corti.

To answer this hypothesis, the following aims were proposed:

1. **To identify the formation of heteromeric channels formed by Cx26S17 and Cx30 through functional and biochemical assays**
   1.1. To determine if Cx26S17F and Cx30 colocalize and interact, forming heteromeric HCs
   1.2. To study whether the Cx26S17F mutant forms hyperactive heteromeric HCs with Cx30.
   1.3. To study if Cx26S17F and Cx30 form functional heteromeric GJCs.

2. **To study functional properties of heteromeric HCs formed by Cx26S17F and Cx30, and the consequences of their expression on cellular viability.**
   2.1. To determine if the co-expression of Cx26S17F and Cx30 favor Ca^{2+} influx in HeLa cells and the sensitivity HCs to extracellular Ca^{2+}.
   2.2. To determine the effect of the mutant heteromeric HCs formed by Cx26S17F with Cx30 on cell viability, in co-transfected HeLa cells
   2.3. To evaluate purinergic evoked-Ca^{2+} signal by a puff of exogenous ATP in Hela cells co-transfected with Cx26S17F / Cx30 or with wild type Cxs.

3. **To study the formation of heteromeric HCs *ex vivo* formed by Cx26S17F and Cx30, the properties of these HCs, and the consequences of their expression in cochlear explants of knock-in Cx26S17F transgenic mice.**
   3.1 To study the cellular, sub-cellular distribution and possible colocalization of Cx26S17F and Cx30 in cochlear explants of $Cx26^{+/floxedS16F}$ mice treated with TAT-Cre and controls.

3.2 To characterize the functional state of HCs, GJCs, and the $[Ca^{2+}]_I$ response to ATP stimulation in the supporting cells of the organ of Corti in cochlear explants of $Cx26^{+/floxedS16F}$ animals treated with TAT-Cre and controls.

MATERIALS AND METHODS

I. HeLa cell culture.

1. Maintenance

HeLa cells were cultured in MEM medium (GIBCO), supplemented with 10% fetal bovine serum (FBS), Glutamax 1X (GIBCO), 1X non-essential amino acids (Invitrogen) and a mixture of Penicillin-Streptomycin 1X solution (Invitrogen) at 37°C, 5% CO_2 and 95% humidity; being maintained in 90 mm, 60 mm and / or 35 mm plates, with 10, 4 and 2 ml MEM, respectively. The culture medium was renewed every other day.

Stable Cell Lines

For stable expression, a cell line was maintained stably expressing Cx26WT without fluorescent tag. These cells were maintained with culture medium plus puromycin as a selection antibiotic at 30 µg/ml.

In order to check the expression of Cxs, in addition to the constant maintenance of antibiotics, periodic immunofluorescences were performed. Protein expression was confirmed in more than 85% of the cells (not shown).

Cell passages

Cell cultures at 70-80% confluence was passaged through trypsinization (Trypsin 1X, Invitrogen) and transferred to a conical tube with 4 ml of complete MEM and centrifuged for 3 minutes at 1800 rpm. The cell pellet was resuspended in 5 ml of complete MEM medium and subsequently seeded in culture plates at an appropriate confluence to obtain 60-70% confluence on the day of the experiment.

For immunocytochemistry experiments, dye uptake, calcium images, proximity ligation assay, FRAP and microinjections, the cells were seeded on glass covers 0.17 mm thick, 12 mm or 25 mm diameter, according to the experiment.

Cell conservation

For long-term maintenance of cell lines in the laboratory, freezing at -80°C in ultra-freezer, or preservation in liquid nitrogen was used. For this, cells were stored in FBS plus 10% DMSO, and subsequently deposited in cryotubes. The cryovials were stored in containers containing isobutanol, which allowed the freezing to be carried out slowly, thereby favoring the integrity of the cells. Once frozen, and after at least 24 h, the cells were changed to containers in the ultra-freezer, or to cryovial holders suitable for conservation in liquid nitrogen. When needed, the cells were quickly thawed and added to a tube with 10 ml of MEM + 10% FBS. The cell suspension was subsequently centrifuged at 1,800 or 2,000 rpm for 3 min, removing the supernatant and the pellet of cells resuspended in 4 ml of fresh medium, to be completely seeded on a 60 mm plate and subsequently maintained as explained previously.

2. Transfections

Plasmid amplification and purification

To express the different Cxs in HeLa cells, which naturally lack Cxs, except Cx45 in minimal amounts, plasmids were used where cDNAs of each of the connexins used were cloned. For the expression of Cx26S17F, the vector pcDNA3.1 CT-GFP-TOPO (Invitrogen) was used, which also contains the green fluorescent protein (GFP) gene, favoring visualization of cells that expressed the mutated Cx.

For Cx30, a plasmid with the connexin cloned in a vector containing msfGFP, kindly donated by Dr. David Spray to the Addgene reservoir (# 69019), was acquired and subsequently cleaved to clone into the pNT-mCherry vector (Clonetech, donated by Dr. María Estela Andrés),

which allowed the visualization of Cx30 in two colors, according to the experiment to be carried out.

For Cx26WT the cDNA cloned in the pcDNA3.1 vector CT-GFP-TOPO (Invitrogen) was available; in addition to Hela cells with stable expression of Cx26WT, without fluorescent tag mentioned previously (see section Stable Cell Lines).

The vectors were amplified by the bacteria transformation method. Briefly, competent *E. coli* XL-1 Blue bacteria were transformed by adding 100 ng of plasmidial DNA, held on ice for 30 minutes, then given a thermal shock of 42°C for 50 s and subsequently incubated for 2 min on ice. Once transformed, the transformed bacteria were recovered in SOC medium for 1 h at 37°C, stirring. Subsequently, it was seeded on agar plates containing antibiotic of suitable selection (kanamycin for pNT-mCherry and ampicillin for the other plasmids). On the morning of the next day, colonies were selected and seeded in 3 ml of LB with antibiotic, kept under stirring and at 37°C until the end of the day. Subsequently, an aliquot was taken and seeded in 15 ml of LB with antibiotic, which was incubated overnight with constant shacking (220 rpm) at 37°C. The next morning, plasmidial DNA extraction was performed using the E.Z.N.A. Endo-Free Plasmid Mini Kit II (Omega Bio-Tek), according to the manufacturer's instructions. Plasmidial DNA was quantified using a Helios spectrophotometer at λ 260nm, and its purity was evaluated by measuring the ratio of absorbance obtained for DNA (λ 260nm) and proteins (λ 280nm), requiring an optimal ratio of 1.7 - 1.9 for an optimal cDNA. Subsequent sequencing of plasmid cDNA was made to verify correct DNA sequences.

Transient transfections

For the temporary expression of the different Cxs in HeLa cells, transient transfections were used by the protocol described for Lipofectamine 2000 (Invitrogen), according to the manufacturer's instructions. Briefly, 1 µg of pNTCx30-mCherry cDNA is added to 50 µl of Opti-mem serum-free medium (Thermo-Fisher). In another tube, Lipofectamine 2000 is added in a 1:

3 (w/v) ratio with the cDNA to be used, i.e. 3 µl for 1µg DNA. For double transfections with Cx26S17F and Cx30, 1 µg of Cx26S17F and 0.7 µg of Cx30 were used; plus 5 µl of Lipofectamine. Both tubes are incubated for 5 min at room temperature, then transfer the mixture of Optimem with Lipofectamine to the tube with cDNA, vigorously homogenized, and then the mixture was incubated at 37 °C for 20 minutes, so that liposomes containing the cDNA could be generated. During that incubation time, the culture medium was changed to 2 ml of fresh Optimem medium, and subsequently the plates with the cells were returned to the incubator. After 20 min, the liposome mixture with cDNA was added to the cells, and the plates were incubated for 2 h and 15 minutes. Subsequently, the Optimem with liposomes was removed, washed with 2 ml of fresh MEM + 10% SFB, removed and then changed to 4 ml of MEM + 10% SFB medium, to ensure that Lipofectamine was not left in the culture medium. The experiments were performed the next morning.

3. Protein distribution and quantification

Immunofluorescence

The cells were seeded on glass coverslips and fixed in a solution of PBS-4% paraformaldehyde for 30 min. Subsequently, cells were permeabilized with PBS-1% Triton X-100 for 30 minutes. After time, the cells were incubated with blocking solution for 30 minutes (PBS 1X-Triton + 2% bovine serum albumin, BSA) to block non-specific immunogenic sites. After the previous step the cells were incubated with primary antibody (ies) (mouse αCx26 1:200, Lifetech; rabbit αCx30, Lifetech), diluted in blocking solution overnight at 4° C, in a humidity chamber. The next day, the cells were washed with permeabilizing solution, 6 times every 5 min to remove unbound antibody and subsequently incubated with corresponding secondary antibody (ies) (αMouse 1:1000, Jackson InmunoResearch; αRabbit 1:1000, Jackson InmunoResearch), diluted in blocking solution, for one hour at room temperature in the dark. The excess of secondary antibody was washed 2 times for 5 min with PBS-Triton X-100, then

labeled cell nuclei with DAPI diluted in PBS, in a humid chamber, protected from light and at room temperature for 10 minutes. The excess was removed again with 4 5-min washes in PBS-Triton, and then a short 2-min wash in PBS without detergent. Finally, the coverslips were immersed in distilled water to remove excess of salts and mounted on a slide with 5 µl of mounting medium (Fluoromont G). The cells were examined with a Nikon Eclipse C1-Plus confocal microscope and EZ-C1 software and analyzed with the FIJI software.

Connexin expression intensities

To quantify intensity of expression of each Cx, ten ROIs of the same area were randomly distributed in the non-appositional membrane area, ten in intracellular space and ten in the apposition zone between two cells. Expression of each Cx was quantified in each optical section of 1 µm of confocal stack images using NIS elements software (NIKON, Japan). Statistical analyzes were made in Graph Pad Prism software.

Colocalization index

To evaluate the colocalization strength of Cx30 with Cx26WT or Cx26S17F, Pearson and Manders´ coefficients were calculated by cellular area in images showing HeLa cells that co-expressed both Cxs, using NIS elements software (NIKON, Japan). Ten ROIs of the same size were randomly distributed in 1 µm optical section in z axis for each cellular compartment, membrane, cytoplasm and the cellular appositional zone (GJ Zone). ROIs that did not show expression of both Cxs, were not considered in this quantification. Threshold of every image was set visually. Statistical analyzes were made in Graph Pad Prism software.

Determination of protein interaction by proximity ligation assay (Duolink)

To evaluate the protein interaction, the Duolink methodology was used according to what the manufacturer indicated (Sigma-Aldrich). Briefly, the technique is based on detecting the interaction of two previously fixed proteins, which must be at a distance less than 40 nm to be

detected. The two proteins of interest were detected using primary antibodies generated in two different hosts (i.e., anti-Cx26 obtained from mouse cells and anti-Cx30, from rabbit) and subsequently incubated with secondary antibodies conjugated with the PLA (Proximity Ligation Assay) probe, one that carries a DNA strand and the other with the complementary antisense strand. Subsequently, the sample was incubated with a ligase, which allowed the PLA probes to hybridize if they were close enough. Then, the sample was incubated with an amplification solution, which consists of cy3-conjugated dNTPs and a polymerase, which will generate an amplification in circles, generating a red fluorescent concatemer. Finally, the samples were assembled using the mounting medium of the same kit, which contains DAPI to counteract the nuclei of the cells. The marks obtained were detected in a Nikon Eclipse C1-Plus confocal microscope and EZ-C1 software and analyzed with the FIJI software.

4. Functional analyses of connexin channels

Determination of the functional state of connexin hemichannels (Dye uptake)

Parental HeLa (HP) or stable expression cells were grown on 25mm diameter coverslips and maintained with MEM medium, as previously described. The day before registration, in the afternoon, transient transfections were performed for the expression of Cx26S17F and Cx30. Records were made at the next morning after transfection.

The culture medium was removed and changed to Hanks recording solution with basal Ca^{2+} (10 mM HEPES, 140 mM NaCl, 5.3 mM KCl, 0.1% glucose, 0.34 mM Na_2HPO_4, 1.26 mM $CaCl_2$, 0.5 mM $MgCl_2$; pH 7.4), or divalent cation-free Hanks (named Ca^{2+}-free Hanks). Both media also contained the YOPRO DNA intercalants (200 nM), ethidium bromide (5 µM) and/or DAPI (1 or 5 µM). Fluorescence microscope pictures were taken in time lapse mode, every 1 minute for 20 min in the basal condition (with extracellular Ca^{2+}), 10 min on Ca^{2+}-free Hanks and then 10 min in the presence of the 100 µM lanthanum or carbenoxolone (CBX) 50 µM. At the beginning and at the end of the recording, phase contrast photographs were taken to assess cell

morphology. These experiments were performed in a NIKON Eclipse TE2000U microscope, with the NIS Elements software and later with the FIJI image analysis software. The analysis of data obtained was performed in Excel and Graph Pad Prism 6.

Determination of the functional state of Gap Junctions

Fluorescence recovery after photobleaching (FRAP)

To evaluate the function of GJs fluorescence recovery after photobleaching (FRAP) approach was used in Hela cells expressing the different connexins. For this, cells were loaded with 1.6 µM calcein-AM (Sigma-Aldrich) dissolved in Hanks with Ca^{2+}, for 30 minutes at 37°C, protected from light. After this time, the excess of calcein was removed with 2 washes of 5 min, with Hanks with Ca^{2+}, protected from light. Then, using 100% power of the confocal microscope laser, fluorescence of one of the cells coupled through GJ was bleached, and subsequently, using the 5% power laser, pictures were taken every 1 min for 10 min total. This technique quantifies the passage of new calcein through GJ over time, from the neighboring coupled cell to the bleached cell, thereby allowing to evaluate the recovery rate of fluorescence over time. These experiments were performed in the Nikon Eclipse C1-Plus confocal microscope and EZ-C1 software and subsequently analyzed with the FIJI software. Data analysis was performed in Excel and Graph Pad Prism 6.

Dye coupling

The function of GJ was studied by diffusion assays of Yellow Lucifer dyes (LY, PM 457, net charge -2, Sigma) between coupled neighboring cells. To do this, parental or transfected HeLa cells grown on glass coverslips were microinjected with a mixture of 4% of LY. Microinjections were performed using a Fentotip II microcapillary (Eppendorf) glass (0.5 µm internal diameter and 0.7 µm external diameter) and the Eppendorf automatic injection system (Femtojet pressure generator and micromanipulator, Inject Man). The cells were injected for 5 seconds, at an

internal capillary pressure of 50-150 hpa. Microinjections were performed in an inverted fluorescence microscope (Nikon Eclipse TE2000U), observing directly the fluorescence of AL. The samples were observed in Nikon Eclipse TE2000U inverted microscope, with Nikon ACT2U software.

5. Ca^{2+} imaging in HeLa cells

ATP induced Ca^{2+} response with Fluo-4

The calcium response to the ATP stimulus was evaluated using the Fluo-4 probe. Briefly, Hela cells expressing the different Cxs under study seeded in 25 mm coverslips were loaded with 3 µM of Fluo-4 dissolved in MEM medium without serum, for 30 min at 37°C. Prior to incubation, Fluo-4 was incubated with pluronic acid (20% in DMSO) in a 1: 1 ratio, for 5 min at room temperature, which favored the incorporation and dispersion of the probe into the cell. After the time, the excess of Fluo-4 was removed with 3 washes of 2 minutes each with Hanks with Ca^{2+}. Then, the coverslip with loaded cells was mounted in the recording chamber and secured to the microscope stage, so as not to lose focus nor field of interest. The visualization of the Fluo-4 was carried out with an argon laser 488, coupled to the microscope. Loaded cells were covered with 1 ml of recording medium (Hanks with or without Ca^{2+}, depending on the experiment) and pictures were taken every 1 second for approximately 2 min, and then 100 µM ATP prepared on the day of the experiment was added. Ca^{2+} response was recorded until the signal returned to baseline levels, or until 8 minutes of total recording. The records were made in a Nikon Eclipse TE2000U microscope, with the NIS Elements software, and subsequently analyzed with the FIJI software. The subsequent data analysis was performed in Excel and Graph Pad Prism 6.

Intracellular Ca^{2+} signal measurement with Fura-2

Basal intracellular Ca^{2+} concentration was evaluated using the Fura-2 double excitation probe (Invitrogen). HeLa cells seeded on 25 mm coverslips expressing the different connexins under study, were loaded with 5 µM Fura-2 diluted in serum-free medium, for 30 minutes at 37°C, and

then washed two times with Hanks solution. Coverslips were placed in the recording chamber filled with 1 ml of Hanks solution and then mounted on the stage adapter in the microscope. Using epifluorescence light, Ca^{2+} response was evaluated at two wavelengths, 340 nm, which is dependent on the binding of the probe to Ca^{2+} and at 380 nm, which is independent, allowing quantification of $[Ca^{2+}]_I$ without background interference. Extracellular $[Ca^{2+}]_e$ was changed every 3 min, from nominal Ca^{2+}-free solution, to 10 µM, 100 µM, 500 µM, 1 mM, 1.5 mM or 1.5 mM plus 10 µM ionomycin. $[Ca^{2+}]_I$ rate in every $[Ca^{2+}]_e$ was quantified (slopes of incorporation and maximum concentration) using NIS elements software and posterior statistical analysis was made in Excel and Graph Pad Prism.

6. Cell death quantification

Annexin V/Propidium iodide assay

Cell death was quantified in HeLa cells expressing different combination of Cxs using Annexin V/Propidium iodide assay (BioLegend ®), according to several modifications to manufacturer's instructions, as the product is optimized for flow cytometry. Briefly, cells seeded in 12 mm coverslips were transfected as described previously and cell death was evaluated at the next morning. Cells were washed twice with RT PBS and 400 ul Annexin V binding buffer were added to 35 mm plate, plus 5 µl of Pacific Blue™ Annexin V and 10 µl of Propidium iodide solution. Solutions were homogenized and cells were incubated for 15 min at RT, protected from light. After incubation time, cells were washed twice with fresh PBS and fixed with 4% PFA for 30 min at RT, protected from light. After fixation, cells were washed and mounted with anti-fade mounting medium Fluoromont-G and observed in Nikon Eclipse C1-Plus confocal microscope and EZ-C1 software and subsequently analyzed with the FIJI software. Data analysis was performed in Excel and Graph Pad Prism 6.

II. Cochlear explant cultures.

1. Maintenance

Cochleae of C57/BL mice were obtained according to the protocols approved by the University's bioethics committee. Briefly, P7 animals (7 days post-natal) were sacrificed by decapitation. Both cochleae were removed by skull dissection and brain removal. Both inner ears located in the temporal bone were isolated, and both cochleae were extracted according to Parker et al, 2010. Briefly, once separated from the spiral ligament, the sensory epithelium was transferred to a plate with medium (Dulbecco's Modified Eagle Medium, supplemented with 10% FBS), ensuring that the tissue adheres to the 12 or 25 mm coverslip, previously treated with Geltrex (Gibco) and incubated for 24 hours at 37°C with 5% CO_2 and 95% humidity. For immunofluorescence, the tissue will be immediately fixed in PBS with 4% PFA for 1 h at room temperature, washed with PBS and left in cold PBS at 4°C until use. For uptake of tracers, FRAP and Calcium imaging, the DMEM medium was removed the next day and washed with Hanks medium with Ca^{2+} to remove excess dye from the culture medium (phenol red). Once clean, the baseline conditions are established in Hanks medium with Ca^{2+} and then incubated with the tracers, as described for each record previously.

Immunofluorescence in cochlear explants

1 DIV cochlear explants were fixed in a solution of PBS-4% PFA for 1 to 3 h at room temperature. Subsequently, the explants were permeabilized with 1X PBS with 1% Triton X-100 for 30 minutes. After time, the explants were incubated with 1 h blocking solution (1X-Triton PBS + 2% BSA; + 2% normal goat serum, NGS) to block non-specific immunogenic sites. Then, the explants were incubated with primary antibody (ies) (mouse αCx26 1:100, Lifetech; rabbit αCx30 1:100, Lifetech), diluted in blocking solution, overnight at 4°C, in a humid chamber. The following day, the explants were washed with permeabilizing solution, 6 times every 5 min to remove

unbound primary antibody and subsequently incubated with corresponding secondary antibody (ies) (αMouse 1:500, Jackson InmunoResearch; αRabbit 1:500, Jackson InmunoResearch), diluted in blocking solution, by 2 h at room temperature, protected from light. The excess of secondary antibody was washed 2 times for 5 min with PBS with Triton X-100, then cell nuclei were labeled with DAPI diluted in PBS, in a humid chamber, protected from light and at room temperature for 10 min. The excess was removed again with 4 5-min washes in PBS-Triton, and then a short 2-min wash in PBS without detergent. Finally, the coverslips were immersed in distilled water to remove excess salts and mounted with 30 µl of mounting medium (Fluoromont G), on a slide with nail polish rings previously drawn, so that they were generated small wells that facilitated the assembly of the cochlea, without damaging its structure. The tissues were examined with a Nikon Eclipse C1-Plus confocal microscope and EZ-C1 software and analyzed with the FIJI software.

Phalloidin assay to identify hair cell stereocilia

Cultured cochleae were incubated with phalloidin-Texas Red (Sigma) dissolved in PBS for 30 min at room temperature, protected from light. After the incubation time finished, the tissue was washed three times per 5 minutes with PBS and fixed with 4% PFA per 30 min. Fixed explants were washed again three times per 5 minutes with PBS, and then stored at 4°C until imaging. Stained stereocilia were examined with a Nikon Eclipse C1-Plus confocal microscope and EZ-C1 software and analyzed with the FIJI software.

Determination of the functional status of HC formed by endogenous connexins in cochlear explants (Dye uptake)

Cochlear explants were grown on coverslips 25 mm in diameter and maintained with DMEM medium, as previously described. Records were made the next morning.

For this, the culture medium was removed and changed by Hanks recording solution with normal Ca^{2+} (10 mM HEPES, 140 mM NaCl, 5.3 mM KCl, 0.1% glucose, 0.34 mM

Na_2HPO_4, 1.26 mM $CaCl_2$, 0.5 mM $MgCl_2$; pH 7.4), or Ca^{2+}-free Hanks. Both media also contained the YOPRO DNA intercalants (200 nM), ethidium bromide (5 µM) and/or DAPI (1 or 5 µM). Fluorescence microscope pictures were taken in time lapse mode, every 30 seconds for 10 minutes in the basal condition (with extracellular Ca^{2+}), 5 min in nominal Ca^{2+}-free solution and then 5 min in the presence of the 100 µM carbenoxolone (CBX). At the beginning and at the end of the recording, phase contrast photographs were taken to assess cell morphology. These experiments were performed in a NIKON Eclipse TE2000U microscope, with the NIS Elements software and later with the FIJI image analysis software. The analysis of data obtained was performed in Excel and Graph Pad Prism 6.

2. Ca^{2+} imaging in cochlear explants

The Ca^{2+} signal response to the ATP stimulus was evaluated using the Fluo-4 probe. Briefly, cochlear explants were grown in 25 mm coverslips and maintained 1 DIV. The next morning, they were loaded with 7.7 µM of Fluo-4 dissolved in MEM medium without serum, for 30 min at 37°C. Prior to incubation, Fluo-4 was incubated with pluronic acid (20% in DMSO) in a 1: 1 ratio, for 5 minutes at room temperature, which favored the incorporation and dispersion of the probe into the cells in the tissue. After the time, the excess of Fluo-4 was removed with 3 washes of 2 min each with Hanks´ solution containing Ca^{2+}. Then, the coverslip with loaded cochlea was mounted in the recording chamber and secured to the microscope stage, so as not to lose focus nor field of interest. The visualization of the Fluo-4 was carried out with a xenon lamp coupled to the microscope, at 488 nm. They were covered with 1 ml of recording medium (Hanks with or without Ca^{2+}, according to the experiment) and pictures were taken every 1 s for approximately 2 min, and then 100 µM ATP prepared on the day of the experiment was added. The calcium response was recorded until the signal returned to baseline levels, or until 8 min of recording. The records were made in a Nikon Eclipse TE2000U microscope, with the NIS Elements software, and subsequently analyzed with the FIJI software. The subsequent data analysis was performed in Excel and Graph Pad Prism 6

III. Study design and statistical analysis

Sample sizes were not statistically pre-determined, but it was estimated based on previous studies, and considering that in vitro experiments were used in transfected cells that can be considered as technical replicates. Despite of that, for every method, experiments were realized in 4 or more different independent cultures and in different days and more than 4 covers per day of experiment were considered. Every double transfected cell in the microscopy field of view was analyzed. For cochlear explants, only 2 animals were used per condition, and 120 ROIs positioned around the nuclei area were analyzed in different cell types. Researcher was not blinded during the experiments, but the experiments were analyzed randomly.

Results are expressed as means ± SEM. For most results data were normally distributed according to Kolmogorov-Smirnov test. In some experiments outliers were removed after its identification by using the ROUT Method (GraphPad Software Inc, La Jolla, CA, USA) using Q= 1%, even it was applied to all experimental data. Statistical comparisons were performed using two-tailed t-test comparison between groups, and results were expressed in the graphs as * $p < 0.05$; ** $p < 0.005$, *** $p<0.001$; **** $p<0.0001$ accordingly. When data was not distributed normally, non-parametric t-test was used (Mann-Whitney test). All statistical analyses were performed using GraphPad Prism 6 software (GraphPad Software Inc, La Jolla, CA, USA).

RESULTS

I.- Syndromic deafness mutation S17F does not affect the compatibility of Cx26 to interact with Cx30.

I.1. Mutant Cx26S17F colocalizes with Cx30 and change the distribution of heteromeric hemichannels in HeLa cells

As mentioned previously, Cx26 form heteromeric channels with Cx30 but not with Cx43. However, a previous report showed that mutation S17F in Cx26 changes the oligomerization compatibility of this protein allowing it an aberrant interaction between mutant Cx26S17F with Cx43, producing malfunctioning heteromeric channels (García et al., 2015). Therefore, we asked whether this mutation could produce the opposite effects with respect to the hetero oligomerization with Cx30, in other words, oligomerization incompatibility between Cx26S17F and Cx30. To answer this question, two strategies in HeLa cells co-transfected with Cx26S17F and Cx30 were used. First, using immunofluorescence and subsequent co-localization analysis, co-localization properties between mutant Cx26S17F and Cx30 were described; and second, whether there is intermolecular interaction between these proteins by proximity ligation assay (PLA, DuoLink ®).

The expression of Cxs was assessed by double immunofluorescence in HeLa cells co-transfected with Cx30 and Cx26 WT (HeLa Cx26WT/Cx30) or with Cx30 and mutated Cx26S17F (HeLa Cx26S7F/Cx30) (Figure 7, panels A and B) and visualized by confocal microscopy. We observed that in both conditions Cx26WT and Cx26S17F co-localize with Cx30. Whereas Cx26WT co-localize perfectly with Cx30 in GJ plaques (Figure 7, panel A), Cx26S17F co-localize with Cx30 mainly in intracellular compartments, with few signals observed in the apposition area, suggesting that mutant Cx26S17F keeps Cx30 in intracellular compartments (Figure 7, panel B). The observation that mutant Cx26S17F and Cx30 co-localize mainly in the

intracellular space, while only a small fraction of them goes to the apposition zone forming GJ, suggest an altered traffic of the vesicles containing both Cxs to the appositional membranes. However, as described before, despite of the suggested abnormal vesicle traffic, it is possible to observe small GJ plaques between two adjoined cells (Figure 7, panel B1).

The high level of co-localization was further confirmed by Pearson correlation index (Figure 7, panel C) for both connexin combinations in every cellular area and did not show statistical difference between Cx26WT or Cx26S17F with Cx30. Pearson values for Cx26WT/Cx30 and Cx26S17F/Cx30 were: in the membrane 0.75 and 0.69 (p=0.5727); intracellular space 0.64 and 0.69 (p=0.5762) and appositional zone 0.69 and 0.77 (p=0.4249), respectively. For details, see Table 1.

To determine if expression of mutant or wild type Cx26 affect the proportion of Cx30 (or vice versa) within a particular sub-cellular area, we decided to apply Manders co-occurrence coefficient. Manders coefficients were calculated using signal of Cx26S17F or Cx26WT over Cx30) as M1 (Figure 7, panel D) and Cx30 over Cx26WT or Cx26S17F as M2 (Figure 7, panel E). Per subcellular area, Manders´ coefficient (M1) for Cx26WT/Cx30 and Cx26S17F/Cx30 are: membrane 1.0 and 0.99; intracellular space 1.0 and 0.97; and gap junction, 1.0 and 0.98, respectively (See Table 2). When co-occurrence of Cx30 over Cx26WT or Cx26S17F are compared (M2), results obtained did not show statistical significances for the signals in the GJ zone (0.98 and 0.99, p=0.162), but in the membrane (p= 0.0134, mean 0.92 and 0.99) and intercellular compartment we observed a small statistical significance between WT and mutant heteromeric channels (0.96 and 0.99, p=0.0204) consistent with the observation that the mutant Cx26S17F kept Cx30 in the intracellular space, which increase the signal for Cx30 in the intracellular compartment (See Table 3).

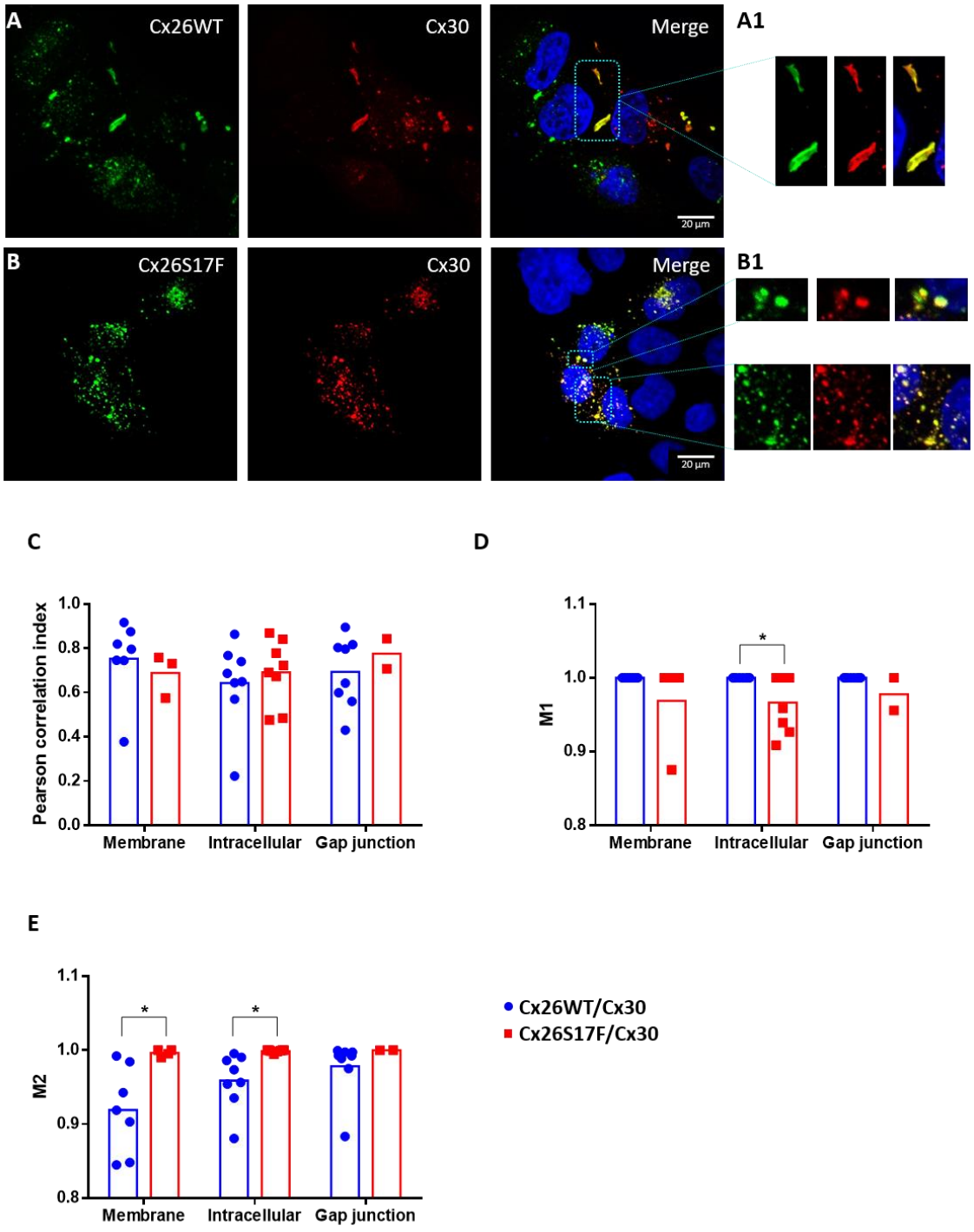
A
Cx26WT
Cx30
Merge
A1
20 µm
B
Cx26S17F
Cx30
Merge
B1
20 µm
C
Pearson correlation index
1.0
0.8
0.6
0.4
0.2
0.0
Membrane
Intracellular
Gap junction
D
M1
1.1
1.0
0.9
0.8
*
Membrane
Intracellular
Gap junction
E
M2
1.1
1.0
0.9
0.8
*
*
Membrane
Intracellular
Gap junction
Cx26WT/Cx30
Cx26S17F/Cx30

Previous page **Figure 7. Mutant Cx26S17F colocalizes with Cx30 and change the distribution of heteromeric hemichannels in HeLa cells**

Co-immunofluorescent detection of wild type or mutant Cx26 and Cx30 in HeLa cells co-expressing Cx30 with Cx26 (A) or with deafness mutant Cx26S17F (B). A) Strong co-localization between wild type Cx26 (green) and Cx30 (red) in GJ plaques observed at appositional membranes between two contacting cells. A1) A magnifying view of GJ plaques observed in A. B) Strong co-localization of Cx30 with mutant Cx26S17F was observed mainly in intracellular compartments, and occasionally with few small plaques in the appositional zone. B1) upper and lower panels show magnifying view of small GJ plaques and intracellular co-localization between Cx30 and mutant Cx26S17F, respectively. C) Average and single values of Pearson correlation index for co-localization between Cx26 WT and Cx30 (blue) or between mutant Cx26S17F and Cx30 (red) by specific sub cellular area. Mean values, SEM and p values are in Table 1. D, E) Manders coefficients were calculated using signal of Cx26S17F or Cx26 over Cx30 as M1 (D) and Cx30 over Cx26 or Cx26S17F as M2 (E). * $p < 0.05$. Mean values, SEM and p values are in Table 2 for M1 and Table 3 for M2.

Table 1. Correlation index Pearson values, SEM and p value of Cx26WT/Cx30 and Cx26S17F/Cx30 per subcellular area

Cx26 WT/Cx30 vs Cx26S17F/Cx30	Mean Cx26WT/Cx30±SEM	Mean Cx26S17F/Cx30±SEM	p value
Mb	0.75 ± 0.07 N=7	0.69 ± 0.06 N=3	0.5727
Intracellular	0.64 ± 0.07 N=8	0.69 ± 0.05 N=8	0.5768
GJ	0.69 ± 0.06 N=8	0.78 ± 0.07 N=2	0.4249

Table 2. Correlation index Manders 1 (Cx26 WT or Cx26S17F, green; over Cx30, red), SEM and p value of Cx26WT/Cx30 and Cx26S17F/Cx30 per subcellular area

Cx26 WT/Cx30 vs Cx26S17F/Cx30	Mean Cx26WT/Cx30±SEM	Mean Cx26S17F/Cx30±SEM	p value
Mb	1.00 ± 0.0 N=7	0.97 ± 0.03 N=4	0.391
Intracellular	1.00 ± 0.0 N=8	0.97 ± 0.01 N=8	0.043
GJ	1.00 ± 0.0 N=8	0.98 ± 0.02 N=2	0.5

Table 3. Correlation index Manders 2 (Cx30, red, over Cx26 WT or Cx26S17F, green), SEM and p value of Cx26WT/Cx30 and Cx26S17F/Cx30 per subcellular area

Cx26 WT/Cx30 vs Cx26S17F/Cx30	Mean Cx26WT/Cx30±SEM	Mean Cx26S17F/Cx30±SEM	p value
Mb	0.92 ± 0.02 N=7	0.99 ± 0.002 N=4	0.0134
Intracellular	0.99 ± 0.0006 N=8	0.99 ± 0.0006 N=8	0.0204
GJ	0.98 ± 0.01 N=8	0.99 ± 0.0001 N=2	0.1626

I.2. Expression of mutant Cx26S17F significantly reduce localization of Cx30 in the appositional zone

To confirm previous observation that mutant Cx26S17F affects the subcellular localization of Cx30, we quantified the expression intensity of different Cxs in specific sub-cellular areas of co-transfected HeLa cells.

As a control, we determined the level of Cx30, Cx26WT or mutant Cx26S17F in different sub-cellular areas in HeLa cells expressing only one type of Cx (homomeric configuration). In this configuration (Figure 8, panel A), Cx30 expressed in HeLa cells remains mainly in the apposition zone (~65% of total), forming GJ plaques, a minor part remains in the intracellular space (~30%) and only a small fraction less than 10% remains in the non-appositional cell membrane, possibly forming free HCs. In the case of Cx26 WT, this protein remains equally distributed in the intracellular space and gap junction plaques (48% in each localization), and less than 10% stays in the non-appositional membrane. Remarkably, as previously reported, we found that homomeric Cx26S17F stays mainly in the intracellular space (more than 85%), confirming that mutation critically affects the traffic the mutant Cx (See Table 4).

On the other hand, the co-expression of mutant Cx26S17F with Cx30 changes the distribution of mutant heteromeric channels, compared to WT channels. Each connexin in WT heteromeric channel (Cx26WT/Cx30, Figure 8, panel B) remains on the same proportion (~40%, see Table 5 for details) in the apposition zone forming GJ plaques and in the intracellular space

as observed in homomeric WT configuration, and ~20% of total protein expression remains in the non-appositional membrane forming free HCs. However, in mutant heteromeric channels (Cx26S17F/Cx30, Figure 8, panel C) each Cx remains mostly in the intracellular space (See Table 6). In fact, Cx26S17F sequesters and retain about ~60% of Cx30 in the intracellular space and reduce the signal of Cx30 in the appositional zone (GJ zone) to less than 20% (Figure 8, panel D. See Table 7 for details).

We also observed that mutant heteromeric HC occasionally form few GJ plaques, which are smaller than the WT heteromeric GJ plaques. To quantify this observation, we determined the GJ size index, by measuring the length of the gap junction plaque of each Cx signal normalized by the length of the appositional zone between two cells, for every optical section of 1 µm thick. Figure 8, panel E shows the GJ size index in each condition, homomeric Cx26 WT and Cx30 form large GJ plaques that cover about the 60% of the appositional zone (63.64 ± 4.53% and 59.04 ± 2.97%, respectively); while homomeric Cx26S17F did not present detectable GJ plaques or they were too small to measure. GJ size index for heteromeric GJ plaques formed by Cx26WT and Cx30 were significantly larger than the formed by Cx26S17F and Cx30, covering 48.65 ± 5.49% and 24.33 ± 4.28% of the appositional zone, respectively (statistical significance p=0.0022). For details, see Table 8.

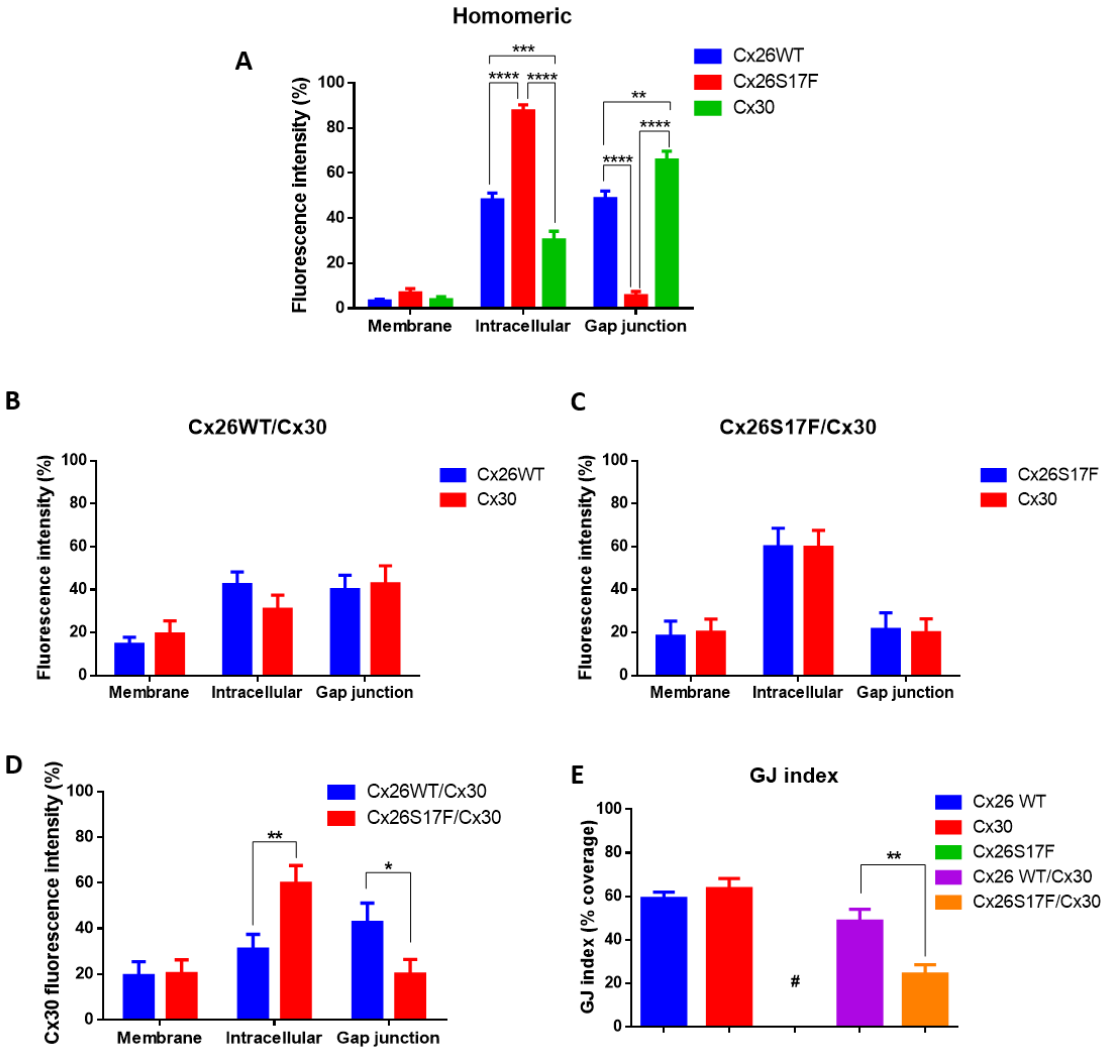

Figure 8. Expression of mutant Cx26S17F significantly reduce localization of Cx30 in the appositional zone

Relative expression of each Cx by subcellular area in cells expressing only one Cx type (A) or cells co-expressing two different Cxs (B, C, D). (A) Cx26WT (blue) is detected mainly in the intercellular space and GJ plaques at the appositional zone and a small proportion in non-appositional membrane. Cx26S17F (red) is observed mainly in the intracellular area with reduced signal in the non-appositional membrane and GJ plaques. Cx30 (green) is located mainly in GJ zone (65.77 + 3.95 %), and less in the intracellular and non-appositional membrane areas. Mean values, SEM and p values are in table 4. B) In cells co-expressing Cx26WT and Cx30, both Cxs were expressed almost in the same proportion in the three cellular compartments. Mean values, SEM and p values are in

table 5. C) In cell co-expressing Cx26S17F and Cx30 both Cxs were expressed almost in identical proportions in each cellular compartment. However, both proteins were detected mainly in intracellular compartments space, while less expression is observed appositional and non-appositional membrane. Mean values, SEM and p values are in table 6. D) Cx30 change its localization when co-expressed with Cx26 or Cx26S17F, indicating that mutant Cx26S17F retain Cx30 in the intracellular space, and only a small proportion goes to the membrane. Mean values, SEM and p values are in table 7. E) Extension of coverage for GJ plaques over the apposition zone (GJ size index) between neighbor cells expressing one Cx type or co-expressing Cx30 with Cx26WT or with Cx26S17F. Cx26WT and Cx30 formed large GJ plaques that covered 59.04 $\pm$ 2.97%, and 63,64 + 4.53% of the appositional zone, respectively. Cx26S17F did not form detectable GJ plaques in HeLa cells. Heteromeric Cx26WT/Cx30 GJ plaques covered 48.65 $\pm$ 5.49% and mutant heteromeric Cx26S17F/Cx30 only covered 24.33 + 4.28 of the appositional zones. Mean values, SEM and p values are in table 8. * $p < 0.05$; ** $p < 0.005$, *** $p<0.001$; **** $p<0.0001$.

Table 4. Intensities of homomeric Cx26 WT, Cx30 or Cx26S17F expression in HeLa cells per subcellular area (Mean ±SEM, N, p value)

		Mean Cx26WT±SEM	Mean Cx30±SEM	Mean Cx26S17F±SEM	p value
Mb	Cx26 WT vs Cx30	3,28 ± 0,79 N=23	3,84 ± 1,26 N=21		0.713
	Cx26 WT vs Cx26S17F	3,29 ± 0,79 N=23		6,82 ± 1,99 N=14	0.1181
	Cx30 vs Cx26S17F		3,84 ± 1,26 N=21	6,82 ± 1,99 N=14	0.2196
Intra	Cx26 WT vs Cx30	48,11 ± 3,04 N=23	30,39 ± 3,8 N=21		0.0008
	Cx26 WT vs Cx26S17F	48,11 ± 3,04 N=23		87,54 ± 2,76 N=14	< 0,0001
	Cx30 vs Cx26S17F		30,39 ± 3,80 N=21	87,54 ± 2,76 N=14	< 0,0001
GJ	Cx26 WT vs Cx30	48,60 ± 3,44 N=23	65,77 ± 3,95 N=21		0.0021
	Cx26 WT vs Cx26S17F	48,60 ± 3,44 N=23		5,64 ± 1,82 N=14	< 0,0001
	Cx30 vs Cx26S17F		65,77 ± 3,95 N=21	5,64 ± 1,82 N=14	< 0,0001

Table 5. Intensities Cx26 WT and Cx30 in heteromeric configuration in HeLa cells per subcellular area (Mean ±SEM, N, p value)

	Cx26WT/Cx30						
	Cx26WT			Cx30			
	Mean	SEM	N	Mean	SEM	N	p value
Membrane	14.59	3.25	20	19.35	6.07	19	0.4879
Intracellular	42.46	5.85	19	30.99	6.50	17	0.1970
Gap junction	40.07	6.65	20	42.69	8.45	19	0.8075

Table 6. Intensities Cx26S17F and Cx30 in heteromeric configuration in HeLa cells per subcellular area (Mean ±SEM, N, p value)

	Cx26S17F/Cx30						
	Cx26S17F			Cx30			
	Mean	SEM	N	Mean	SEM	N	p value
Membrane	18.41	6.93	18	20.21	6.09	18	0.8462
Intracellular	60.06	8.58	18	59.78	7.88	18	0.9807
Gap junction	21.53	7.72	18	20.01	6.47	18	0.8809

Table 7. Relative intensity of Cx30 when interacting with Cx26 WT or Cx26S17F in HeLa cells per subcellular area (Mean ±SEM, N, p value)

	with Cx26WT		with Cx26S17F		Cx30
	Mean	SEM	Mean	SEM	p value
Membrane	19.35	6.07	20.21	6.09	0.92
Intracellular	30.99	6.50	59.78	7.88	0.008 *
Gap junction	42.69	8.45	20.01	6.47	0.04

Table 8. Percentage of GJ coverage of the apposition zone in HeLa cells expressing homomeric Cx26 WT, Cx30 and heteromeric Cx26WT/Cx30 and Cx26S17F/Cx30 (Mean ±SEM, N, p value)

	Mean ± SEM	N	p value
Cx26WT	59.04 ± 2.97	53	0.3823
Cx30	63.64 ± 4.53	29	
Cx26WT/Cx30	48.65 ± 5.49	13	0.0022
Cx26S17F/Cx30	24.33 ± 4.28	12	

I.3. Cx26S17F interacts with Cx30, forming mutant heteromeric HC

The morphometric analyses of subcellular localization mentioned above support the hypothesis that mutant Cx26S17F interact with Cx30, but it does not prove it. In order to more directly assess this question, we performed proximity ligation assay (PLA, Duolink ®) which detects proteins with primary antibodies, that subsequently are labeled with secondary antibodies conjugated with complementary oligonucleotides. As shown in Figure 9, cells that co-express Cx30 with Cx26 WT (Figure 9, panel A) or Cx26S17F (Figure 9, panel B) present strong positive signals of interaction with PLA assay indicating that both proteins are close enough to interact (less than 40 nm) suggesting that Cx30 can form heteromeric HCs with both WT and mutant Cx26.

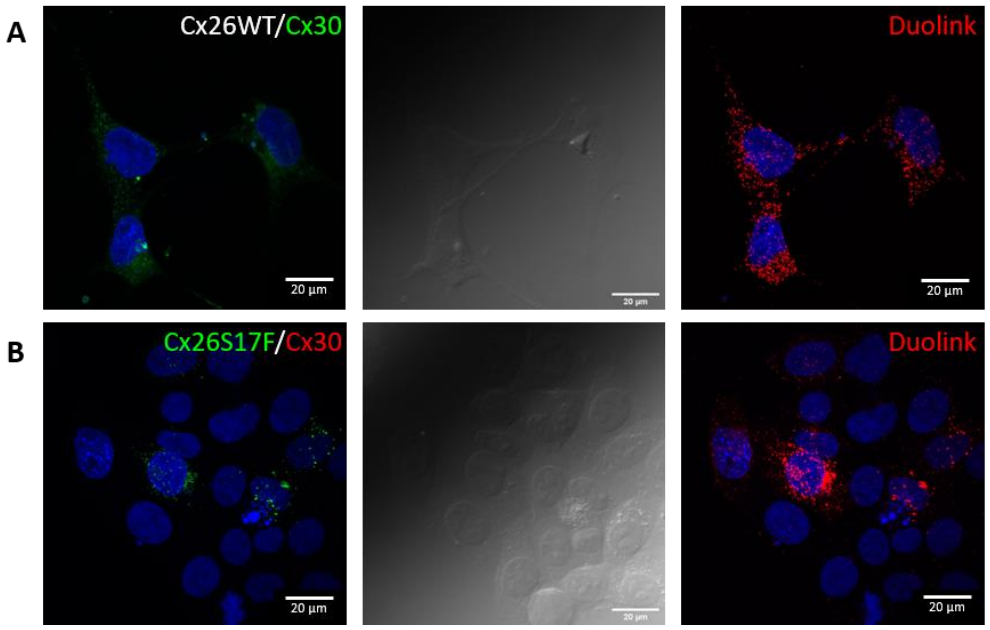

Figure 9. Cx26S17F interacts with Cx30, forming mutant heteromeric HC

PLA with anti-Cx26 and anti-Cx30 antibodies was used to demonstrate interaction between Cx30 and Cx26 WT or mutant Cx26S17F in HeLa cells co-expressing both proteins. (A) WT heteromeric Cx26 (not labeled) and Cx30 (green) in the left panel show robust interaction between both Cxs, seen as a red signal in the right panel. General morphology of cells is shown in middle panel. Scale bar, 20 µm. (B) HeLa cells in the left panel co-expressing Cx26S17F (green) and Cx30 (not shown) also show strong

interaction signal, indicating that Cx30 oligomerizes with WT and mutated Cx26. Scale bar, 20 µm.

II.- Mutant Cx26S17F is functional *trans* dominant-negative of Cx30 gap junction channels

II.1. Co-expression of Cx26S17F with Cx30 strongly reduces intercellular gap junctional communication

Previous study showed that mutant Cx26S17F form non-functional heteromeric GJCs with Cx43 (García et al., 2015), supporting a functional trans dominant-negative effect of mutant Cx26 over Cx43. To study if Cx26S17F also exert a trans dominant-negative effect over Cx30, different dye coupling techniques were used to determine the effect of co-expression of Cx26 WT or mutant Cx26S17F with Cx30 on the functional state of GJ channels. First, intercellular diffusion of fluorescent tracer calcein-AM (623 Da; net charge of z = -4; medial axial diameter of 6,5 Å) was measured using FRAP analysis between contacting cells transfected or co-transfected with the different Cx combination (Figure 10, panel A).

HeLa cells expressing different Cxs were incubated with calcein-AM (acetomethoxy group), because calcein alone cannot freely diffuse through plasma membrane. After transporting it into the cells, intracellular esterases remove the acetomethoxy group and calcein gets trapped inside cells, giving out strong green fluorescence in live cells (Figure 10, panel A).

Using a 100% laser power, calcein present in one coupled cell in a cluster of cells was bleached, and then the recovery of new calcein (i.e. the recovery of fluorescence) through functional GJs was measured from unbleached cells to the bleached cell over time. Therefore, the rate of fluorescence recovery (slope of fluorescence increments) is an index of the magnitude of functional state of GJCs present in the bleached cell.

Using this approach, we demonstrated that homotypic/homomeric GJCs formed by WT Cx26 and/or Cx30 have a similar fluorescent recovery rate of calcein (Figure 10, panel B).

However, when HeLa cells co-expressed Cx26S17F/Cx30 heteromeric GJs, the recovery of fluorescence was statistically slower than observed in WT heteromeric GJ, suggesting that Cx26S17F has a trans dominant-negative effect over Cx30 ($p<0.0001$) (Figure 10, panel C). See Table 9 for details.

Because the Cx composition determines the permeability properties of GJ channels, we evaluated the permeability of GJCs by using a different fluorescent tracer, Lucifer yellow (LY: 457.3 Da; net charge of z = -2; median axial diameter of 9.9 Å). The tracer was microinjected into one cell in a cluster of cells that express or co-express the different Cx combination, and the diffusion of LY from the injected cell to its contacting cells was determined (Figure 10, panel D). With this approximation, no microinjected cell expressing GJ formed by Cx26S17F/Cx30 transferred LY to the neighbor cell, while cell expressing homotypic or heteromeric GJCs formed by WT Cxs had more than 75% incidence of LY coupling. These experiments suggest that heteromeric GJCs formed by mutant Cx26S17F and Cx30 are not permeable to LY (9.9 Å) but may be slightly permeable to the smaller tracer calcein (6.6 Å).

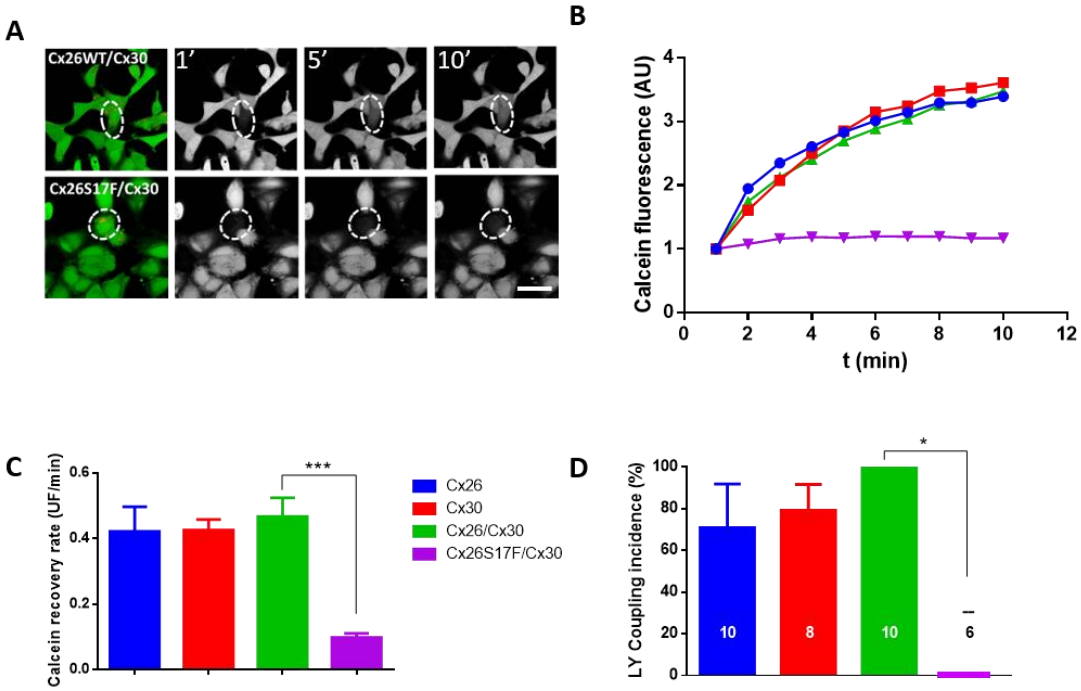

Previous page **Figure 10. Co-expression of Cx26S17F with Cx30 strongly reduces intercellular gap junctional communication**

HeLa cells expressing homomeric Cx26WT and Cx30 and co-expressing heteromeric Cx26WT/Cx30 and Cx26S17F/Cx30 were incubated with calcein-AM, giving green signal of calcein in live cells. Selected cells expressing Cxs of interest were bleached and the recovery of fluorescence was measured taking confocal pictures every minute for 10 min. Panel A shows representative pictures of HeLa cells expressing GJ formed by Cx26WT and Cx30 (upper panels) or Cx26S17F and Cx30 (lower panels), and the recovery of the fluorescence over time (from left to right): unbleached coupled cell marked with a dashed line and then at 1, 5 and 10 minutes after bleaching. Scale bar, 50 µm. Representative recoveries are shown in panel B, with Cx26WT response shown in blue, Cx30 in red, WT heteromeric Cx26WT/Cx30 GJ channel response in green and mutant heteromeric Cx26S17F/Cx30 GJ channel response in purple. Colors represent the same Cxs in every panel. Total recovery rate is shown in C. Mutant heteromeric Cx26S17F/Cx30 has a very slow recovery rate compared to WT heteromeric Cx26WT/Cx30 (***p<0.001). Mean values, SEM and p values are in table 9. (D) GJ functionality was also tested by LY microinjection, expressed as the percentage of incidence of LY coupling and number of experiments in each bar. Heteromeric mutant Cx26S17F/Cx30 GJ was not permeable to LY; Mann-Whitney test, * p<0.05.

Table 9. FRAP recovery rates comparison of homomeric Cx26WT v/s Cx30, and heteromeric Cx26WT/Cx30 v/s Cx26S17F/Cx30 (Mean, SEM and p value)

	Mean ± SEM	N	p value
Cx26WT	0,42 ± 0,08	13	0.9564
Cx30	0,43 ± 0,03	4	
Cx26WT/Cx30	0,47 ± 0,06	8	0.0003
Cx26S17F/Cx30	0,1 ± 0,01	9	

III.-. Heteromeric HC formed by Cx26S17F and Cx30 are hyperactive and less sensitive to extracellular Ca^{2+} and La^{3+}.

III.1. Heteromeric HC formed by Cx26S17F/Cx30 have hyperactive function and do not respond to connexin blocker La^{3+}.

HC function was evaluated using the incorporation of ethidium (Etd) from the extracellular to the intracellular space, in basal or resting conditions (1.26 mM Ca^{2+}), then in absence of extracellular divalent cations (Ca^{2+}_e free) to increase open probability of the connexin HCs, and finally, in Ca^{2+}_e free with non-selective connexin blocker La^{3+}.

When HeLa cells were expressing WT homomeric (Cx26 or Cx30 expressed alone) and WT heteromeric (Cx26/Cx30) channels most cells showed very low Etd uptake rates in basal conditions (Figure 11, panels A-C). However, under resting conditions most cells co-expressing mutant heteromeric Cx26S17F/Cx30 presented larger uptake rates compared to cells expressing WT homomeric or heteromeric HC formed by Cx26 and/or Cx30 (Figure 11, panel D), that in average were almost fourth time larger than the uptake rate observed in cells co-expressing wild type Cx26/Cx30 (Figure 11, panel E; $p<0.0001$).

When extracellular Ca^{2+} was removed, Etd uptake increased in most cells expressing Cx26 WT or Cx30 (Figure 11, panels A and B) and also in cells co-expressing Cx26WT/Cx30, but in the last ones with less extension, except some cells that present very large uptake rates (Figure 11, panel C). Moreover, under free extracellular Ca^{2+} condition some cells co-expressing Cx26S17F/Cx30 increased Etd uptake, but in less extension than WT condition (Figure 11, panel D and E). The consolidated averaged data showed that under free extracellular Ca^{2+} condition cells expressing Cx26 or Cx30 or co-expressing both wild type connexins increased the Etd uptake rate more than three times, while cells co-expressing Cx26S17F/Cx30 only did it twice (Figure 11, panel E). In addition, increased Etd uptake rate observed in cells expressing Cx26S17F/Cx30 was not reduced by the HC blocker La^{3+} as in cells co-expressing WT Cxs

($p<0.001$). These results demonstrate that Cx26S17F/Cx30 form hyperactive heteromeric HCs since they showed altered sensitivity to extracellular Ca^{2+} and could not be inhibited by the Cx HC blocker La^{3+}, suggesting that mutant heteromeric HC formed by Cx26S17F and Cx30 present aberrant gating properties.

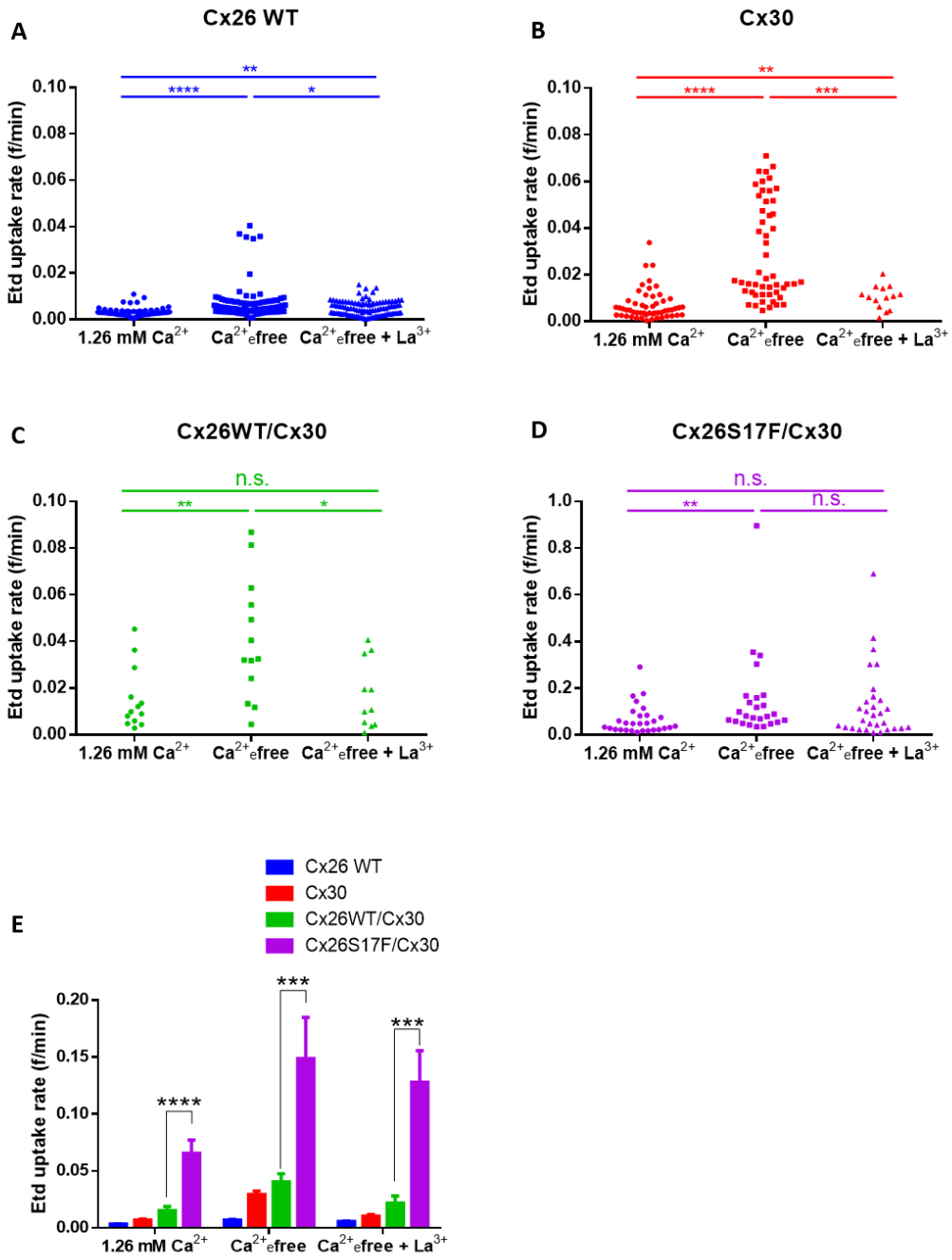

Previous page **Figure 11. Heteromeric HC formed by Cx26S17F/Cx30 have hyperactive function and do not respond to connexin blocker La^{3+}.**

HC functionality was evaluated with Etd uptake approach over time, with cells bathed in Hanks solution with 1.26 mM Ca^{2+} per 10 minutes, then in Ca^{2+} free solution (5 min) to increase the opening of HCs and finally with the Cx HC blocker La^{3+} (100 µM) (5 min). Etd uptake rate in every individual HeLa cell considered in the experiment expressing homomeric Cx26WT HC (A, blue); Cx30 HC (B, red), heteromeric WT Cx26/Cx30 HC (C, green) and mutant Cx26S17F/Cx30 HCs (D, purple). (E) Consolidated data in basal, Ca^{2+}_e free and Ca^{2+}_e free + La^{3+} for all Cx HCs evaluated. Remarkably, in basal condition, heteromeric Cx26S17F/Cx30 HC showed higher activity than Cx26WT/Cx30 HC ($p<0.0001$). In Ca^{2+}_e free solution, all types of HCs formed by different Cxs increased Etd uptake rate, but in less extension for Cx16S17F/Cx30 HCs. Interestingly when La^{3+} was added to the recording solution mutant heteromeric Cx26S17F/Cx30 showed significantly higher HC activity compared to WT heteromeric Cx26/Cx30 HC. Mann-Whitney test, * $p < 0.05$; ** $p < 0.005$, *** $p<0.001$; **** $p<0.0001$.

III.2. HeLa cells co-expressing mutant heteromeric Cx26S17F/Cx30 channels showed less sensitivity to $[Ca^{2+}]_e$ compared to cells co-expressing heteromeric Cx26WT/Cx30 channels.

Since HC made of Cx26 WT are permeable to Ca^{2+} (Fiori et al., 2012), we decided to study the possibility that cells expressing heteromeric HC formed by Cx26S17F/Cx30 present higher Ca^{2+} flux from extracellular to intracellular compartments. Intracellular $[Ca^{2+}]$ signal rate was measured in HeLa cells co-expressing Cx26WT/Cx30 or Cx26S17F/Cx30 heteromeric HCs, using the ratiometric Ca^{2+} sensor Fura-2, at ascendant extracellular Ca^{2+} concentrations (Figure 12, panel A). Using this approach, we observed that the Ca^{2+} rate augmented at increasing extracellular Ca^{2+} concentrations showing a bell-shaped response with peaks increments at 100 µM and 500 µM of extracellular Ca^{2+}, in cells co-expressing Cx26/Cx30 and Cx26S17F/Cx30, respectively. On contrary, at higher $[Ca^{2+}]_e$ intracellular Ca^{2+} rate increment was dramatically reduced in cells co-expressing Cx26WT/Cx30 but modestly reduced in cells co-expressing Cx26S17F/Cx30, consistent with the fact that HC are closing at higher extracellular Ca^{2+} concentrations, but not in the mutant heteromeric condition, supporting the idea that heteromeric HCs made by Cx26S17F/Cx30 have lower sensibility to $[Ca^{2+}]_e$

To better understand the flux increment in the $[Ca^{2+}]_i$ at different $[Ca^{2+}]_e$ in both WT and mutant heteromeric Cx combinations, a normalization was made using the ratio between fluorescence signal increments at different $[Ca^{2+}]_e$ over fluorescence at 10 µM $[Ca^{2+}]_e$, which was the lower extracellular Ca^{2+} concentration used (Figure 12, panel B). Both Cx combinations show similar Ca^{2+} influx increments at 100 µM $Ca^{2+}{}_e$, however at 500 µM $[Ca^{2+}]_e$ have a significant reduced flux of Ca^{2+} in the cells co-expressing Cx26WT/Cx30, but not in cells co-expressing Cx26S17F/Cx30, where we still observed increments in Ca^{2+} flux. Remarkably, with this analysis is yet more evident that at higher extracellular Ca^{2+} concentration there is no influx of extracellular Ca^{2+} into cells co-expressing wild type Cx26/Cx30, yet the cells co-expressing Cx26S17F/Cx30 present large Ca^{2+} influx. Finally we did not observe differences in the slope

rate of Ca^{2+} signals increments in the ascendant part of the curve, at lower $[Ca^{2+}]_e$, between cells co-expressing WT Cxs versus cells co-expressing Cx26S17F/Cx30, suggesting, that although HC made by Cx26S17F/Cx30 are hyperactive they are not more permeable to extracellular Ca^{2+}.

Overall, these experiments suggest that heteromeric HCs made by Cx26WT/Cx30, or Cx26S17F/Cx30, are both permeable to extracellular Ca^{2+}. However, HCs made by Cx26S17F/Cx30 are significantly less sensitive to extracellular Ca^{2+} for HC closing, which is consistent with dye uptake experiments and with the idea that this mutant heteromeric HCs are hyperactive, allowing major Ca^{2+} influx at resting conditions. Whether if HCs are still open or permeability was affected, is an open question to be answered in the future.

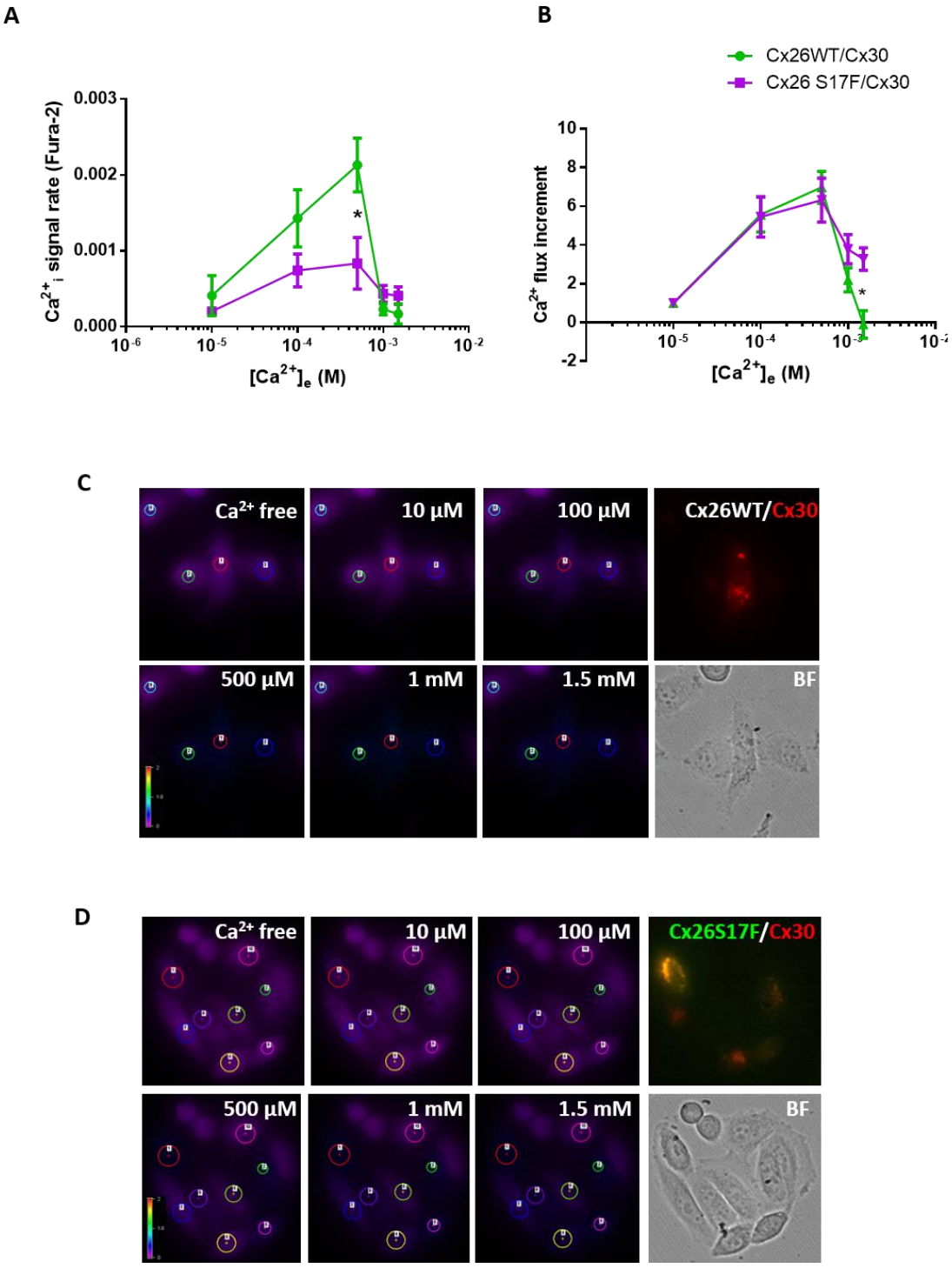
A
B
Cx26WT/Cx30
Cx26 S17F/Cx30
Ca^{2+}_i signal rate (Fura-2)
Ca^{2+} flux increment
$[Ca^{2+}]_e$ (M)
C
Ca^{2+} free
10 µM
100 µM
Cx26WT/Cx30
500 µM
1 mM
1.5 mM
BF
D
Ca^{2+} free
10 µM
100 µM
Cx26S17F/Cx30
500 µM
1 mM
1.5 mM
BF

Previous page **Figure 12. HeLa cells co-expressing mutated heteromeric Cx26S17F/Cx30 channels showed lees sensibility to $[Ca^{2+}]_e$ compared to cells co-expressing WT heteromeric Cx26WT/Cx30 channels.**

Ca^{2+} signals were determined by FURA-2. (A) Ca^{2+} signal rate indicated by the slopes of intracellular Ca^{2+} increments at different $[Ca^{2+}]_e$ in HeLa cells co-expressing Cx26WT/Cx30 (green) or mutant heteromeric Cx26S17F/Cx30 (purple). Mean slopes, SEM and p values are detailed in table 10. (B) Normalized Ca^{2+} flux increment respect to uptake Ca^{2+} rate at 10 µM. Peak of Ca^{2+} flux was reach at same concentration for both Cx combination around 500 µM, higher extracellular Ca^{2+} concentration produce an almost complete reduction in the uptake rate of extracellular Ca^{2+} flux in cells co-expressing Cx26WT/Cx30, but not in cells expressing Cx26S17F/Cx30, where even at 1.5 mM extracellular Ca^{2+} produce a significant Ca^{2+} influx.

IV.- Co-expression of Cx26S17F/Cx30 HCs increases cellular damage and death

IV.1. Expression of mutant heteromeric Cx26S17F/Cx30 HCs increase cell death in HeLa cells

As a general observation during this thesis work, we noticed that cells co-expressing Cx26S17F/Cx30 has a low expectancy of survival after transfection, so we decided to quantify this phenomenon by using the annexin V and Propidium iodide (PI) assay, for labeling damaged cells (like early apoptosis) and necrotic cells, respectively.

Using this approach, we observed that only 20% of HeLa cells co-expressing Cx26WT/Cx30 are labeled with annexin V and 11% of them are labeled with PI, values that were similar to the observed in non-transfected HeLa cell cultures (Figure 13, panels A and C). On the other hand, HeLa cells co-expressing Cx26S17F/Cx30 have the higher level of cell damage or early apoptosis, as more than 65% of the cells are labeled with annexin V (Figure 13, panels B and C). In addition, almost 30% cells co-expressing mutant heteromeric Cx26S17F/Cx30 present also strong positivity to PI, indicating that some damaged cells were already necrotic. Even when these experiments are preliminary results and more replication and quantification is still required, the observed result is in line with the effect observed in cells expressing other hyperactive HCs described in the literature.

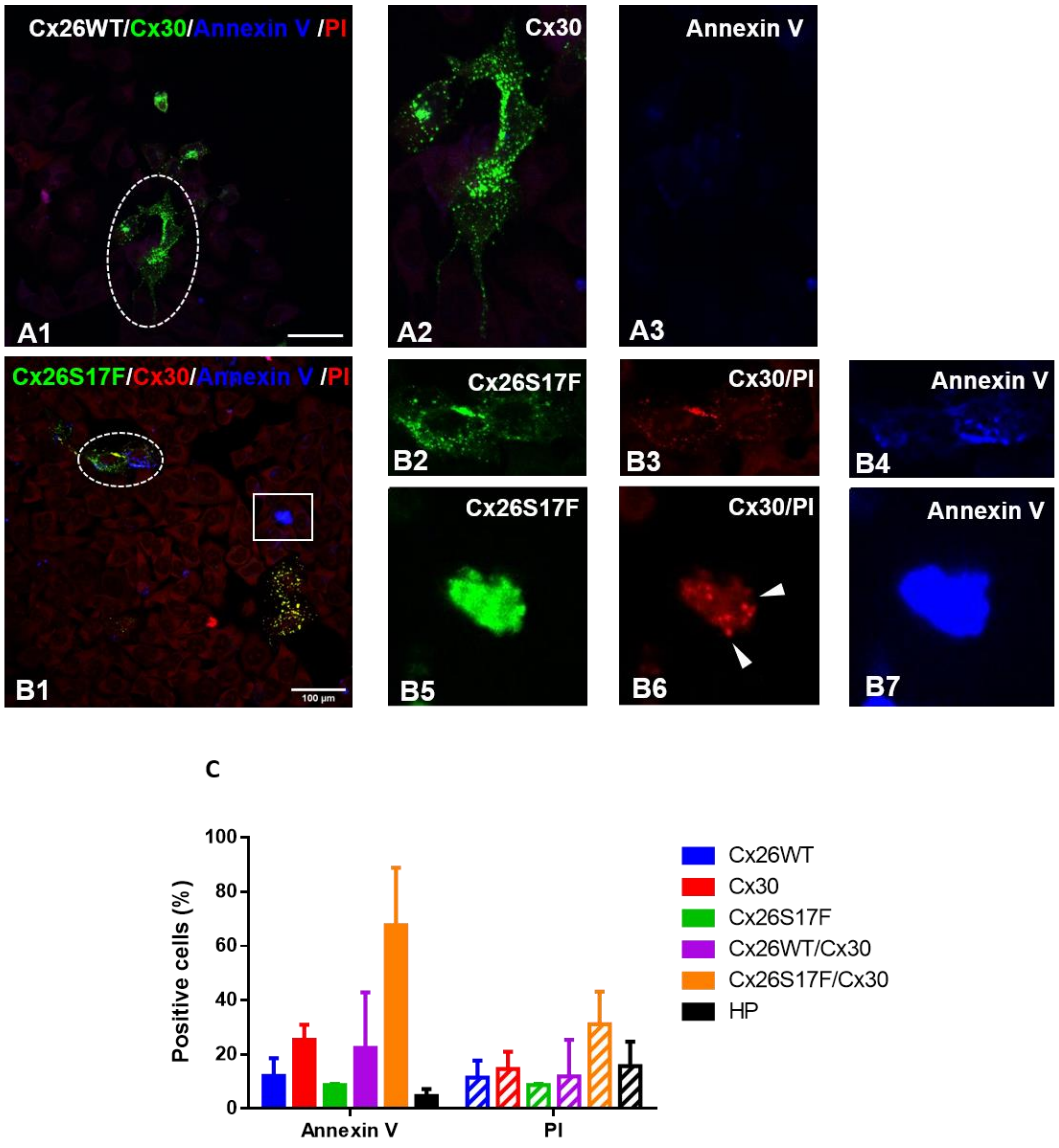

Figure 13. Expression of mutant heteromeric Cx26S17F/Cx30 HCs increase cell death in HeLa cells

Representative image of HeLa cells co-expressing WT heteromeric Cx26 (no tag) and Cx30 (green) (A1), with a magnified view of the highlighted zone in A2, showing no signal for annexin V (A3) (B1) HeLa cells co-expressing mutant Cx26S17F (green) and Cx30 (red), with PI and annexin V signals. Cells highlighted with a dotted line is showed in B2 for Cx26S17F (green), B3 for Cx30 and PI background signal (red) and annexin V signal in the membrane (B4, blue)

Another focal plane of B1 is shown where the highlighted cell in a white square is in focus. Expression Cx26S17F (green, B5) PI positive signal and Cx30, distinguished by arrowheads (red, B6) show positive signal for annexin V (B7) with a rounded morphology typical of a dead cell. Scale bar, 100 µm. (C) Percentage of cell death in HeLa cells expressing different Cxs. Filled bars show percentage of damaged cells or early apoptotic cells positive for annexin V and hatched bars for PI. Statistical analysis has not been performed yet, due to low number of experiments to date.

V.- Expression of Cx26S17F in mouse cochlear explants changes the sub-cellular distribution of connexins in supporting cells of the organ of Corti.

V.1. Cochlear explants as a model to study inner ear connexins

In order to understand the effects of expression of mutant Cx26S17F in the inner ear, we used cochlear explants from WT and from the transgenic mouse line $Cx26^{+/floxS17F}$, a mouse strain that carries Cx26S17F mutation downstream to Cx26 gene flanked by loxP sequences that do not show any phenotype (Schütz et al., 2011). The F1 progeny product of the crossing of a female $Cx26^{+/floxS17F}$ with a male mouse bearing Cre recombinase expresses Cx26S17F instead of Cx26 WT, and present skin phenotype and deafness (Schütz et al., 2011). However, using the same strategy than the article of (Schütz et al., 2011) we observed that F1 progeny of KI Cx26S17F mouse present high incidence of lethal phenotypes with most deaths before two-three days of life, before full development of mouse inner ear, therefore we decided to use another strategy in which, instead of crossing mouse line $Cx26^{+/floxS17F}$ with Cre mouse line, we did induce the expression of conditional knock-in of Cx26S17F (cKI Cx26S17F) by treatment of cochlear explants with Cre-recombinase recombinant protein, coupled to a TAT sequence, allowing the diffusion of exogenous Cre-recombinase enzyme into the cells.

Cochlear explants were made with the valuable help of Dr. Helmuth Sanchez. Briefly, to obtain the explants, temporal bone was removed from the skull of WT and $Cx26^{+/floxS17F}$ p7 mice, and the whole cochlea was isolated under a stereo microscope (Figure 14, panel A, zoom 4x). After isolation, cochlear explants were seeded in a commercial matrix and kept with culture media for up to 1 or 2 days to make experiments (Parker et al., 2010) *(see Material and Methods section)*.

After 1 day in vitro (1 DIV), cochlear explants show all cellular types in perfect condition (Figure 14, panel B), and spiral limbus and sensory epithelium are distinguished. Figure 14, panel C show a magnified view of the cochlear explant in brightfield and a nuclear stain (DAPI),

which allows recognition of several cell types: ISC, inner supporting cells; IHC, inner hair cells; PC, pillar cells; OHC, outer hair cells; OSC, outer supporting cells and F, fibrocytes. With DAPI, it is possible to identify nuclei of supporting cells being smaller than hair cells. To determine the integrity of cochlear cells we observed morphology of hair cell stereocilia with phalloidin using super-resolution fluorescent microscopy, since it is a very sensitive structure that might break after mechanical stress. As seen in Figure 14, panel D, cochlear explants kept the integrity of cellular morphology, including perfectly aligned stereocilia, indicating that explants cultures (24-48 h) keeps the normal aspect of the fine structure of the organ of Corti, making it as a suitable model to study the effect of expression of deafness mutations in *ex-vivo* studies.

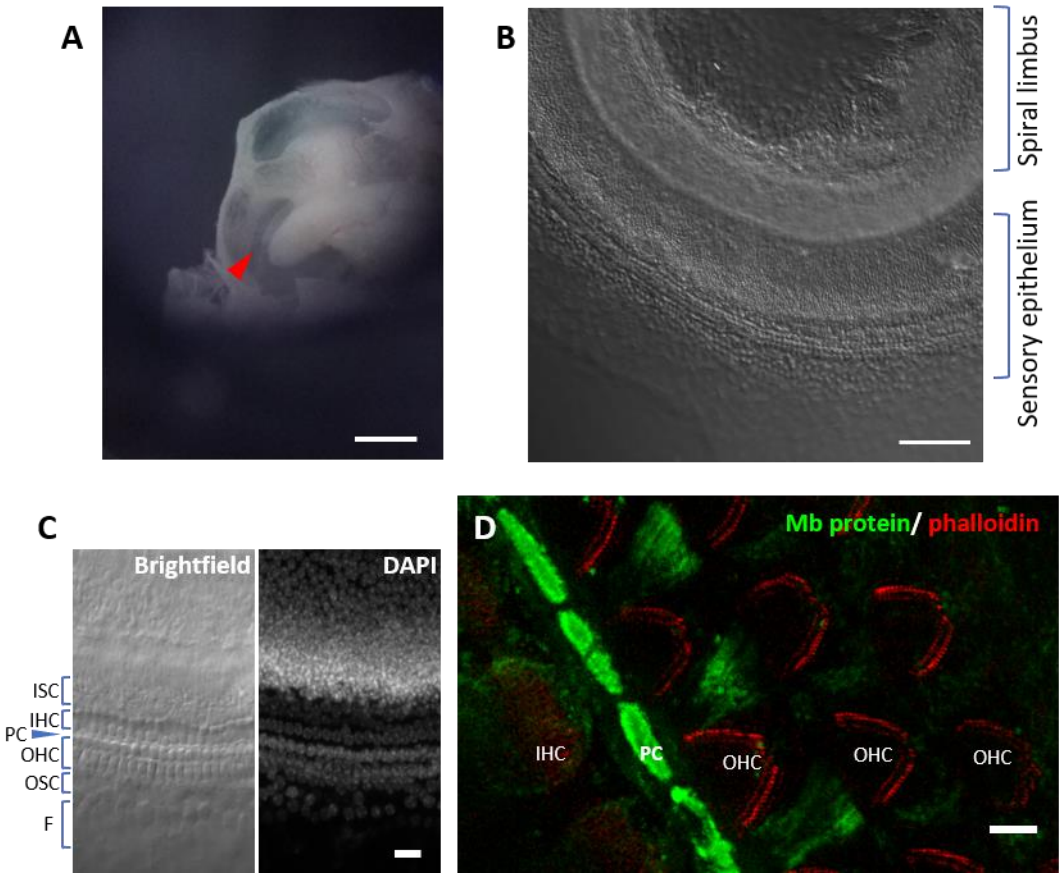

Figure 14. Cochlear explants as a model to study inner ear connexins

Dissection of a cochlea from a P7 mouse (A). The bony labyrinth of the cochlea is visible, where sensory epithelium is highlighted with a red arrowhead. Scale 0.5 mm. (B) Cochlear explant showing the sensory epithelium and the residual spiral limbus next to it. Scale bar, 100 µm. (C) Cell types in the organ of Corti, in the sensory epithelium. ISC, inner supporting cells; IHC, inner hair cells; PC, Pillar cells; OHC, outer hair cells; OSC, outer supporting cells; F, fibroblasts and mesenchymal cells. DAPI stain showing different sizes in cell nuclei. Scale bar, 20 µm. (D) Phalloidin stain (red) showing intact stereocilia located in the apical part of hair cells, indicating integrity in the morphology of the cochlear tissue. Scale bar, 2 µm.

V.2. Expression of cKI Cx26S17F in cochlear explants change the distribution of the protein in supporting cells of the organ of Corti.

Immunofluorescence was carried out in order to visualize possible effects of expression of Cx26S17F on sub-cellular localization of Cxs in the cultured explants from $Cx26^{+/floxS17F}$ mice incubated with or without (control) TAT-Cre enzyme. In control explants, Cx26 WT (green) and Cx30 (red) were co-expressed in supporting cells of the organ of Corti where they strongly co-localize (Figure 15, panel B). Panel B1 of figure 15 shows a magnified view of outer supporting cells (OSC, top row) were Cx26 and Cx30 co-localized in fibrocytes and Hensen, Claudius and Böettcher cells, forming large heteromeric GJ plaques. Middle row shows pillar cells, which form the tunnel of Corti, and Deiters cells, also showing GJ plaques of a bigger size than the GJ observed in OSC. Bottom row shows expression of inner supporting cells, were a massive amount of small heteromeric GJ plaques made by both Cxs can be observed. An orthogonal view of the highlighted zone in doted cyan line is shown in B2, where Cx distribution is observed mostly in the bottom but also in the upper part of supporting cells. Cell nuclei are stained with DAPI.

On the other hand, when $Cx26^{+/floxS17F}$ cochlear explants are treated with TAT-Cre (Figure 15, panel C), and cKI Cx26S17F is expressed, several changes can be noticed: OSC and ISC shows expression of Cx26S17F and Cx30 mostly in the intracellular space, where they co-localize, and in few small GJ plaques. However, we did not observe changes in Cx expression in pillar and Deiters cells. These results suggest that expression of cKI Cx26S17F in explants of the organ of Corti change the subcellular distribution of Cx26 and Cx30 in OSC and ISC to a more intracellular localization, without affecting Dieters and pillar cells. An orthogonal view of the highlighted zone in doted cyan line is shown in C2, where Cx distribution is observed but also, a change in the nuclei morphology of supporting cells.

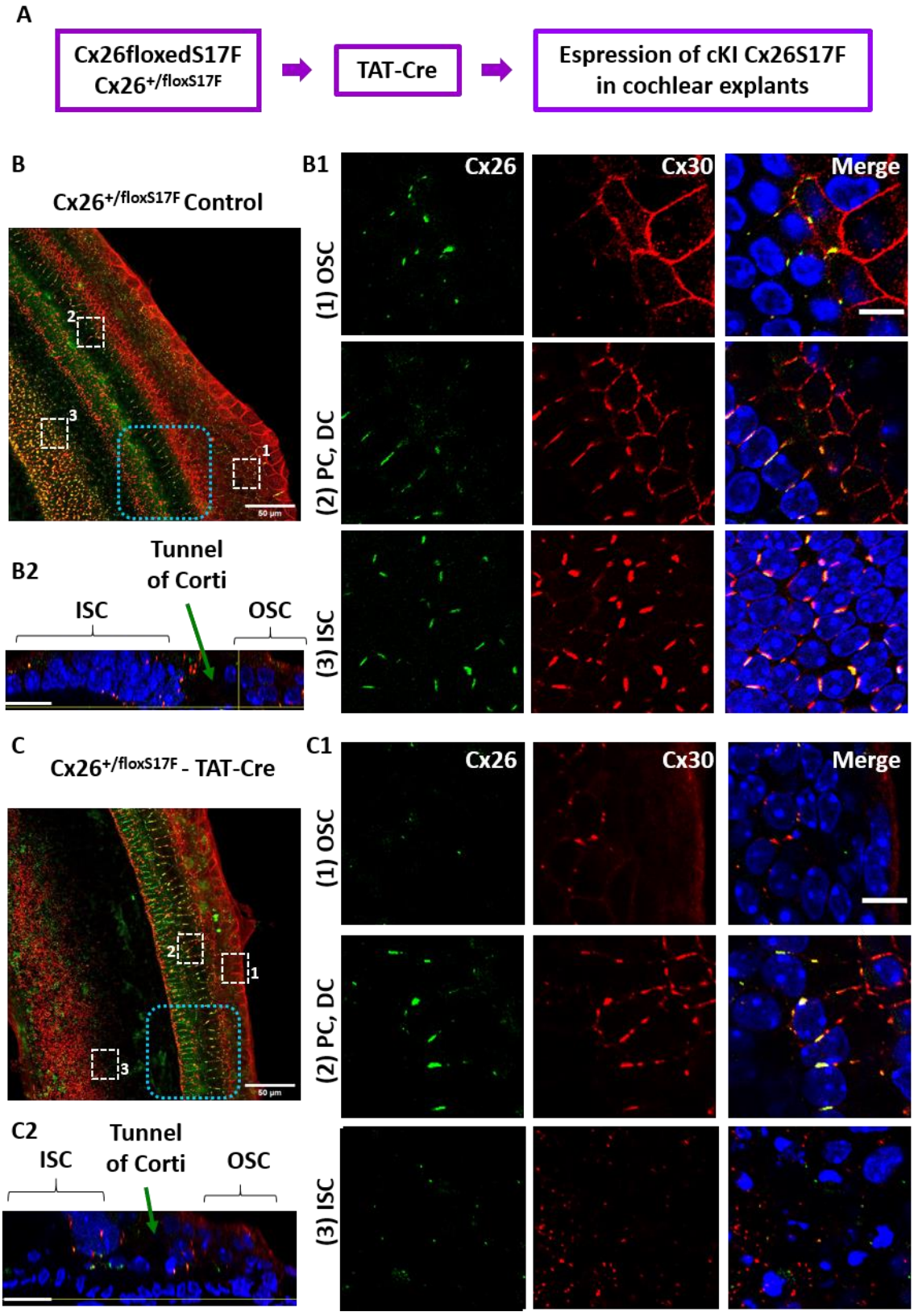
A
Cx26flox S17F
Cx26+/floxS17F
TAT-Cre
Espression of cKI Cx26S17F
in cochlear explants
B
Cx26+/floxS17F Control
B1
Cx26
Cx30
Merge
(1) OSC
(2) PC, DC
(3) ISC
B2
Tunnel
of Corti
ISC
OSC
C
Cx26+/floxS17F - TAT-Cre
C1
Cx26
Cx30
Merge
(1) OSC
(2) PC, DC
(3) ISC
C2
ISC
Tunnel
of Corti
OSC

Previous page **Figure 15. Expression of Cx26S17F in cochlear explants change the distribution of the protein in supporting cells of the organ of Corti.**

Cochlear explants from $Cx26^{+/floxS17F}$ were used to induce the expression of mutant Cx26S17F in supporting cells of the organ of Corti, adding diffusible TAT-Cre to culture media and inducing the expression of conditional knock-in *ex vivo* (A). Control cochlea (B) showed typical distribution of Cx26 (green) and Cx30 (red), forming beautiful heteromeric GJ plaques, as seen in the magnified views of 1 µm thick in (B1) of OSC (1), PC and DC (2) and ISC (3). Scale bar, 5 µm. (B2) Transversal view of highlighted zone in doted cyan line in B. Scale bar, 20 µm. Expression of cKI Cx26S17F (C) changed distribution of mutant Cx26S17F and Cx30. Scale bar, 50 µm. Magnified views of highlighted squares in C are shown in 1 µm thick optic cuts in C1, where diminishing formation of GJ plaques and retaining both Cxs in the intracellular space in OSC (1), as previously observed in vitro; while in ISC expression of GJ is totally lost (3). PC and DC do not show an extreme phenotype (2) are observed, respectively. Scale bar, 5 µm. (C2) Transversal view of highlighted zone in doted cyan line in C. Scale bar, 20 µm.

VI.- Expression of Cx26S17F produce HCs hyperactivity in supporting cells of the organ of Corti and damage of hair cells

VI.1. cKI Cx26S17F expression in cochlear explants increases activity of supporting cells HC

Because the observation in HeLa cells that co-expression of Cx26S17F with Cx30 produces hyperactive heteromeric HCs with loss of channel closure by extracellular Ca^{2+}, we decided to study if the same HC property could be observed in the cochlear explants that express Cx26S17F. Using DAPI as a HC-activity tracer, explants were kept in Hanks solution with 1.26 mM Ca^{2+} (same concentration as in the perilymph) for 10 minutes, then in nominal Ca^{2+}-free Hanks solution (close to endolymph Ca^{2+} concentration) for another 5 minutes to increase open probability of HC and finally, HC activity was blocked with Cx blocker carbenoxolone (CBX, 100 µM) (Majumder et al., 2010; Sirko et al., 2019) to demonstrate specificity in the Cx response.

In control explants OSC, PC and ISC (blue dots and bars) show low DAPI uptake in basal conditions (1.26 mM $[Ca^{2+}]_e$), that increases when Ca^{2+} is removed from the register solution. Then, HC were blocked with CBX, which significantly reduced the uptake rate of DAPI in these cells. On contrary, in cochlear explants treated with TAT-Cre dye uptake rates basal conditions observed in OSC, PC and ISC were significantly higher, more than three times, compared to controls explants. The higher DAPI uptake rates observed in explants treated with TAT-Cre did not change significantly when basal medium was replaced by nominal Ca^{2+}-free Hanks solution and also after treatment with HC blocker CBX (Figure 16 panels A, B and C shows consolidated DAPI uptake rates from three independent experiments; and D, E and F are representative individual experiments from each condition)

The above observations suggest two important things in our model. First, they indicate presence of Cx HCs in supporting cells in control explants, since the activity registered here was

modulated by Cx-based channel blocker CBX and by $[Ca^{2+}]_e$. This strongly suggest presence of Cx HC in normal cochlea. And second, the expression of cKI Cx26S17F in cochlear explants induces the formation of hyperactive HCs, possible by the generation of aberrant heteromeric HCs formed between mutant Cx26 and Cx30, with reduced regulation by extracellular Ca^{2+}.

It is worth to mention that hair cells do not express Cxs nor Panxs, a related type of proteins that also form HC. In this experimental approach, we observed a very fast and almost instantaneous DAPI uptake in inner and outer hair cells that were not affected by HC blocker CBX, suggesting that DAPI may have been incorporated to these cells through a different type of channel or may represent damage of hair cells, as it is suggested in preliminary results shown in Figure 17.

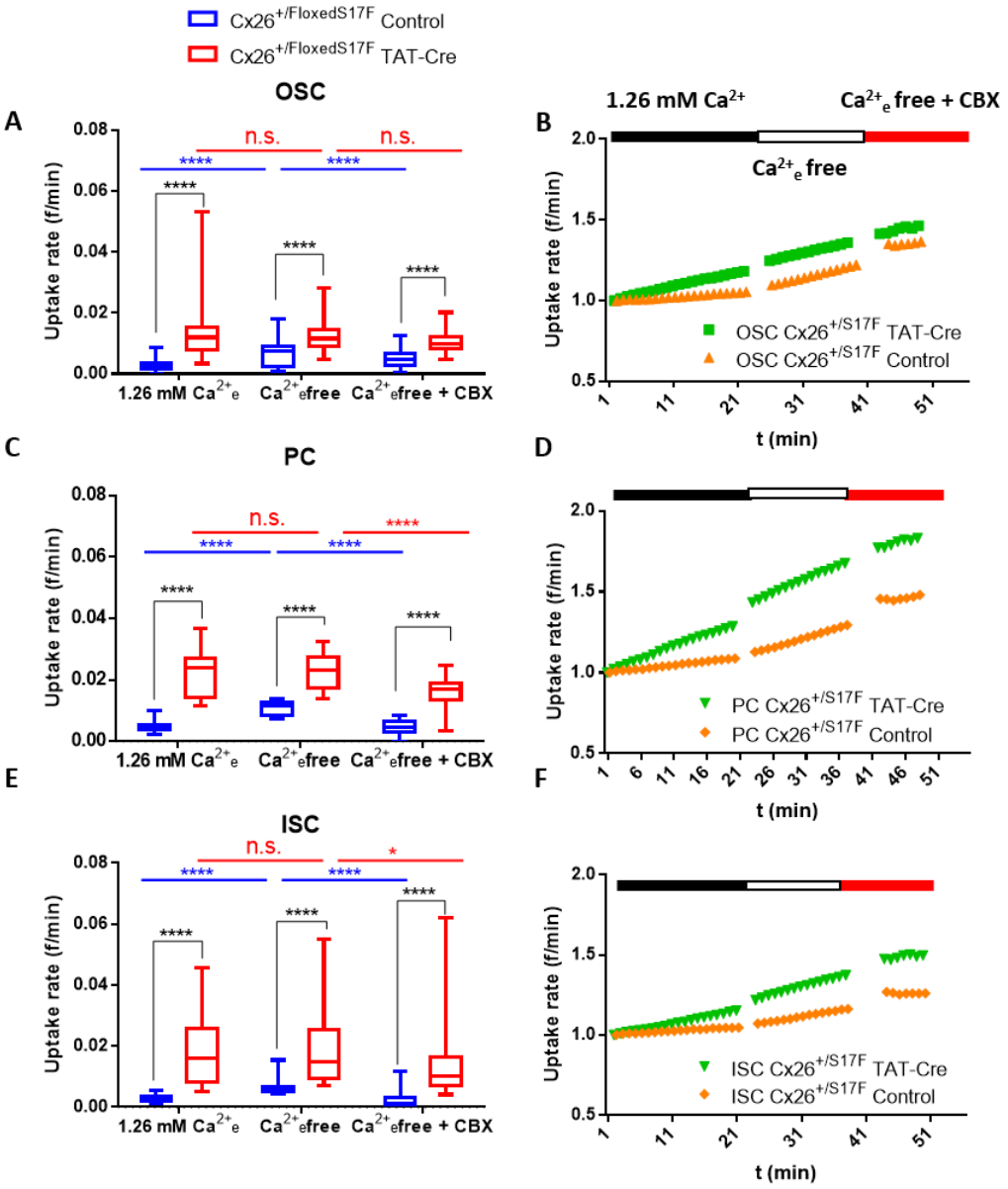

Figure 16. cKI Cx26S17F expression in cochlear explants increases activity of supporting cells HC

Uptake rate of DAPI by OSC (A), PC (C) and ISC (E) in control (blue) and TAT-Cre (red) cochlear explants of $Cx26^{+/floxedS17F}$ mice, shown as box and whiskers plot with minimum and maximum values, box representing 25 and 75 percentiles, and a central line showing median values. Intragroup comparisons are presented in (control) and red (TAT-Cre). Representative mean cell responses (B, D and F, respectively) in control (orange) and cKI explants (green). * $p<0.05$; **** $p<0.0001$.

VI.2. Mutation Cx26S17F affects morphology of hair cell's stereocilia in cochlear explants

Then, we evaluated the general state of hair cell by stereocilia stain with phalloidin, a molecule that binds to actin, in WT and cKI Cx26S17F cochlear explants.

Cochlear explants from a P7 WT mouse show V-shaped stereocilia in the OHC, and a more horizontal shape in IHC stereocilia bundles (Figure 17, panel A), as described elsewhere (Stauffer and Holt, 2007; Ciganović et al., 2017; Ashmore, 2008).

Figure 17, panel B shows hair cell stereocilia in a severe phenotype of cKI Cx26S17F cochlear explant, which loses the general arrangement and several stereocilia are lost especially in the IHC.

Carrier mouse $Cx26^{+/floxS17F}$ hair cells stereocilia do not show a marked difference related to WT explants (Figure 17, panel C). Consistently, $Cx26^{+/floxS17F}$ cochlear explants treated with TAT-Cre recombinase for the *ex vivo* expression of cKI Cx26S17F showed loss of stereocilia, as observed in Figure 17, panel D. The general phenotype was less severe than in the constitutive KI Cx26S17F F1 mice from the crossing of $Cx26^{+/floxS17F}$ carrier mouse and CMV-Cre mouse (Figure 17, panel B), maybe because the expression of Cx26S17F started only when TAT-Cre was applied to the culture, 16 h before the experiments.

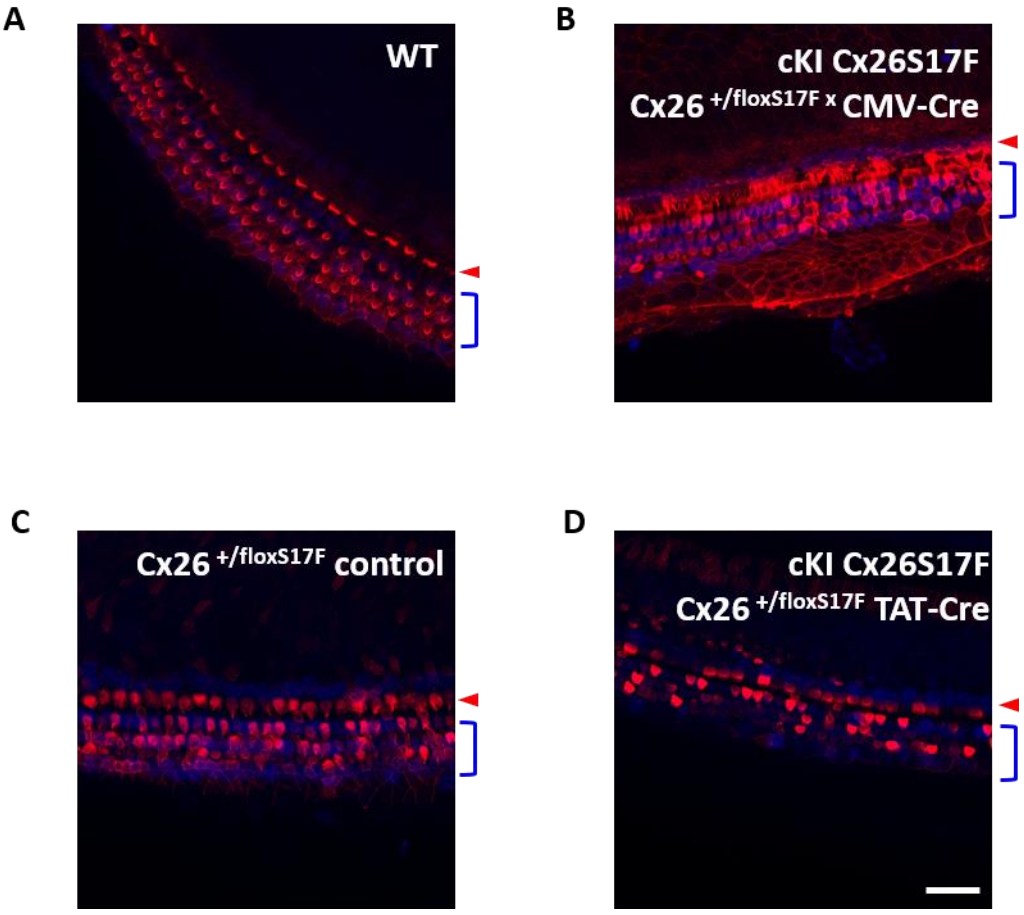

Figure 17. Mutation Cx26S17F affects morphology of hair cell's stereocilia in cochlear explants

Red arrowhead show the single row of IHC, and blue bracket shows the three rows of OHC in cochlear explants of WT (A); mutant cKI Cx26S17F, a F1 mouse when crossing $Cx26^{+/floxS17F}$ with CMV-Cre, which resembles the KID syndrome in the ear and skin (B); a control $Cx26^{+/floxS17F}$ mouse, which carries Cx26S17F mutation but do not express it, then having a normal phenotype (C); and $Cx26^{+/floxS17F}$ treated with TAT-Cre, which allows the expression of cKI Cx26S17F *ex vivo*. Scale bar, 30 µm.

VII.- Expression of Cx26S17F in HeLa cells and cochlear supporting cells differentially affect purinergic signaling

VII.1. ATP-induced intracellular Ca^{2+} response is reduced in cells expressing mutant Cx26S17F/Cx30

Since ATP is an important physiological and pathological mediator, and since HeLa cells express many purinergic receptors that are also expressed in the cochlea and the skin, we decided to analyze the effect of expression of aberrant heteromeric hyperactive HCs on the Ca^{2+} response induced by ATP in Hela cells transfected with different Cxs.

HeLa cells expressing different Cxs were incubated with Fluo-4, a sensitive non-ratiometric Ca^{2+} indicator. After incubation, cells were washed and kept in Hanks buffer with 1.26 mM Ca^{2+} or in Ca^{2+} free solution, and intracellular Ca^{2+} signal was measured using an epifluorescence microscope. To stimulate cells, 100 µM ATP was added to the recording solution, and Ca^{2+} response was quantified.

In Ca^{2+} free solution, cells expressing mutant heteromeric Cx26S17F/Cx30 has a decreased response to purinergic stimulus compared to cells expressing WT Cx26/Cx30 (**** $p<0.0001$). Peak amplitude is decreased compared to Cx26WT/Cx30 (** $p<0.005$), and peak duration, which was shorter than Ca^{2+} response cells expressing Cx26WT/Cx30 (**** $p<0.0001$)

Cells expressing heteromeric WT HCs (Cx26WT/Cx30) has a significantly higher ATP-induced Ca^{2+} response than cells expressing mutant heteromeric Cx26S17F/Cx30 in presence of Ca^{2+}_e (* $p<0.05$). The decreased response is evident in the peak amplitude (**** $p<0.0001$), but the time of this small response is similar as observed in cells expressing WT heteromeric HC.

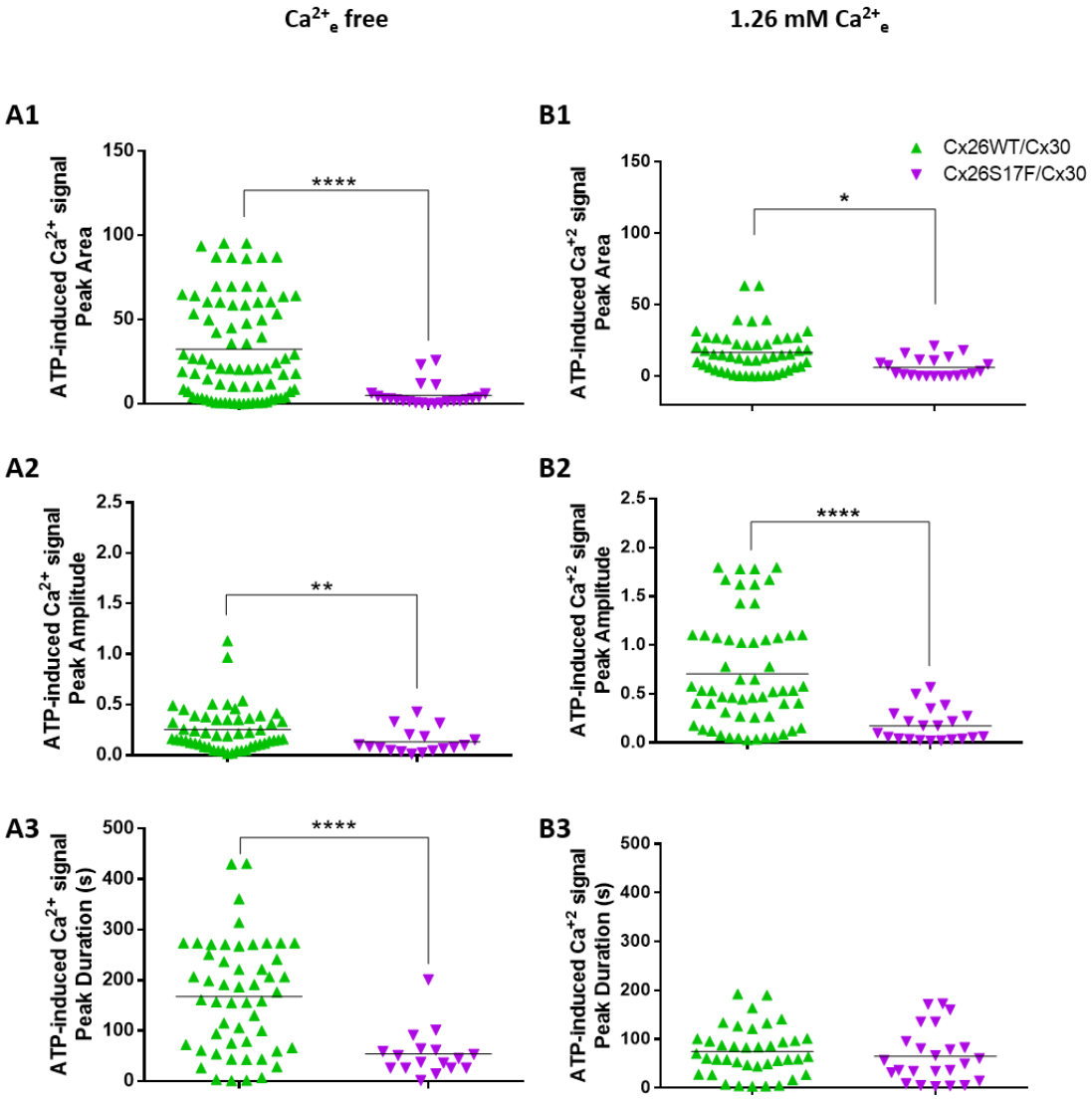

Figure 18. ATP-induced intracellular Ca^{2+} response is reduced in cells expressing mutant Cx26S17F/Cx30

HeLa cells expressing heteromeric Cx26S17F/Cx30 (purple) has a decreased response to ATP in absence or presence of Ca^{2+}_e (peak area, A1 and B1). Peak amplitude (A2 and B2) and peak duration (A3 and B3) are also decreased in cells expressing Cx26S17F/Cx30, but cells expressing WT heteromeric Cx26WT/Cx30 (green) showed a bigger amplitude in presence of Ca^{2+}_e and bigger peak duration in absence of Ca^{2+}_e. * $p < 0.05$; ** $p < 0.005$, **** $p<0.0001$.

VII.2. cKI Cx26S17F expression in cochlear explants show altered ATP-induced Ca^{2+} response in absence or presence of $[Ca^{2+}]_e$

Using Fluo-4 Ca^{2+} sensor, ATP-induced Ca^{2+} response was measured in supporting cells of control and cKI Cx26S17F. As mentioned previously, ATP released during development is very important to synchronize and maintain hair cells, induce Ca^{2+} waves in supporting cells during development and adult organ of Corti, induce K^+ currents in supporting cells, among other physiological functions; and is one of the molecules that can pass through Cx HCs and GJ channels.

Having hyperactive HCs or non-functional GJ channels in supporting cells of the organ of Corti might be related to KID, since it has been described here that HeLa cells expressing Cx26S17F/Cx30 has increased $[Ca^{2+}]_i$, hyperactive HC, non-functional GJ channels and altered response to purinergic stimulus. Considering that, we evaluated Ca^{2+} response to purinergic stimulus (ATP, 100 µM) in control and cKI Cx26S17F cochlear explants from P7 $Cx26^{+/floxS17F}$ mice, in absence or presence of $[Ca^{2+}]_e$.

OSC and PC Ca^{2+} response is shown in absence (Figure 19, panel A) and presence (Figure 19, panel B) of $[Ca^{2+}]_e$. In Ca^{2+}-free solution, $Cx26^{+/floxS17F}$ cochlear explants treated with TAT-Cre recombinase (cKI Cx26S17F) decreases response to purinergic stimulus compared to non-treated explants. When explants are incubated in basal Ca^{2+} condition (Figure 19, panel B), similar to perilymph (1.26 mM), cKI Cx26S17F expression increases Ca^{2+} response to ATP. On contrary, expression of mutant Cx26S17F in ISC increases Ca^{2+} response in absence of $[Ca^{2+}]_e$ when compared to control; but in presence of $[Ca^{2+}]_e$, they do not show differences in their Ca^{2+} response.

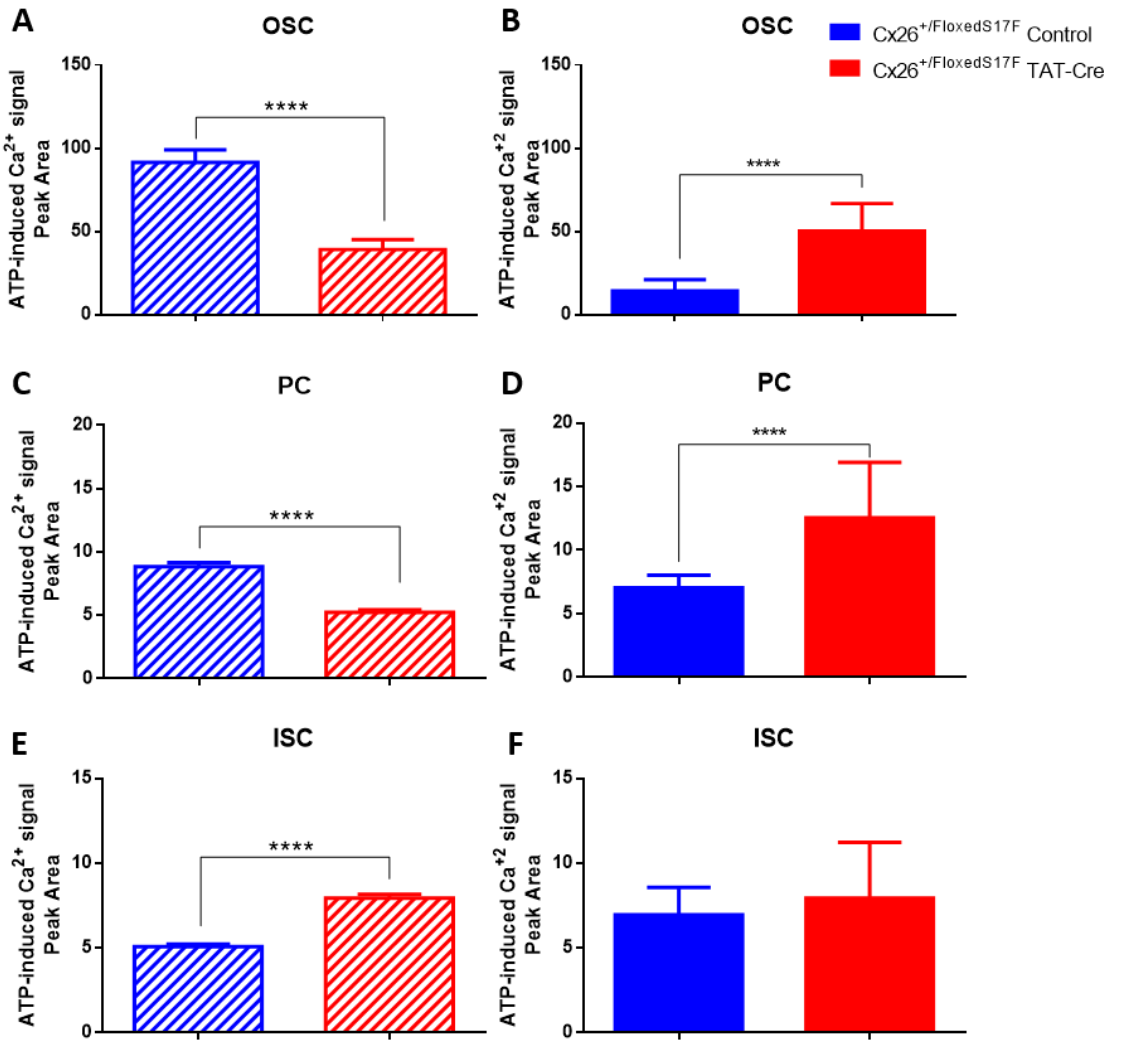

Figure 19. cKI Cx26S17F expression in cochlear explants show altered ATP-induced Ca^{2+} response in absence or presence of $[Ca^{2+}]_e$

In Ca^{2+}-free register solution, OSC (A) and PC (C) of cKI Cx26S17F cochlear explants showed decreased response to 100µM ATP, while ISC (E) showed increased response, compared to non-treated $Cx26^{+/floxS17F}$ explants. (**** $p<0.0001$). Meanwhile, in 1.26 mM $[Ca^{2+}]_e$, cKI Cx26S17F cochlear explants showed increased response to the same exogenous ATP concentration in OSC (B) and PC (D) (****$p<0.0001$). No significant difference was observed in ISC (p 0.0763). These observations suggest strong influence on $[Ca^{2+}]_e$ and activity of supporting cells HC.

DISCUSSION AND CONCLUSIONS

In the present work, we demonstrate the formation of mutant heteromeric HCs formed by Cx26S17F and Cx30 producing hyperactive HCs and non-functional GJCs in HeLa cells. Remarkably, these mutant heteromeric HCs present reduced sensibility to extracellular Ca^{2+} regulation, which is also related to increased cell death. The expression of Cx26S17F in cochlear explants expressing the cKI also induced the formation of hyperactive HC in supporting cells of the organ of Corti, which was associated to increased damage in sensorial hair cells stereocilia. These results support a pathological mechanism of syndromic deafness in which dysregulation of HCs and loss of function in GJ channels impact cochlear homeostasis. This is the first study showing functional characterization functional of HCs and GJCs in cochlea expressing syndromic mutations in Cx26.

I.- Syndromic deafness mutation S17F does not affect the compatibility of Cx26 to interact with Cx30.

Previously, our laboratory reported the interaction of mutated Cx26S17F with Cx43 producing aberrant hyperactive HCs and non-functional GJCs associated with increased intracellular calcium (García et al., 2015). The previous observation was surprising because it has been known for long time that Cx26 and Cx43 were non-compatible Cxs to form heteromeric channels (Rouan et al., 2001). Hence, these results implicate that mutation S17F changes the Cx26 oligomerization compatibility. The interaction between Cx26S17F and Cx43 may explain the symptoms in the skin where both Cxs are co-expressed; however, Cx26 is co-expressed with Cx30 and not with Cx43 in supporting cells of the organ of Corti in the cochlea. It is well described that Cx26 and Cx30 interact and form functional heteromeric HCs and GJCs (Yum et al., 2007) but it is unknown whether S17F mutation may alter the regular compatibility between

Cx26 and Cx30, this question is relevant since mutation S17F seems to modify Cx26 compatibility.

Here, using transfected HeLa cells and co-localization analysis, we demonstrate that Cx30 colocalizes with both Cx26 WT and mutated Cx26S17F (Figures 7, 8 and 9). Pearson and Manders colocalization coefficients strongly support that Cx30 colocalized with Cx26 WT and Cx26S17F (Figure 7). Proximity Ligation Assay further confirmed direct interactions of Cx30 with Cx26 WT or Cx26S17F (Figure 9). While in WT heteromeric condition, Cx26 and Cx30 co-localize mainly in GJ plaques between two adjacent cells, with minor localization in intracellular compartment, the opposite was found for Cx26S17F/Cx30 heteromeric HCs where these Cxs co-localize mostly in intracellular compartment (Figures 7 and 8), suggesting an altered traffic due to the mutation. Despite of that, some HCs made by Cx30 and Cx26S17F can go to the plasma membrane because small GJ plaques formed by Cx26S17F/Cx30 were still observed between two adjoined cells. Similar results were observed for the interaction of Cx43 with Cx26S17F, where the co-localization of these Cxs is mainly intracellular with few and small GJ plaques (García et al., 2015). The finding that mutant Cx26S17F affects the trafficking of other co-expressed Cxs, is in agreement with the observation that other KID mutations in Cx26 like G12R and D50N, also affect the traffic of Cx HCs (Common et al., 2003; Meşe et al., 2007; García et al., 2015). Interestingly, similar results were also obtained with mutations in Cx31 (R42P, 66delD, G12R, G12D and C86S) that cause a skin disorder called Erythrokeratodermia variavilis (Meşe et al., 2007). These findings support a common mechanism of syndromic deafness mutations with skin phenotype that involved mislocalization of HCs and GJ channels. Vesicles containing Cxs are released from the endoplasmic reticulum, as for W-type connexins Cx26 and Cx30 (Smith et al., 2012), to go to the membrane, in the case of Cx26, using microtubules that carry the vesicles as a cargo (Martin et al., 2001; Koval, 2006). In that vesicles, HCs travel in close configuration, and remain closed until specific ions, molecules or voltages open the HCs (Laird, 2006). Understand the mechanism of the inappropriate traffic of

heteromeric HC formed by Cx26S17F/Cx30 is a still an open question and also a future projection of this study to be addressed.

Overall, these morphological results indicate that even when Cx26S17F change the capability of Cx26 to interact with Cx43 (García et al., 2015; Rouan et al., 2001), it does not affect the interaction of mutant Cx26 with Cx30. In β-connexins, as in Cx26 (GJB2) and Cx30 (GJB6), S17 is a well conserved residue in the polypeptide chain, while in α-connexins, this serine occupies position 18 (Beyer et al., 2012); being a critic residue in the maintenance of the pore structure, since interactions between N-terminal and TM1 help to maintain the channel open during gating process (Beyer et al., 2012; García et al., 2016b). In addition, amino acid residues in Cx26 involved in oligomerization with other Cxs seems to be mainly located in the N-terminal and TM1 (García et al., 2016b; Segretain and Falk, 2004).

There is a “selectivity signal” in the N-terminal that allows the interaction between two connexins to form heteromeric HC (Segretain and Falk, 2004; Lagree et al., 2003; Thévenin et al., 2013). In addition, other Cx signals may be Cx specific and located in the TM1 and TM3 (Martinez et al., 2011; Jara et al., 2012). The protein domains involved in the interaction are mainly composed of hydrophobic residues, which is the case of TM segments. Indeed, TM1 also has these hydrophobic residues, making it part of the “selectivity signal” in Cx subunits (Martínez et al., 2011; Jara et al., 2012; Segretain and Falk, 2004). Therefore, our results support an hypothesis in which Cx-Cx compatibility for oligomerization requires more than one specific domain, since mutation S17F in the NT domain affects the compatibility to interact with Cx43, but it does no change the normal property Cx26 to interact with Cx30, indicating that this mutation is not sufficient to transform completely the pattern of Cx26 compatibility.

By itself, Cx30 has several interesting features that can explain the capacity to interact with mutant Cx26S17F. It has been described that Cx30 can interact with Cxs of groups α and β, having the ability to interact with 7 different Cxs to form heterotypic GJs (Harris, 2001). Then, the capacity to form heterotypic GJ also suggest that the Cxs is able to form heteromeric HCs with

the same Cxs (Harris, 2001) being a very promiscuous Cx in terms of compatibility. Also, Cx30 has a different way to assemble GJ plaques, without using ZO-1, but β-actin directly (Defourny et al., 2019). It is possible to speculate that even when Cx26S17F by itself is not functional and remains mainly in the intracellular space, and also sequesters Cx30 to the intracellular area, the minor part of heteromeric channels that in fact goes to the membrane, is due to trafficking properties of Cx30. The use of antibodies to block these accessory proteins would help to evaluate these ideas. On the other hand, it would be interesting to determine if the vesicles containing CxS17F/Cx30 released from the ER might be interacting with the cytoskeleton in an altered fashion that may lead to traffic problems inside the cell or if the vesicles interact with other molecules in their pathway affecting the general homeostasis of the cell.

II.- Mutant Cx26S17F is functional *trans* dominant-negative of Cx30 gap junction channels

We evaluated the functional state of GJ channels by two different approaches, by FRAP and microinjection, using calcein and Lucifer yellow as permeability tracers, respectively (Figure 10). Only a slight amount of calcein was recovered in a bleached cell expressing Cx26S17F/Cx30 GJ channels (Figure 10, panel C), but no activity was observed when LY was used as tracer of GJ function (Figure 10, panel D). This contrast with the high intercellular coupling that we observed between cells expressing WT Cx26 or 30 or co-expressing both Cxs, which is consistent with previous publications (Yum et al., 2007). Observations presented in this research suggests a *trans* dominant-negative effect of Cx26S17F over Cx30. Trans dominant negative effect is a common feature in non-syndromic and also syndromic deafness of Cx mutations over the WT protein, in this case not the same Cx26 WT but Cx30 WT function (Yum et al., 2010); while “dominant negative” refers to one mutation in an allele, affecting the WT allele in a gene (for comprehensive revision see (García et al., 2016b). However, some mutations also have a mild negative effect, in which GJ channels present reduced transfer of specific second messengers, such as IP3, but maintain the transfer of ionic current intact through these

channels (García et al., 2016b). This observation is very important in the context of the cochlea, because cochlear sensory epithelium is a poorly vascularized tissue (Pickles, 2015). Looking a sagittal cut of *scala media*, the irrigated tissue would be only the *stria vascularis*, where the perilymph is generated from blood serum (Mammano, 2018; Li–dong et al., 2008; Kikuchi et al., 2000a) Irrigation in the sensory epithelial tissue is made up by cochlear artery, in the ¾ upper portion of the cochlea. In the fourth lower part there is the vestibulocochlear artery irrigating the tissue. All of these anatomical features are important because the gap junction network connecting supporting cells and the network in the lateral wall are the principal way of cells to obtain nutrients, secondary messengers, and all physiological molecules relevant for the correct function of the auditory tissue (Pickles, 2015; Johnson et al., 2017; Ceriani et al., 2019; Zhao et al., 2005). If the gap junction network is not working properly, all cells depending on them might be affected. Recycling of K^+, IP_3 transport, ATP and Ca^{2+} transport, among others, would be altered (Majumder et al., 2010; Piazza et al., 2007; Zhao and Yu, 2006; Verselis, 2017; Jagger and Forge, 2015; Forge et al., 2003b). In addition, some animal models of non-syndromic deafness produced by expression of mutant Cx26 have shown that lack or reduction in GJ function alter the proper development of the cochlea (Zhu et al., 2015; Johnson et al., 2017; Nickel and Forge, 2008) which is consistent with the importance of GJ network for cochlear function and development. Finally, with the experiments presented here it is impossible to determine whether heteromeric mutant GJCs present changes in single channel properties. However, because the cell that co-express Cx26S17F and Cx30 still present some intercellular transfer of calcein, which has a molecular radius of 6.5 Aº (Tambutté et al., 2011) but not to Lucifer yellow that has a slightly bigger radius of 9.9 Aº (Heyman and Burt, 2008) and considering that both tracers are anionic, we cannot discard that this mutant heteromeric GJC can be functional but with a reduced pore size.

III.- Heteromeric HC formed by Cx26S17F and Cx30 are hyperactive and less sensitive to extracellular Ca^{2+} and La^{3+}

We evaluated the function of Cx26S17F/Cx30 HCs by dye uptake approach (Figure 11), where we observed that mutant heteromeric HC are hyperactive and do not respond properly to extracellular Ca^{2+} nor La^{3+}, suggesting an abnormal gating by extracellular cations; which is in accordance with the functional properties of other mutations involved in KID syndrome (García et al., 2015, 2016a; Mhaske et al., 2013). According to literature, Ca^{2+} binding site might be located in the extracellular side of the pore at D50 and K61 that, when Ca^{2+} bound to those residues, destabilizes open state probability of HC, keeping them in a closed state (Lopez et al., 2016). Also, previous reports from our laboratory and others show that the mutation G12R, also located in the NT, has a disrupted fast and slow gating, which favors the open state probability of those mutated HC, and it is independent of $[Ca^{2+}]_e$. Molecular dynamics of this mutation shows that there is a displacement in the NT which favors an abnormal interaction with the intracellular loop, that disrupt the fast and slow gating (García et al., 2018; Sanchez et al., 2016). Even when we cannot assert that this disrupted mechanism might be happening with the S17F mutation, they certainly have several functional hallmarks in common. Future electrophysiological studies assessing unitary currents in Cx26S17F/Cx30 may help to understand this question. The fact that mutant heteromeric Cx26S17F/Cx30 HC do not respond to Ca^{2+} nor La^{3+} suggest that both cations may be acting in the same binding sites, however, little is known about the binding site of La^{3+}. La^{3+} was thought to physically block the HC pore, but it was demonstrated that reversing the voltage polarity in attempt to force La^{3+} cations to unblock the pore did not work (Brokamp et al., 2012). Others suggest that La^{3+} may be affecting the lipid environment in the plasmatic membrane (Hauser et al., 1975), but it is still a matter of debate (Brokamp et al., 2012).

There are two mechanisms proposed to the blockage of Cx HCs by extracellular Ca^{2+}: A) electrostatic mechanism by which the binding of Ca^{2+} into the extracellular side of the pore generates a large and positive electrostatic potential that hinders cation flux. This hypothesis

was strongly supported by a crystallographic structure of the Cx26 channel in a Ca^{2+} bound configuration that shows no major structural changes around the pore (Bennett et al., 2016). However, two independent studies did not support this hypothesis. Lopez and colleagues show that the small charged MTSES (2-sulfonatoethyl methanethiosulfonate) reagent and Cd^{2+} can pass through the putative Ca^{2+} binding site, suggesting that the gating of Cx26 HCs promoted by Ca^{2+} is not electrostatic (Lopez et al., 2016). On the other hand, analysis of the water permeability of Cx46 HCs expressed in *Xenopus* oocytes under hypotonic conditions, in Ca^{2+}-free and high Ca^{2+} medium, shows that Ca^{2+} binding to HCs reduced the passage of water indicating that extracellular Ca^{2+} binding promotes the closing of a physical gate in the channel (Pinto et al., 2017). B) The second hypothesis is that binding of extracellular Ca^{2+} induce a physical blockage, like a plug that clogs the HC, impairing normal flux of ions and molecules. This hypothesis is strongly supported by structural studies with atomic force microscopy showing that in the presence of Ca^{2+} the extracellular mouth of the channel narrows (Müller et al., 2002). It is unknown how the mutation S17F can affect the gating properties induced by Ca^{2+} in heteromeric HCs, but previous reports suggested that Ca^{2+} binds only to the closed state of HCs by a voltage independent mechanism (Pinto et al., 2017) hence it is possible that this mutation may uncouple Ca^{2+} binding with the gating mechanism. Remarkably, a detailed analysis of the activation and deactivation channel kinetics suggests that Ca^{2+} and voltage sensors are allosterically coupled to promote hemichannel closing (Pinto et al., 2017).

Until now, the effect of the mutation S17F on the configuration of Cx26 is still unknown. As mentioned previously, S17 is located in the N-terminal of the protein, a domain involved in gating, selectivity and polarity of the channel; while Ca^{2+} and La^{3+} regulates HCs by the extracellular side of the membrane, in an undocked configuration (Brokamp et al., 2012; Lopez et al., 2013; García et al., 2018). These observations suggest that mutation S17F may be affecting the quaternary structure of the protein, causing a conformational change in the HC that cannot be regulated properly. Residue S17 is involved in the hinge that allows the NT to get into the pore. The 6 N terminals of each connexin in a HC form a funnel-like shape which constrict

the cytoplasmic side of the pore, which in Cx26 WT is about 14 Å diameter (Beyer et al., 2012; Retamal et al., 2015; Maeda et al., 2009). When mutation S17F is present, this mechanism might be damaged or altered avoiding the hinge to flex properly due to the aromatic ring in the radical group of phenylalanine. Therefore, the presence of a phenylalanine in this position may prevent the proper constriction of the pore, altering the regular salt bridges that bind TM1 with NT inside the pore or more drastically NT might not get into the pore at all. This may result in a bigger pore that allows the passage of molecules even in presence of cations in the extracellular milieu. Also, mutation S17F may alter the quaternary structure of the Cx26 impeding the response to Ca^{2+}_e regulation masking the sensors or by allosteric impediment. All of these consequences highlight the critical impact that mutations in highly conserved residues can have. In this regard, mutations in a well conserved residue as Ser17 shows several examples among other α and β Cxs, including Cx26S17Y, where the mutation leads the patient to present non syndromic hearing impairment when expressed as compound heterozygosity with the c.35delG mutation (Tóth et al., 2004) and Cx32S17Y mutation is involved in Charcot-Marie-Tooth disease (Brožková et al., 2010) for β Cxs. In α Cxs, serine is in the position 18, where the mutation Cx43S18P leads to Oculodentodigital dysplasia (Paznekas et al., 2003)

Then we asked whether the mutant heteromeric Cx26S17F/Cx30 has an increased intracellular $[Ca^{2+}]_{I,}$ since Ca^{2+} is one of the ions and molecules that can pass through HC (Fiori et al., 2012) and is a second messenger in the purinergic pathway, that may be altered in the KID pathology. Using Fura-2 ratiometric sensor, we observed that $[Ca^{2+}]_I$ influx was higher at 1 and 1.5 mM $[Ca^{2+}]_e$ in HeLa cells expressing Cx26S17F/Cx30, consisting with the lower sensitivity to extracellular Ca^{2+} discussed above (Figure 12, panel A). In addition, under basal conditions the Ca^{2+} flux increment was higher in the mutant heteromeric HC, suggesting that $[Ca^{2+}]_I$ stays elevated in HeLa cells expressing Cx26S17F/Cx30 HC related to WT counterpart (Figure 12, panel B). This observation was important because increased $[Ca^{2+}]_I$ may lead to cell death, which can be part of the symptoms of KID pathophysiology (Terrinoni et al., 2010; Vinken et al., 2011, 2006; Decrock et al., 2011). Increased intracellular Ca^{2+} concentration may also

affect functionality of HC and GJ channels. For example, several Cxs present regulation by Ca^{2+}/CaM through the intracellular side, where Ca^{2+} binds CaM, which in turn can bind to Cx intracellular domains (IL or CT). CT domain binds IL in a Ca^{2+}/CaM-dependent way, opening the HC at around 500 nm $[Ca^{2+}]_i$ in a mechanism called “ball and chain” (De Vuyst et al., 2006). Interestingly, for GJ channels, an increment in $[Ca^{2+}]_I$ has the opposite effect, closing the GJ as observed by the loss of junctional conductance (Peracchia, 2004), also in a Ca^{2+}/CaM dependent way (Peracchia, 2020). Even when it is still unknown whether calmodulin binds Cx26 or Cx30, there are putative binding sites that need to be explored, since we observed an increment in the $[Ca^{2+}]_I$ in cells expressing Cx26S17F/Cx30.

IV.- Co-expression of Cx26S17F and Cx30 HCs increases cellular damage and death

Given the altered functions in HC and GJs, and the increased $[Ca^{2+}]_i$ and the low sensitivity to HC regulation by divalent cations, we evaluated the level of cell damage and cell death in transfected HeLa cell. Consistent with the previous observations, we found increased cellular damage and death in cells expressing Cx26S17F and Cx30 (Figure 13).

There are several cases where hyperactive HC due to mutations in Cxs has been related to increased release of ATP and activation of purinergic receptors, leading to an increment in the $[Ca^{2+}]_I$ (Retamal et al., 2015). For instance, Clouston syndrome due to Cx30 G11R or A88V mutations shows hyperactive HCs, with increased release of ATP to the extracellular space and increased $[Ca^{2+}]_I$ which leads to cell death (Essenfelder et al., 2005). In normal cardiac tissue, cardiomyocytes express Cx43 (reviewed in Retamal et al., 2015); however, several mutations related to heart disease as in I31M, G143S, G138R lead to hyperactive HCs which allow the release of ATP. In that tissue, ATP released from mutant hyperactive HCs activates P2Y2, leading to increased $[Ca^{2+}]_I$ and the expression of several proteins trough a ERK mediated pathway (Lu et al., 2012). Cx43 G138R is also involved in

Oculodentodigital dysplasia (Dobrowolski et al., 2007) and enteric gliotransmission (Grubišić and Parpura, 2017), where in the intestine Cx43 G138R HCs increase the release of ATP and activation of P2Y1/4 purinergic receptors, which increases cell death (Grubišić and Parpura, 2017).

Cx43 is also expressed in astrocytes, which in normal circumstances Cx43 HC are normally closed. In several neurodegenerative diseases, as in ischemia and Alzheimer's disease HCs are hyper activated, leading to release of ATP and glutamate, among other molecules. Neurodegenerative diseases like encephalitis, Alzheimer's disease, amyotrophic lateral sclerosis and Parkinson's disease show a common feature of inflammation, which induces formation of ROS that also open Cx43 HC in glial cells, allowing increased release of ATP and other signaling molecules, that leads to neuronal death (Retamal et al., 2015; Orellana et al., 2012; He et al., 2020; Giaume et al., 2017).

V.- Expression of Cx26S17F in mouse cochlear explants changes the sub-cellular distribution of connexins in supporting cells of the organ of Corti.

To understand how these critical observations may be affecting the cochlea, in particular the supporting cells of the organ of Corti (Figure 14), we used cochlear explants from $Cx26^{+/floxedS17F}$, which is a mouse strain that carries Cx26S17F but do not express it, until floxed Cx26 WT gene (GjB2) is cleaved by Cre enzyme. When that cleavage occurs, Cx26 WT gene is removed and Cx26S17F is expressed in every cell that should have the WT Cx and is regulated under the same Cx26 WT promoter. To express cKI Cx26S17F in cochlear explants, we first attempted to use a crossing between $Cx26^{+/floxedS17F}$ strain with CMV-Cre mouse strain, in order to replicate the entire KID syndrome in the whole animal (Schutz, 2011). However, the lethality rate was too high, so we induced the flox-Cre mechanism with a diffusible TAT-Cre enzyme that can pass the cell membrane due to the TAT sequence from viral origin (Figure 15).

VI.- Expression of Cx26S17F produce HCs hyperactivity in supporting cells of the organ of Corti and damage of hair cells

As observed previously in HeLa cells, cKI Cx26S17F cochlear explants showed a change in the distribution of Cx26, as well as in Cx30 (Figure 15). Mutant heteromeric HCs remain mainly in the intracellular space in inner and outer supporting cells of the organ of Corti, with smaller GJ plaques observed frequently (not quantified), and increased HC function (Figure 15, panel C). Pillar cells and Deiters cells did not show and evident change in the subcellular distribution of Cx26 or Cx30 (Figure 15, panel C), but they did show altered functions, as increased HC activity evaluated by dye uptake (Figure 16, panel C). Inner supporting cells located next to inner hair cells and deeper in the GER area showed a highly disrupted expression of Cx26 and Cx30, with smaller GJ plaques and a very punctuated phenotype, compared to non-treated cochlear explants (Figure 15).

As mentioned above, proper GJ function has biological relevance in an non-vascularized or low vascularized tissue like the organ of Corti, because GJ network allows the metabolic coordination and cell synchronization between supporting cells (Kikuchi et al., 2000b; Meşe et al., 2007; Pickles, 2015). The lack of function in GJ channels appears to be a common feature in syndromic and non-syndromic deafness, with a few exceptions, indicating the importance of these channels for audition. Also, different mutations cause different degrees of deafness, which is highly related with the GJ function described for each specific mutation in GJB2 (Martínez et al., 2009; Jara et al., 2012; García et al., 2016b), with the exception of A40V and G45E, that even when their phenotypes includes severe deafness, their GJs still work properly (García et al., 2016b).

Even when HC expression in normal tissue has been controversial (Verselis, 2017; Sáez and Leybaert, 2014), it has been suggested that connexin HCs in the cochlea are located in the apical portion of supporting cells, being covered (filled) with endolymph, the scala media fluid that lacks Ca^{2+} (Pickles, 2015). HCs in supporting cells might be important allowing the pass of

important molecules like ATP (Anselmi et al., 2008; Burnstock and Dale, 2015; Lee and Marcus, 2008; Verselis, 2017; Zhao et al., 2005; Ortolano et al., 2008). In development, this is especially relevant because ATP release is involved in the tuning process of hair cells firing, synchronizing depolarization and consequent release of glutamate (Bulankina and Moser, 2012; Mammano, 2018; Dayaratne et al., 2014; Pickles, 2015). A hyperactive HC would disrupt this highly controlled process; and leading to supporting cell death, affecting its homeostasis and increasing its intracellular calcium concentration. So, we evaluated dye uptake by Cx HCs, in basal (1.26 mM Ca^{2+}, same as the perilymph Ca^{2+} concentration), in Ca^{2+}-free solution (as in endolymph) and then we added Cx blocker CBX, to assure that this was a connexin-formed channel function. Using this approach, we observed two important events, as mentioned previously in the result section (Figure 16). First, our data strongly indicates the expression of Cx HCs in normal tissue, since they behaved as expected HC in control cochleae: they responded to variations in extracellular [Ca^{2+}], increasing uptake rate when Ca^{2+} was removed, and this activity was blocked by CBX (Mammano, 2013; Ceriani et al., 2019; Sirko et al., 2019). And second, in cochlea explants treated with TAT-Cre, mutated HC present in supporting cells showed a hyperactive profile, and they were active in presence of extracellular Ca^{2+} (Figure 16). To our knowledge, this is the first demonstration of hyperactive HC induced by expression of Cx26 with syndromic deafness mutation in real cochlear tissue. It is a challenge to extrapolate this result as a possible pathological mechanism for syndromic deafness, mainly because this is an acute effect of expression of mutant Cx26, instead of a real model in which expression could occur early in development (Schütz et al., 2011); however, the fact that this increased HC activity was associated to damage of hair cell in the explants treated with TAT-Cre (Figure 17), support the hypothesis that deregulation of HC activity affect the homeostasis of sensory cells. The preliminary results with cochlear explants from the cKI animal expressing Cx26S17 support the previous hypothesis, because the organ of Corti present overall normal morphology but it also shows loss of hair cells stereocilia (Figure 17). The mechanism by which hyperactive HC from supporting cells damage hair cells needs to be dilucidated in further studies, however, it can be

inferred that this damage could be related with more ATP release through HC and activation of purinergic receptor in hair cells. In this regard, it would be interesting to quantify ATP release though HC in cochlear explants of cKI Cx26S17 and WT animals, and to evaluate hair cell damage with annexin V in presence of broad spectrum purinergic blocker suramin and blockers of specific purinergic receptors to understand a possible relation between those phenomena.

An important feature to be considered will be to understand the function of GJ channels in cKI Cx26S17F cochlear explants, and how it could affect the transport of molecules and ions like IP3, Ca^{2+} and K^{+}, among others. Also, to understand the impact of this mutation on HCs and GJs during auditory development, since we used a conditional KI model that expressed the mutation only at P7.

VII.- Expression of Cx26S17F in HeLa cells and cochlea supporting cells differentially affect purinergic signaling

Finally, we briefly evaluated Ca^{2+} responses induced by exogenous ATP in control and cKI Cx26S17F cochlear explants and in transfected HeLa cells, in absence and presence of $[Ca^{2+}]_e$. We evaluated the response to a purinergic stimulus with a puff of 100 µM ATP in HeLa cells co-transfected with Cx26S17F and Cx30 (Figure 18) and observed that cells expressing mutant Cx26S17F/Cx30 showed lower Ca^{2+} responses than cells expressing Cx26WT/Cx30. Similarly, in cochlear explants of cKI Cx26S17F mice (Figure 19), outer supporting cells have lower Ca^{2+} responses induced by ATP compared to control explants. However, in absence of $[Ca^{2+}]_e$, the Ca^{2+} response in ISC was higher than control. This observation might be related to different types of purinergic metabotropic receptors present in those cells, since the Ca^{2+} response observed came from intracellular stores (Horváth et al., 2016; Piazza et al., 2007). Ca^{2+} waves can be spread through GJ, as the ion and IP_3 second messenger can pass through GJ (Beltramello et al., 2005; Mammano and Bortolozzi, 2017; Majumder et al., 2010), but

according to observations in HeLa cells, GJ might be disrupted in this model. In presence of $[Ca^{2+}]_e$, Ca^{2+} response induced by exogenous ATP was higher in cKI Cx26S17F supporting cells that in control cochleae. Again, this observation might be due to different purinergic receptors, which in this case can be metabotropic and ionotropic, allowing the pass of extracellular Ca^{2+} through purinergic and hyperactive Cx HC. Further experiments will help to understand these observations.

As a future projections of this research it would be interesting to determine the release of ATP by HC in WT and mutant conditions, in transfected HeLa cells as well as in cochleae of cKI Cx26S17F and WT animals, in order to understand if purinergic signaling is altered in these systems. As mentioned previously ATP is an important regulator of inner ear development (Anselmi et al., 2008; Verselis, 2017) thus an excessive release of ATP or its metabolites may alter the proper function of the organ of Corti. It will be important to understand how the mutation might be altering the $[Ca^{2+}]_i$ due to altered purinergic signaling and/or altered buffering of calcium that has entered by hyperactive channels. In addition, it should be necessary to address the possibility of recovering hearing in a cKI Cx26S17F mice by intracochlear treatment with purinergic blockers, and to integrate all this knowledge in order to get therapeutic help to patients who express Cx26S17F mutation in the inner ear.

In conclusion, the data presented here can contribute to the understanding of the pathological mechanisms that produce severe to profound deafness in KID syndrome.

A

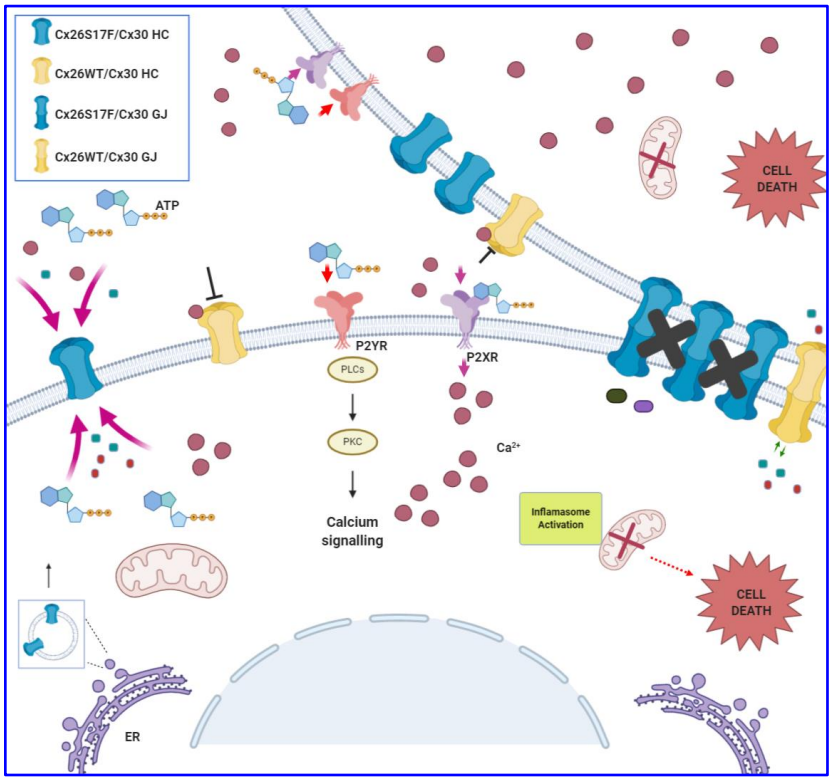
Cx26S17F/Cx30 HC
Cx26WT/Cx30 HC
Cx26S17F/Cx30 GJ
Cx26WT/Cx30 GJ
ATP
CELL DEATH
P2YR
P2XR
PLCs
PKC
Ca2+
Calcium signalling
Inflamasome Activation
CELL DEATH
ER

B

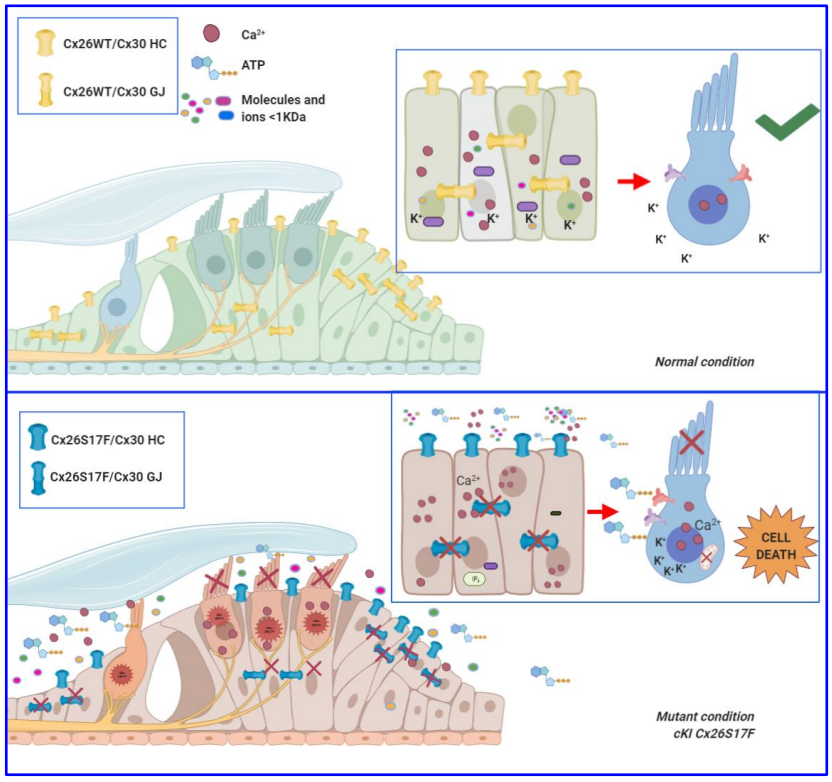
Cx26WT/Cx30 HC
Cx26WT/Cx30 GJ
Ca2+
ATP
Molecules and ions <1KDa
K+
Normal condition
Cx26S17F/Cx30 HC
Cx26S17F/Cx30 GJ
Ca2+
CELL DEATH
Mutant condition
cKI Cx26S17F

Previous page **Figure 20. Graphic conclusions.**

Mutant heteromeric HCs formed by Cx26S17F and Cx30 produce hyperactive HCs and non-functional GJCs in HeLa cells, which also show reduced sensibility to extracellular Ca^{2+} regulation, finally related to increased cell death. These results may represent a pathological mechanism of syndromic deafness in which dysregulation of HC and loss of function in GJ channels impact cochlear homeostasis.

REFERENCES

Ahmad, S., S. Chen, J. Sun, and X. Lin. 2003. Connexins 26 and 30 are co-assembled to form gap junctions in the cochlea of mice. *Biochem. Biophys. Res. Commun.* 307:362–368. doi:10.1016/S0006-291X(03)01166-5.

Alvarez, A., I. del Castillo, A. Pera, M. Villamar, M.A. Moreno-Pelayo, F. Moreno, R. Moreno, and M.C. Tapia. 2003. De novo mutation in the gene encoding connexin-26 (GJB2) in a sporadic case of keratitis-ichthyosis-deafness (KID) syndrome. *Am. J. Med. Genet. A*. 117A:89–91. doi:10.1002/ajmg.a.10851.

Anselmi, F., V.H. Hernandez, G. Crispino, A. Seydel, S. Ortolano, S.D. Roper, N. Kessaris, W. Richardson, G. Rickheit, M.A. Filippov, H. Monyer, and F. Mammano. 2008. ATP release through connexin hemichannels and gap junction transfer of second messengers propagate Ca2+ signals across the inner ear. *Proc. Natl. Acad. Sci.* 105:18770–18775. doi:10.1073/pnas.0800793105.

Ashmore, J. 2008. Cochlear outer hair cell motility. *Physiol. Rev.* 88:173–210. doi:10.1152/physrev.00044.2006.

Ashmore, J.F., and H. Ohmori. 1990. Control of intracellular calcium by ATP in isolated outer hair cells of the guinea-pig cochlea. *J. Physiol.* 428:109–31. doi:10.1113/jphysiol.1990.sp018203.

Avshalumova, L., J. Fabrikant, and A. Koriakos. 2014. Overview of skin diseases linked to connexin gene mutations. *Int. J. Dermatol.* 53:192–205. doi:10.1111/ijd.12062.

Baroja-Mazo, A., M. Barberà-Cremades, and P. Pelegrín. 2013. The participation of plasma membrane hemichannels to purinergic signaling. *Biochim. Biophys. Acta - Biomembr.* 1828:79–93. doi:10.1016/j.bbamem.2012.01.002.

Beltramello, M., V. Piazza, F.F. Bukauskas, T. Pozzan, and F. Mammano. 2005. Impaired permeabilty to Ins(1,4,5)P3 in a mutant connexin underlies recessive hereditary deafness. *Nat. Cell Biol.* 7:63–69. doi:10.1038/ncb1205.

Bennett, B.C., M.D. Purdy, K.A. Baker, C. Acharya, W.E. McIntire, R.C. Stevens, Q. Zhang, A.L. Harris, R. Abagyan, and M. Yeager. 2016. An electrostatic mechanism for Ca2+-mediated regulation of gap junction channels. *Nat. Commun.* 7:8770. doi:10.1038/ncomms9770.

Berger, A.C., J.J. Kelly, P. Lajoie, Q. Shao, and D.W. Laird. 2014. Mutations in Cx30 that are linked to skin disease and non-syndromic hearing loss exhibit several distinct cellular pathologies. *J. Cell Sci.* 127:1751–1764. doi:10.1242/jcs.138230.

Beyer, E.C., G.M. Lipkind, J.W. Kyle, and V.M. Berthoud. 2012. Structural organization of intercellular channels II. Amino terminal domain of the connexins: Sequence, functional roles, and structure. *Biochim. Biophys. Acta - Biomembr.* 1818:1823–1830. doi:10.1016/j.bbamem.2011.10.011.

Brokamp, C., J. Todd, C. Montemagno, and D. Wendell. 2012. Electrophysiology of Single and Aggregate Cx43 Hemichannels. *PLoS One*. 7:1–11. doi:10.1371/journal.pone.0047775.

Brožková, D., R. Mazanec, J. Haberlová, I. Sakmaryová, I. Šubrt, and P. Seeman. 2010. Six new gap junction beta 1 gene mutations and their phenotypic expression in czech patients with charcot-marie-tooth disease. *Genet. Test. Mol. Biomarkers*. 14:3–7. doi:10.1089/gtmb.2009.0093.

Bulankina, A. V., and T. Moser. 2012. Neural circuit development in the mammalian cochlea. *Physiology*. 27:100–112. doi:10.1152/physiol.00036.2011.

Burnstock, G. 2006. Purinergic signalling. *Br. J. Pharmacol.* 147:172–181. doi:10.1038/sj.bjp.0706429.

Burnstock, G., and N. Dale. 2015. Purinergic signalling during development and ageing.

Purinergic Signal. 11:277–305. doi:10.1007/s11302-015-9452-9.

Ceriani, F., A. Hendry, J. Jeng, S.L. Johnson, F. Stephani, J. Olt, M.C. Holley, F. Mammano, J. Engel, C.J. Kros, D.D. Simmons, and W. Marcotti. 2019. Coordinated calcium signalling in cochlear sensory and non-sensory cells refines afferent innervation of outer hair cells. *EMBO J.* 38:1–19. doi:10.15252/embj.201899839.

Ciganović, N., A. Wolde-Kidan, and T. Reichenbach. 2017. Hair bundles of cochlear outer hair cells are shaped to minimize their fluid-dynamic resistance. *Sci. Rep.* 7:1–9. doi:10.1038/s41598-017-03773-y.

Common, J.E.A., W.L. Di, D. Davies, H. Galvin, I.M. Leigh, E.A. O'Toole, and D.P. Kelsell. 2003. Cellular mechanisms of mutant connexins in skin disease and hearing loss. *Cell Commun. Adhes.* 10:347–351. doi:10.1080/cac.10.4-6.347.351.

Corey, D.P. 2009. Cell biology of mechanotransduction in inner-ear hair cells. *F1000 Biol. Rep.* 1:1–4. doi:10.3410/b1-58.

Cotrina, M.L., J.H.-C. Lin, A. Alves-Rodrigues, S. Liu, J. Li, H. Azmi-Ghadimi, J. Kang, C.C.G. Naus, and M. Nedergaard. 1998. Connexins regulate calcium signaling by controlling ATP release. *Proc. Natl. Acad. Sci.* 95:15735–15740. doi:10.1073/pnas.95.26.15735.

Dayaratne, M.W.N., S.M. Vlajkovic, J. Lipski, and P.R. Thorne. 2014. Kolliker's organ and the development of spontaneous activity in the auditory system: implications for hearing dysfunction. *Biomed Res. Int.* 2014:367939. doi:10.1155/2014/367939.

Decrock, E., M. Vinken, M. Bol, K. D'Herde, V. Rogiers, P. Vandenabeele, D. V. Krysko, G. Bultynck, and L. Leybaert. 2011. Calcium and connexin-based intercellular communication, a deadly catch? *Cell Calcium*. 50:310–321. doi:10.1016/j.ceca.2011.05.007.

Defourny, J., N. Thelen, and M. Thiry. 2019. Mechanisms of Development Cochlear connexin 30 homomeric and heteromeric channels exhibit distinct assembly mechanisms. *Mech. Dev.*

155:8–14. doi:10.1016/j.mod.2018.10.001.

Dobrowolski, R., A. Sommershof, and K. Willecke. 2007. Some oculodentodigital dysplasia-associated Cx43 mutations cause increased hemichannel activity in addition to deficient gap junction channels. *J. Membr. Biol.* 219:9–17. doi:10.1007/s00232-007-9055-7.

Essenfelder, G.M., G. Larderet, G. Waksman, and J. Lamartine. 2005. Gene structure and promoter analysis of the human GJB6 gene encoding connexin30. *Gene*. 350:33–40. doi:10.1016/j.gene.2004.12.048.

Falk, M.M., R.M. Kells, and V.M. Berthoud. 2014. Degradation of connexins and gap junctions. *FEBS Lett.* 588:1221–1229. doi:10.1016/j.febslet.2014.01.031.

Fiori, M.C., V. Figueroa, M.E. Zoghbi, J.C. Sáez, L. Reuss, and G.A. Altenberg. 2012. Permeation of calcium through purified connexin 26 hemichannels. *J. Biol. Chem.* 287:40826–40834. doi:10.1074/jbc.M112.383281.

Fisher, J.A.N., F. Nin, T. Reichenbach, R.C. Uthaiah, and A.J. Hudspeth. 2012. The Spatial Pattern of Cochlear Amplification. *Neuron*. 76:989–997. doi:10.1016/j.neuron.2012.09.031.

Forge, A., D. Becker, S. Casalotti, J. Edwards, N. Marziano, and G. Nevill. 2003a. Gap Junctions in the Inner Ear : Comparison of Distribution Patterns in Different Vertebrates and Assessement of Connexin Composition in Mammals. *J. Comp. Neurol.* 231:207–231. doi:10.1002/cne.10916.

Forge, A., N.K. Marziano, S.O. Casalotti, D.L. Becker, and D. Jagger. 2003b. The inner ear contains heteromeric channels composed of cx26 and cx30 and deafness-related mutations in cx26 have a dominant negative effect on cx30. *Cell Commun. Adhes.* 10:341–346. doi:10.1080/15419060390263010.

García, I.E., F. Bosen, P. Mujica, A. Pupo, C. Flores-Muñoz, O. Jara, C. González, K. Willecke, and A.D. Martínez. 2016a. From Hyperactive Connexin26 Hemichannels to Impairments in

Epidermal Calcium Gradient and Permeability Barrier in the Keratitis-Ichthyosis-Deafness Syndrome. *J. Invest. Dermatol.* 136:574–583. doi:10.1016/j.jid.2015.11.017.

García, I.E., J. Maripillán, O. Jara, R. Ceriani, A. Palacios-Muñoz, J. Ramachandran, P. Olivero, T. Perez-Acle, C. González, J.C. Sáez, J.E. Contreras, and A.D. Martínez. 2015. Keratitis-Ichthyosis-Deafness Syndrome-Associated Cx26 Mutants Produce Nonfunctional Gap Junctions but Hyperactive Hemichannels When Co-Expressed With Wild Type Cx43. *J. Invest. Dermatol.* 135:1338–1347. doi:10.1038/jid.2015.20.

García, I.E., P. Prado, A. Pupo, O. Jara, D. Rojas-Gómez, P. Mujica, C. Flores-Muñoz, J. González-Casanova, C. Soto-Riveros, B.I. Pinto, M.A. Retamal, C. González, and A.D. Martínez. 2016b. Connexinopathies: a structural and functional glimpse. *BMC Cell Biol.* 17:S17. doi:10.1186/s12860-016-0092-x.

García, I.E., F. Villanelo, G.F. Contreras, A. Pupo, B.I. Pinto, J.E. Contreras, and T.P. Acle. 2018. The syndromic deafness mutation G12R impairs fast and slow gating in Cx26 hemichannels. 150.

Van Geel, M., M.A.M. Van Steensel, W. Küster, H.C. Hennies, R. Happle, P.M. Steijlen, and A. König. 2002. HID and KID syndromes are associated with the same connexin 26 mutation. *Br. J. Dermatol.* 146:938–942. doi:10.1046/j.1365-2133.2002.04893.x.

Gerido, D.A., A.M. DeRosa, G. Richard, and T.W. White. 2007. Aberrant hemichannel properties of Cx26 mutations causing skin disease and deafness. *Am. J. Physiol. Physiol.* 293:C337–C345. doi:10.1152/ajpcell.00626.2006.

Giaume, C., J.C. Sáez, W. Song, L. Leybaert, and C.C. Naus. 2017. Connexins and pannexins in Alzheimer's disease. *Neurosci. Lett.* doi:10.1016/j.neulet.2017.09.006.

Godillot, C., M. Severino-Freire, V. Michaud, F. Boralevi, C. Labrèze, V. Guigonis, G. Onnis, F. Morice-Picard, and J. Mazereeuw-Hautier. 2019. Keratitis-Ichthyosis-Deafness Syndrome: Early Death Caused by the GJB2 Mutation p.Gly12Arg. *Acta Derm. Venereol.* 0.

doi:10.2340/00015555-3218.

Gossman, D.G., and H.-B. Zhao. 2008. Hemichannel-mediated inositol 1,4,5-trisphosphate (IP3) release in the cochlea: a novel mechanism of IP3 intercellular signaling. *Cell Commun. Adhes.* 15:305–15. doi:10.1080/15419060802357217.

Grubišić, V., and V. Parpura. 2017. Two modes of enteric gliotransmission differentially affect gut physiology. *Glia*. 65:699–711. doi:10.1002/glia.23121.

Harris, A.L. 2001. Emerging issues of connexin channels: biophysics fills the gap. 34. 325–472 pp.

Harris, A.L. 2007. Connexin channel permeability to cytoplasmic molecules. *Prog. Biophys. Mol. Biol.* 94:120–143. doi:10.1016/j.pbiomolbio.2007.03.011.

Hauser, H., M.C. Phillips, B.A. Levine, and R.J.P. Williams. 1975. Ion-Binding to Phospholipids: Interaction of Calcium and Lanthanide Ions with Phosphatidylcholine (Lecithin). *Eur. J. Biochem.* 58:133–144. doi:10.1111/j.1432-1033.1975.tb02357.x.

He, J.T., X.Y. Ll, L. Yang, and X. Zhao. 2020. Astroglial connexins and cognition: Memory formation or deterioration? *Biosci. Rep.* 40:1–11. doi:10.1042/BSR20193510.

Heyman, N.S., and J.M. Burt. 2008. Hindered diffusion through an aqueous pore describes invariant dye selectivity of Cx43 junctions. *Biophys. J.* 94:840–854. doi:10.1529/biophysj.107.115634.

Horváth, T., G. Polony, Fekete, M. Aller, G. Halmos, B. Lendvai, A. Heinrich, B. Sperlágh, E.S. Vizi, and T. Zelles. 2016. ATP-evoked intracellular Ca2+ signaling of different supporting cells in the hearing mouse hemicochlea. *Neurochem. Res.* 41:364–375. doi:10.1007/s11064-015-1818-4.

Hudspeth, A.J. 2008. Making an Effort to Listen: Mechanical Amplification in the Ear. *Neuron*. 59:530–545. doi:10.1016/j.neuron.2008.07.012.

Jagger, D.J., and A. Forge. 2015. Connexins and gap junctions in the inner ear – it's not just about K+ recycling. *Cell Tissue Res.* 360:633–644. doi:10.1007/s00441-014-2029-z.

Jara, O., R. Acuna, I.E. García, J. Maripillán, V. Figueroa, J.C. Sáez, R. Araya-Secchi, C.F. Lagos, T. Perez-acle, V.M. Berthoud, E.C. Beyer, and A.D. Martínez. 2012. Critical role of the first transmembrane domain of Cx26 in regulating oligomerization and function. *Mol. Biol. Cell*. 23:3299–3311. doi:10.1091/mbc.E11-12-1058.

Johnson, S.L., F. Ceriani, O. Houston, R. Polishchuk, E. Polishchuk, G. Crispino, V. Zorzi, F. Mammano, and W. Marcotti. 2017. Connexin-Mediated Signaling in Nonsensory Cells Is Crucial for the Development of Sensory Inner Hair Cells in the Mouse Cochlea. *J. Neurosci.* 37:258–268. doi:10.1523/JNEUROSCI.2251-16.2016.

Jonard, L., D. Feldmann, C. Parsy, S. Freitag, M. Sinico, C. Koval, M. Grati, R. Couderc, F. Denoyelle, C. Bodemer, S. Marlin, and S. Hadj-Rabia. 2008. A familial case of Keratitis-Ichthyosis-Deafness (KID) syndrome with the GJB2 mutation G45E. *Eur. J. Med. Genet.* 51:35–43. doi:10.1016/j.ejmg.2007.09.005.

Kang, J., N. Kang, D. Lovatt, A. Torres, Z. Zhao, J. Lin, and M. Nedergaard. 2008. Connexin 43 Hemichannels Are Permeable to ATP. *J. Neurosci.* 28:4702–4711. doi:10.1523/JNEUROSCI.5048-07.2008.

Kikuchi, T., J.C. Adams, Y. Miyabe, E. So, and T. Kobayashi. 2000a. Potassium ion recycling pathway via gap junction systems in the mammalian cochlea and its interruption in hereditary nonsyndromic deafness. *Med. Electron Microsc.* doi:10.1007/s007950070001.

Kikuchi, T., R.S. Kimura, D.L. Paul, T. Takasaka, and J.C. Adams. 2000b. Gap junction systems in the mammalian cochlea. *Brain Res. Rev.* doi:10.1016/S0165-0173(99)00076-4.

Koval, M. 2006. Pathways and control of connexin oligomerization. *Trends Cell Biol.* 16:159–166. doi:10.1016/j.tcb.2006.01.006.

Lagree, V., K. Brunschwig, P. Lopez, N.B. Gilula, G. Richard, and M.M. Falk. 2003. Specific amino-acid residues in the N-terminus and TM3 implicated in channel function and oligomerization compatibility of connexin43. *J. Cell Sci.* 116:3189–3201. doi:10.1242/jcs.00604.

Laird, D.W. 2006. Life cycle of connexins in health and disease. *Biochem. J.* 394:527–543. doi:10.1042/BJ20051922.

Lauf, U., B.N.G. Giepmans, P. Lopez, S. Braconnot, S.C. Chen, and M.M. Falk. 2002. Dynamic trafficking and delivery of connexons to the plasma membrane and accretion to gap junctions in living cells. *Proc. Natl. Acad. Sci. U. S. A.* 99:10446–10451. doi:10.1073/pnas.162055899.

Lee, J.H., and D.C. Marcus. 2008. Purinergic signaling in the inner ear. *Hear. Res.* 235:1–7. doi:10.1016/j.heares.2007.09.006.

Lee, J.R., A.M. Derosa, and T.W. White. 2009. Connexin Mutations Causing Skin Disease and Deafness Increase Hemichannel Activity and Cell Death when Expressed in Xenopus Oocytes. *J. Invest. Dermatol.* 129:870–878. doi:10.1038/jid.2008.335.

Lee, J.R., and T.W. White. 2009. Connexin-26 mutations in deafness and skin disease. *Expert Rev. Mol. Med.* 11:e35. doi:10.1017/S1462399409001276.

Leybaert, L., K. Braet, W. Vandamme, L. Cabooter, P.E.M. Martin, and W.H. Evans. 2003. Connexin channels, connexin mimetic peptides and ATP release. *Cell Commun. Adhes.* doi:10.1080/15419060390262985.

Li–dong, Z., L. Jun, H. Yin–yan, S. Jian–he, and Y. Shi–ming. 2008. Supporting Cells–a New Area in Cochlear Physiology Study. *J. Otol.* 3:9–17. doi:http://dx.doi.org/10.1016/S1672-2930(08)50002-X.

Lilly, E., C.G. Bunick, A.M. Maley, S. Zhang, M.K. Spraker, A.J. Theos, K.L. Vivar, L. Seminario-

Vidal, A.E. Bennett, R. Sidbury, Y. Ogawa, M. Akiyama, B. Binder, S. Hadj-Rabia, R.A. Morotti, E.J. Glusac, K.A. Choate, G. Richard, and L.M. Milstone. 2019a. More than keratitis, ichthyosis, and deafness: Multisystem effects of lethal GJB2 mutations. *J. Am. Acad. Dermatol.* doi:10.1016/j.jaad.2018.09.042.

Lilly, E., M. Strickler, L.M. Milstone, and C.G. Bunick. 2019b. Alterations in connexin 26 protein structure from lethal keratitis-ichthyosis-deafness syndrome mutations A88V and G45E. *J. Dermatol. Sci.* 2–5. doi:10.1016/j.jdermsci.2019.07.002.

Locke, D., F. Kieken, L. Tao, P.L. Sorgen, and A.L. Harris. 2011. Mechanism for modulation of gating of connexin26-containing channels by taurine. *J. Gen. Physiol.* 138:321–339. doi:10.1085/jgp.201110634.

Lohman, A.W., and B.E. Isakson. 2014. Differentiating connexin hemichannels and pannexin channels in cellular ATP release. *In* FEBS Letters.

Lopez, W., J. Gonzalez, Y. Liu, A.L. Harris, and J.E. Contreras. 2013. Insights on the mechanisms of Ca2+ regulation of connexin26 hemichannels revealed by human pathogenic mutations (D50N/Y). *J. Gen. Physiol.* 142:23–45. doi:10.1085/jgp.201210893.

Lopez, W., J. Ramachandran, A. Alsamarah, Y. Luo, A.L. Harris, and J.E. Contreras. 2016. Mechanism of gating by calcium in connexin hemichannels. *Proc. Natl. Acad. Sci. U. S. A.* 113:E7986–E7995. doi:10.1073/pnas.1609378113.

Lu, D., S. Soleymani, R. Madakshire, and P.A. Insel. 2012. ATP released from cardiac fibroblasts via connexin hemichannels activates profibrotic P2Y2 receptors. *FASEB J.* 26:2580–2591. doi:10.1096/fj.12-204677.

Maeda, S., S. Nakagawa, M. Suga, E. Yamashita, A. Oshima, Y. Fujiyoshi, and T. Tsukihara. 2009. Structure of the connexin 26 gap junction channel at 3.5 A resolution. *Nature*. 458:597–602. doi:10.1038/nature07869.

Maeda, S., and T. Tsukihara. 2011. Structure of the gap junction channel and its implications for its biological functions. *Cell. Mol. Life Sci.* 68:1115–1129. doi:10.1007/s00018-010-0551-z.

Majumder, P., G. Crispino, L. Rodriguez, C.D. Ciubotaru, F. Anselmi, V. Piazza, M. Bortolozzi, and F. Mammano. 2010. ATP-mediated cell-cell signaling in the organ of corti: The role of connexin channels. *Purinergic Signal.* 6:167–187. doi:10.1007/s11302-010-9192-9.

Mammano, F. 2013. ATP-dependent intercellular Ca2+ signaling in the developing cochlea: Facts, fantasies and perspectives. *Semin. Cell Dev. Biol.* 24:31–39. doi:10.1016/j.semcdb.2012.09.004.

Mammano, F. 2018. Inner Ear Connexin Channels : Roles in Development and Maintenance of Cochlear Function. doi:10.1101/cshperspect.a033233.

Mammano, F., and M. Bortolozzi. 2017. Ca2+ signaling, apoptosis and autophagy in the developing cochlea: Milestones to hearing acquisition. *Cell Calcium*. doi:10.1016/j.ceca.2017.05.006.

Martin, P.E.M., G. Blundell, S. Ahmad, R.J. Errington, and W.H. Evans. 2001. Multiple pathways in the trafficking and assembly of connexin 26, 32 and 43 into gap junction intercellular communication channels. *J. Cell Sci.* 114:3845–3855.

Martínez, A.D., R. Acuña, V. Figueroa, J. Maripillan, and B. Nicholson. 2009. Gap-junction channels dysfunction in deafness and hearing loss. *Antioxid. Redox Signal.* 11:309–22. doi:10.1089/ars.2008.2138.

Martínez, A.D., V. Hayrapetyan, A.P. Moreno, and E.C. Beyer. 2002. Connexin43 and connexin45 form heteromeric gap junction channels in which individual components determine permeability and regulation. *Circ. Res.* 90:1100–1107. doi:10.1161/01.RES.0000019580.64013.31.

Martínez, A.D., J. Maripillan, R. Acuña, P.J. Minogue, V.M. Berthoud, and E.C. Beyer. 2011.

Different domains are critical for oligomerization compatibility of different connexins. *Biochem. J.*

Marziano, N.K., S.O. Casalotti, A.E. Portelli, D.L. Becker, and A. Forge. 2003. Mutations in the gene for connexin 26 (GJB2) that cause hearing loss have a dominant negative effect on connexin 30. *Hum. Mol. Genet.* 12:805–812. doi:10.1093/hmg/ddg076.

Meşe, G., G. Richard, and T.W. White. 2007. Gap junctions: Basic structure and function. *J. Invest. Dermatol.* 127:2516–2524. doi:10.1038/sj.jid.5700770.

Mhaske, P. V., N.A. Levit, L. Li, H.-Z. Wang, J.R. Lee, Z. Shuja, P.R. Brink, and T.W. White. 2013. The human Cx26-D50A and Cx26-A88V mutations causing keratitis-ichthyosis-deafness syndrome display increased hemichannel activity. *AJP Cell Physiol.* 304:C1150–C1158. doi:10.1152/ajpcell.00374.2012.

Mittal, R., A.P. Patel, D. Nguyen, D.R. Pan, V.M. Jhaveri, J.R. Rudman, A. Dharmaraja, D. Yan, Y. Feng, P. Chapagain, D.J. Lee, S.H. Blanton, and X.Z. Liu. 2018. Genetic basis of hearing loss in Spanish, Hispanic and Latino populations. *Gene*. 647:297–305. doi:10.1016/j.gene.2018.01.027.

Müller, D.J., G.M. Hand, A. Engels, G.E. Sosinsky, A. Engel, and G.E. Sosinsky. 2002. Conformational changes in surface structures of isolated connexin 26 gap junctions. *EMBO J.* 21:3598–3607. doi:10.1093/emboj/cdf365.

Nickel, R., and A. Forge. 2008. Gap junctions and connexins in the inner ear: Their roles in homeostasis and deafness. *Curr. Opin. Otolaryngol. Head Neck Surg.* doi:10.1097/MOO.0b013e32830e20b0.

Oh, S., and T.A. Bargiello. 2015. Voltage regulation of connexin channel conductance. *Yonsei Med. J.* 56:1–15. doi:10.3349/ymj.2015.56.1.1.

Okmen, F., I. Hortu, U. Jafarova, M. Imamoglu, H. Ekici, and A.M. Ergenoglu. 2019. Antenatal

Findings of Keratitis-Ichthyosis-Deafness Syndrome. *J. Obstet. Gynaecol. Canada*. 1–3. doi:10.1016/j.jogc.2019.06.005.

Orellana, J. a., P.J. Sáez, C. Cortés-campos, R.J. Elizondo, K.F. Shoji, S. Contreras-Duarte, V. Figueroa, V. Velarde, J.X. Jiang, F. Nualart, J.C. Sáez, M. a. García, E. Rojczyk-Gołębiewska, A. Pałasz, R. Wiaderkiewicz, R. Elizondo-Vega, C. Cortes-Campos, M.J. Barahona, K. a. Oyarce, C. a. Carril, M. a. García-Robles, J. Flament-Durand, J.P. Brion, A. Nasiadka, M.D. Clark, R.M. Paredes, J.C. Etzler, L.T. Watts, J.D. Lechleiter, D.A. Bechtold, A.S.I. Loudon, W.H. Kaye, C.E. Wierenga, U.F. Bailer, A.N. Simmons, and A. Bischoff-grethe. 2012. Glucose increases intracellular free Ca 2+ in tanycytes via ATP released through connexin 43 hemichannels. *Trends Neurosci.* 36:631–642. doi:10.1002/glia.21246.

Ortolano, S., G. Di, G. Crispino, F. Anselmi, F. Mammano, and J.A. Chiorini. 2008. Coordinated control of connexin 26 and connexin 30 at the regulatory and functional level in the inner ear.

Parker, M., A. Brugeaud, and A.S.B. Edge. 2010. Primary Culture and Plasmid Electroporation of the Murine Organ of Corti. *J. Vis. Exp.* 2–7. doi:10.3791/1685.

Paznekas, W.A., S.A. Boyadjiev, R.E. Shapiro, O. Daniels, B. Wollnik, C.E. Keegan, J.W. Innis, M.B. Dinulos, C. Christian, M.C. Hannibal, and E.W. Jabs. 2003. Connexin 43 (GJA1) mutations cause the pleiotropic phenotype of oculodentodigital dysplasia. *Am. J. Hum. Genet.* 72:408–418. doi:10.1086/346090.

Peracchia, C. 2004. Chemical gating of gap junction channels Roles of calcium , pH and calmodulin. 1662:61–80. doi:10.1016/j.bbamem.2003.10.020.

Peracchia, C. 2020. Calmodulin-mediated regulation of gap junction channels. *Int. J. Mol. Sci.* 21. doi:10.3390/ijms21020485.

Piazza, V., C.D. Ciubotaru, J.E. Gale, and F. Mammano. 2007. Purinergic signalling and

intercellular Ca2+ wave propagation in the organ of Corti. *Cell Calcium*. 41:77–86. doi:10.1016/j.ceca.2006.05.005.

Pickles, J.O. 2015. Auditory pathways: Anatomy and physiology. *Handb. Clin. Neurol.* 129:3–25. doi:10.1016/B978-0-444-62630-1.00001-9.

Pinto, B.I., A. Pupo, I.E. García, K. Mena-Ulecia, A.D. Martínez, R. Latorre, and C. Gonzalez. 2017. Calcium binding and voltage gating in Cx46 hemichannels. *Sci. Rep.* 7:15851. doi:10.1038/s41598-017-15975-5.

Ramírez-Camacho, R., J.R. García-Berrocal, A. Trinidad, J.A. González-García, J.M. Verdaguer, A. Ibáñez, A. Rodríguez, and R. Sanz. 2006. Central role of supporting cells in cochlear homeostasis and pathology. *Med. Hypotheses*. 67:550–555. doi:10.1016/j.mehy.2006.02.044.

Retamal, M.A., E.P. Reyes, I.E. Garcí-a, B. Pinto, A.D. Martí-nez, and C. González. 2015. Diseases associated with leaky hemichannels. *Front. Cell. Neurosci.* 9:1–10. doi:10.3389/fncel.2015.00267.

Richard, G., F. Rouan, C.E. Willoughby, N. Brown, P. Chung, M. Ryynänen, E.W. Jabs, S.J. Bale, J.J. DiGiovanna, J. Uitto, and L. Russell. 2002. Missense Mutations in GJB2 Encoding Connexin-26 Cause the Ectodermal Dysplasia Keratitis-Ichthyosis-Deafness Syndrome. *Am. J. Hum. Genet.* 70:1341–1348. doi:10.1086/339986.

Rouan, F., T.W. White, N. Brown, a M. Taylor, T.W. Lucke, D.L. Paul, C.S. Munro, J. Uitto, M.B. Hodgins, and G. Richard. 2001. Trans-Dominant Inhibition of Connexin-43 By Mutant Connexin-26: Implications for Dominant Connexin Disorders Affecting Epidermal Differentiation. *J. Cell Sci.* 114:2105–2113.

Sáez, J.C., V.M. Berthoud, M.C. Brañes, A.D. Martínez, and E.C. Beyer. 2003. Plasma membrane channels formed by connexins: Their regulation and functions. *Physiol. Rev.* 83:1359–1400. doi:10.1152/physrev.00007.2003.

Sáez, J.C., and L. Leybaert. 2014. Hunting for connexin hemichannels. *FEBS Lett.* 588:1205–1211. doi:10.1016/j.febslet.2014.03.004.

Sanchez, H.A., N. Slavi, M. Srinivas, and V.K. Verselis. 2016. Syndromic deafness mutations at Asn 14 differentially alter the open stability of Cx26 hemichannels. *J. Gen. Physiol.* 148:25–42. doi:10.1085/jgp.201611585.

Sanchez, H.A., and V.K. Verselis. 2014. Aberrant Cx26 hemichannels and keratitis-ichthyosis-deafness syndrome: insights into syndromic hearing loss. *Front. Cell. Neurosci.* 8:1–10. doi:10.3389/fncel.2014.00354.

Schütz, M., T. Auth, A. Gehrt, F. Bosen, I. Körber, N. Strenzke, T. Moser, and K. Willecke. 2011. The connexin26 S17F mouse mutant represents a model for the human hereditary keratitis-ichthyosis-deafness syndrome. *Hum. Mol. Genet.* 20:28–39. doi:10.1093/hmg/ddq429.

Scott, C.A., D. Tattersall, E.A. O'Toole, and D.P. Kelsell. 2012. Connexins in epidermal homeostasis and skin disease. *Biochim. Biophys. Acta - Biomembr.* 1818:1952–1961. doi:10.1016/j.bbamem.2011.09.004.

Segretain, D., and M.M. Falk. 2004. Regulation of connexin biosynthesis, assembly, gap junction formation, and removal. *Biochim. Biophys. Acta - Biomembr.* 1662:3–21. doi:10.1016/j.bbamem.2004.01.007.

Shuja, Z., L. Li, S. Gupta, G. Meşe, and T.W. White. 2016. Connexin26 Mutations Causing Palmoplantar Keratoderma and Deafness Interact with Connexin43, Modifying Gap Junction and Hemichannel Properties. *J. Invest. Dermatol.* 136:225–235. doi:10.1038/JID.2015.389.

Sirko, P., J.E. Gale, and J.F. Ashmore. 2019. Intercellular Ca 2 + signalling in the adult mouse cochlea. *J. Physiol.* 1:303–317. doi:10.1113/JP276400.

Skinner, B.A., M.C. Greist, and A.L. Norins. 1981. The Keratitis, Ichthyosis, and Deafness (KID) Syndrome. *JAMA Dermatology*. 117:285–289. doi:10.1001/archderm.1981.01650050041019.

Smith, T.D., A. Mohankumar, P.J. Minogue, E.C. Beyer, V.M. Berthoud, and M. Koval. 2012. Cytoplasmic amino acids within the membrane interface region influence connexin oligomerization. *J. Membr. Biol.* 245:221–230. doi:10.1007/s00232-012-9443-5.

Söhl, G., S. Maxeiner, and K. Willecke. 2005. Expression and functions of neuronal gap junctions. *Nat. Rev. Neurosci.* 6:191–200. doi:10.1038/nrn1627.

Söhl, G., and K. Willecke. 2003. Cell Communication & Adhesion An Update on Connexin Genes and their Nomenclature in Mouse and Man An Update on Connexin Genes and their Nomenclature in Mouse and Man. *Cell Commun. Adhes.* 9061:173–180. doi:10.1080/15419060390262877.

Stauffer, E.A., and J.R. Holt. 2007. Sensory transduction and adaptation in inner and outer hair cells of the mouse auditory system. *J. Neurophysiol.* 98:3360–3369. doi:10.1152/jn.00914.2007.

Van Steensel, M.A.M., M. Van Geel, M. Nahuys, J. Henk Sillevis Smitt, and P.M. Steijlen. 2002. A novel connexin 26 mutation in a patient diagnosed with keratitis-ichthyosis-deafness syndrome. *J. Invest. Dermatol.* 118:724–727. doi:10.1046/j.1523-1747.2002.01735.x.

Sun, J., S. Ahmad, S. Chen, W. Tang, Y. Zhang, P. Chen, and X. Lin. 2004. Cochlear gap junctions coassembled from Cx26 and 30 show faster intercellular Ca2+ signaling than homomeric counterparts. *AJP Cell Physiol.* 288:C613–C623. doi:10.1152/ajpcell.00341.2004.

Suzuki, T., T. Takamatsu, and M. Oyamada. 2003. Expression of Gap Junction Protein Connexin43 in the Adult Rat Cochlea: Comparison with Connexin26. *J. Histochem. Cytochem.* 51:903–912. doi:10.1177/002215540305100705.

Tambutté, E., S. Tambutté, N. Segonds, D. Zoccola, A. Venn, J. Erez, and D. Allemand. 2011. Calcein labelling and electrophysiology: Insights on coral tissue permeability and calcification. *Proc. R. Soc. B Biol. Sci.* 279:19–27. doi:10.1098/rspb.2011.0733.

Taruno, A. 2018. ATP release channels. *Int. J. Mol. Sci.* 19. doi:10.3390/ijms19030808.

Terrinoni, A., A. Codispoti, V. Serra, B. Didona, E. Bruno, R. Nisticò, M. Giustizieri, M. Alessandrini, E. Campione, and G. Melino. 2010. Connexin 26 (GJB2) mutations, causing KID Syndrome, are associated with cell death due to calcium gating deregulation. *Biochem. Biophys. Res. Commun.* 394:909–914. doi:10.1016/j.bbrc.2010.03.073.

Thévenin, A.F., T.J. Kowal, J.T. Fong, R.M. Kells, C.G. Fisher, and M.M. Falk. 2013. Proteins and mechanisms regulating gap-junction assembly, internalization, and degradation. *Physiology*. 28:93–116. doi:10.1152/physiol.00038.2012.

Thorne, P.R., and G.D. Housley. 1996. Purinergic signalling in sensory systems. *Semin. Neurosci.* 8:233–246. doi:10.1006/smns.1996.0030.

Tóth, T., S. Kupka, B. Haack, K. Riemann, S. Braun, F. Fazakas, H.-P. Zenner, L. Muszbek, N. Blin, M. Pfister, and I. Sziklai. 2004. GJB2 mutations in patients with non-syndromic hearing loss from Northeastern Hungary . *Hum. Mutat.* 23:631–632. doi:10.1002/humu.9250.

Tritsch, N.X., and D.E. Bergles. 2010. Developmental regulation of spontaneous activity in the mammalian cochlea. *J. Neurosci.* 30:1539–1550. doi:10.1523/JNEUROSCI.3875-09.2010.

Verselis, V.K. 2017. Connexin hemichannels and cochlear function. *Neurosci. Lett.* doi:10.1016/j.neulet.2017.09.020.

Vinken, M., E. Decrock, E. De Vuyst, R. Ponsaerts, C. D'hondt, G. Bultynck, L. Ceelen, T. Vanhaecke, L. Leybaert, and V. Rogiers. 2011. Connexins: Sensors and regulators of cell cycling. *Biochim. Biophys. Acta - Rev. Cancer*. 1815:13–25.

doi:10.1016/j.bbcan.2010.08.004.

Vinken, M., T. Vanhaecke, P. Papeleu, S. Snykers, T. Henkens, and V. Rogiers. 2006. Connexins and their channels in cell growth and cell death. *Cell. Signal.* 18:592–600. doi:10.1016/j.cellsig.2005.08.012.

De Vuyst, E., E. Decrock, L. Cabooter, G.R. Dubyak, C.C. Naus, W.H. Evans, and L. Leybaert. 2006. Intracellular calcium changes trigger connexin 32 hemichannel opening. *EMBO J.* 25:34–44. doi:10.1038/sj.emboj.7600908.

Wan, G., G. Corfas, and J.S. Stone. 2013. Inner ear supporting cells: Rethinking the silent majority. *Semin. Cell Dev. Biol.* 24:448–459. doi:10.1016/j.semcdb.2013.03.009.

Willecke, K., J. Eiberger, J. Degen, D. Eckardt, A. Romualdi, M. Guldenagel, U. Deutsch, G. Sohl, M. Güldenagel, U. Deutsch, G. Söhl, M. Guldenagel, U. Deutsch, G. Sohl, M. Güldenagel, U. Deutsch, G. Söhl, M. Guldenagel, U. Deutsch, and G. Sohl. 2002. Structural and functional diversity of connexin genes in the mouse and human genome. *Biol.Chem.* 383:725–737. doi:10.1515/BC.2002.076.

Wiszniewski, L., A. Limat, J.H. Saurat, P. Meda, and D. Salomon. 2000. Differential expression of connexins during stratification of human keratinocytes. *J. Invest. Dermatol.* 115:278–285. doi:10.1046/j.1523-1747.2000.00043.x.

Xu, J., and B.J. Nicholson. 2013. The role of connexins in ear and skin physiology - Functional insights from disease-associated mutations. *Biochim. Biophys. Acta - Biomembr.* 1828:167–178. doi:10.1016/j.bbamem.2012.06.024.

Yotsumoto, S., T. Hashiguchi, X. Chen, N. Ohtake, and A. Tomitaka. 2003. Cutaneous Biology Novel mutations in GJB2 encoding connexin-26 in Japanese patients with keratitis – ichthyosis – deafness syndrome. 649–653.

Yum, S.W., J. Zhang, and S.S. Scherer. 2010. Dominant connexin26 mutants associated with

human hearing loss have trans-dominant effects on connexin30. *Neurobiol. Dis.* 38:226–236. doi:10.1016/j.nbd.2010.01.010.

Yum, S.W., J. Zhang, V. Valiunas, G. Kanaporis, P.R. Brink, T.W. White, and S.S. Scherer. 2007. Human connexin26 and connexin30 form functional heteromeric and heterotypic channels. *Am. J. Physiol. - Cell Physiol.* 293:C1032–C1048. doi:10.1152/ajpcell.00011.2007.

Zhao, H.-B., N. Yu, and C.R. Fleming. 2005. Gap junctional hemichannel-mediated ATP release and hearing controls in the inner ear. *Proc. Natl. Acad. Sci.* 102:18724–18729. doi:10.1073/pnas.0506481102.

Zhao, H.B., and N. Yu. 2006. Distinct and gradient distributions of connexin26 and connexin30 in the cochlear sensory epithelium of guinea pigs. *J. Comp. Neurol.* 499:506–518. doi:10.1002/cne.21113.

Zhu, Y., L. Zong, L. Mei, and H.-B. Zhao. 2015. Connexin26 gap junction mediates miRNA intercellular genetic communication in the cochlea and is required for inner ear development. *Sci. Rep.* 5:15647. doi:10.1038/srep15647.

Zong, L., Y. Zhu, R. Liang, and H.-B. Zhao. 2016. Gap junction mediated miRNA intercellular transfer and gene regulation: A novel mechanism for intercellular genetic communication. *Sci. Rep.* 6:19884. doi:10.1038/srep19884.

Zou, J., M. Salarian, Y. Chen, R. Veenstra, C.F. Louis, and J.J. Yang. 2014. Gap junction regulation by calmodulin. *FEBS Lett.* 588:1430–1438. doi:10.1016/j.immuni.2010.12.017.Two-stage.